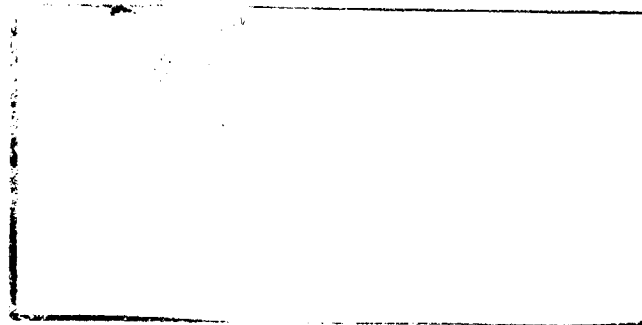


N O T I C E

THIS DOCUMENT HAS BEEN REPRODUCED FROM
MICROFICHE. ALTHOUGH IT IS RECOGNIZED THAT
CERTAIN PORTIONS ARE ILLEGIBLE, IT IS BEING RELEASED
IN THE INTEREST OF MAKING AVAILABLE AS MUCH
INFORMATION AS POSSIBLE

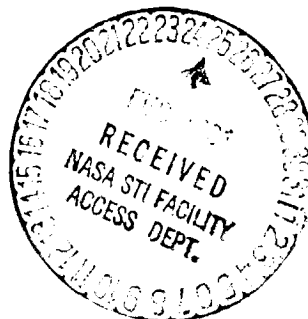
NASA ~~EX~~
NASA CR- 160087



(NASA-CR-160087) THE LOCKHEED OSO-8
PROGRAM. ANALYSIS OF DATA FROM THE MAPPING
X-RAY HELIOMETER EXPERIMENT Final Report,
24 Jun. 1975 - 31 Aug. 1980 (Lockheed
Missiles and Space Co.) 151 p HC A08/MF A01 G3/92

N81-17971

Unclassified
43553



LOCKHEED

MISSILES & SPACE COMPANY, INC. • SUNNYVALE, CALIFORNIA

THE LOCKHEED OSO-8 PROGRAM
FINAL REPORT

Task IB: Analysis of Data from the
Mapping X-Ray Heliometer Experiment

L.W. Acton, C.J. Wolfson, D.W. Datlowe
J.M. Mosher, D.T. Roethig & K.L. Smith

THE LOCKHEED OSO-8 PROGRAM

Analysis of Data from the Mapping X-Ray Heliometer Experiment

**L.W. Acton, Principal Investigator
C.J. Wolfson, Project Manager**

**D.W. Datlowe
J.M. Mosher
D.T. Roethig
K.L. Smith**

**Lockheed Palo Alto Research Laboratory
Department 52-12, Building 202
3251 Hanover Street
Palo Alto, California 94304**

30 September 1980

Final Report for the Period 24 June 1975 - 31 August 1980

Prepared for

**GODDARD SPACE FLIGHT CENTER
Greenbelt, Maryland 20771**

TECHNICAL REPORT STANDARD TITLE PAGE

1. Report No.	2. Government Accession No.	3. Recipient's Catalog No.	
4. Title and Subtitle THE LOCKHEED OSO-8 PROGRAM Analysis of Data from the Mapping X-Ray Heliometer Experiment		5. Report Date 30 September 1980	6. Performing Organization Code
7. Author(s) L.W. Acton, C.J. Wolfson, D.W. Datlowe J.M. Mosher, D.T. Roethig, K.L. Smith		8. Performing Organization Report No. LMSC/D766866	
9. Performing Organization Name and Address Lockheed Palo Alto Research Laboratory Dept. 52-12, Bldg. 202 3251 Hanover Street Palo Alto, California 94304		10. Work Unit No.	11. Contract or Grant No. NAS5-22411 Task IB
12. Sponsoring Agency Name and Address NASA Goddard Space Flight Center Greenbelt, Maryland 20771		13. Type of Report and Period Covered Final (Type III) June 24, 1975 - Aug. 31, 1980	
14. Sponsoring Agency Code			
15. Supplementary Notes			
16. Abstract <p>The purpose of this portion of the Lockheed OSO-8 Program was to analyze, interpret and disseminate data gathered by the Mapping X-Ray Heliometer experiment. The final report describes the extent of the analysis effort, and other activities associated with the preservation and documentation of the data set. The main scientific results, which are related to the behavior of individual solar activity regions in the energy band 1.5 - 15 keV, are summarized, and a complete bibliography of publications and presentations is given. Copies of key articles are also provided.</p>			
17. Key Words (Selected by Author(s)) OSO-8 / Mapping X-Ray Heliometer / Solar Activity		18. Distribution Statement	
19. Security Classif. (of this report) Unclassified	20. Security Classif. (of this page) Unclassified	21. No. of Pages 150	22. Price*

*For sale by the Clearinghouse for Federal Scientific and Technical Information, Springfield, Virginia 22151.

PREFACE

The present report describes activities completed under NAS5-22411 Task Ib. The objective of this portion of the contract was to analyze, disseminate and report results based on data gathered by the Mapping X-Ray Heliometer Experiment on OSC-8 between June 23, 1975 and September 30, 1978. The primary contents of the report are reprints and pre-prints of articles appearing in major scientific publications. These cover a wide range of subjects related to solar X-ray activity. Unpublished results, including those from the extra-solar program are briefly summarized. Efforts in the areas of documenting, cataloging and preserving the data are also described.

TABLE OF CONTENTS

	Page
1. Introduction.....	1
2. Scope of Data	
2.1 Quick Look Data.....	3
2.2 Production Data.....	3
2.3 Coverage.....	3
3. Software Development.....	5
4. Extent of Data Analysis and Documentation.....	14
5. Dissemination of Reduced Data	
5.1 Contributions to the NOAA Solar Forecast Center.....	16
5.2 Publication of Daily Maps by the World Data Center.....	16
5.3 Archival Data for the National Space Science Data Center.....	18
5.4 Miscellaneous Publications of Data.....	21
6. Principal Scientific Results	
6.1 Evolution of Young Active Regions.....	21
6.2 Preflare Phenomena.....	23
6.3 Postflare Relaxation.....	25
6.4 Flare Geometries.....	25
6.5 Sympathetic Flares.....	25
6.6 Spectral Observations.....	26
6.7 Statistical Properties of Active Region X-Ray Emission.....	27
6.8 CRF's and Active Filaments.....	27
6.9 Ultraviolet Flashes.....	32
6.10 Eclipses.....	32
6.11 Radio Bursts.....	32
6.12 Observations of Extra-Solar Sources.....	33
7. New Technology.....	33
Appendix A: Publications and Presentations of the X-Ray Data Analysis Program.....	37
Appendix B: Additional Collaborators in the Data Analysis Program.....	42
Appendix C: Tabulation of Requests for Lockheed X-Ray Data.....	43

Table of Contents (Continued)

	Page
Appendix D: "2-30 keV X-Ray Data from OSO-8".....	45
Appendix E: "Early Evolution of an X-Ray Emitting Solar Active Region".....	54
Appendix F: "A Search for Microwave Emission from Solar X-Ray Bright Point Flares".....	68
Appendix G: "OSO-8 Observations of the Soft X-Ray Continuum in Solar Flares".....	74
Appendix H: "Evolution of the X-Ray Emitting Corona Preceding and After Major Solar Events".....	77
Appendix I: "X-Ray Emission Associated with Filament Activity".....	89
Appendix J: "A Summary of Lockheed X-Ray Data for McMath 14943 and for the Flare of November 22, 1977".....	93
Appendix K: "Does the Emission Measure Decrease During the Start of a Soft X-Ray Flare?".....	102
Appendix L: "An Investigation of the 1.9 \AA Feature in Solar-Flare X-Ray Spectra".....	107
Appendix M: "Predictions of Solar X-Ray Fluxes Based on Sunspot Structure".....	114
Appendix N: "The Height Structure of Solar Active Regions at X-Ray Wavelengths as Deduced from OSO-8 Limb Crossing Observations".....	122
Appendix O: "X-Rays, Filament Activity and Flare Prediction"....	134
Bibliography	142
Index	143

LIST OF ILLUSTRATIONS

	Page
Figure 2.3-1: Daily total outputs of the full sun.....	4
Figure 3-1: Sample printout of engineering information.....	7
Figure 3-2: Printout of an MXRH memory.....	8
Figure 3-3: MXRH histogram map of the X-ray sun.....	10
Figure 3-4: Comparison of observed and predicted spectra.....	11
Figure 3-5: MXRH light curve.....	12
Figure 3-6: Resolution of intensity light curve into temperature and emission measure components.....	13
Figure 5.2-1: The two formats of daily map published in <u>Solar-Geophysical Data (Prompt Reports)</u>	17
Figure 5.3-1: Sample printout of solar coverage times from the National Space Science Data Center submission....	19
Figure 5.3-2: Sample "page" of daily data plots from the National Space Science Data Center submission....	20
Figure 6.1-1: Light curves demonstrating the difference in flare activity between young and mature regions...	22
Figure 6.2-1: Three sample light curves from the pre-flare study.....	24
Figure 6.8-1: Maps and light curve of a flare associated with an eruptive prominence.....	28
Figure 6.8-2: Location of the X-ray source relative to the prominence eruption.....	29
Figure 6.8-3: Interpretation of the event in terms of temperature and emission measure.....	30
Figure 6.8-4: A possible model of the eruption of a filament....	31
Figure 6.12-1: Map showing Sco X-1.....	34
Figure 6.12-2: Map showing the Crab Nebula.....	35
Figure 6.12-3: Map made looking in the direction of Jupiter.....	36

LIST OF TABLES

	<u>Page</u>
Table 1.1: Experiment Summary.....	2
Table 3.1: Basic Software Capabilities.....	6
Table 4.1: Extent of Data Processing.....	15

1. INTRODUCTION

The following report summarizes a portion of the work performed under Contract NASS-22411, as dictated by the guidelines contained therein. Contract NASS-22411 included the obligation to perform three major tasks:

- (a) orbital operations of the Lockheed Mapping X-Ray Heliometer experiment on OSO-8 (Task Ia)
- (b) the analysis and dissemination of data therefrom (Task Ib)
- and (c) the analysis of data from the University of Colorado high resolution ultraviolet spectrometer experiment on OSO-8 (Task II).

The results of Task Ia have been previously reported (Wolfson, Acton, and Smith, 1978)*, and those of Task II are being described in a separate but concurrent report (Bruner, 1980). The present report therefore confines itself to activities undertaken under Task Ib.

Complete details as to the Mapping X-Ray Heliometer (MXRH) instrument itself have been provided in the Final Report to the instrument development contract (Wolfson, Acton, and Gilbreth, 1975), and are summarized in the TECHNICAL MANUAL (1975). Basically, it consists of six proportional counter detectors arrayed behind three one-dimensional collimators fixed to the rotating wheel section of the satellite. As these sweep across the sun, the now-familiar histogram X-ray map is produced (Figure 3-3). The counts forming each of the histogram bins, or "area segments", are further sorted into 16 energy-related pulse-height channels, from which the approximate spectrum of the emitting plasma can be deduced. The instrumental parameters are summarized in Table 1.1.

The work performed under this phase of the contract involved a number of related tasks: (a) documenting and processing the data received; (b) developing the software necessary for its analysis; (c) distributing partially reduced data to the solar community on a near real-time basis; (d) interpreting the results in terms of physical mechanisms; (e) publishing the conclusions; and (f) forming an archival set of reduced data for preservation in the National Space Science Data Center. Our accomplishments in each of these areas are detailed in the sections which follow.

* (Publications developed under the present phase of the contract are listed in Appendix A. All other references are given in the Bibliography.)

TABLE 1.1

**EXPERIMENT SUMMARY
MAPPING X-RAY HELIOMETER**

PHYSICAL SIZE:	ONE OSO-8 WHEEL COMPARTMENT
WEIGHT:	86 LBS
POWER:	9.5 WATTS
TM RATE:	580 BITS/SEC
DETECTION SYSTEM:	ODA TYPE COLLIMATORS PROPORTIONAL COUNTERS
SPECTRAL RANGE:	2 - 30 KEV
SPECTRAL RESOLUTION:	< 20% FWHM AT 6 KEV
ANGULAR RESOLUTION:	2 ARC MIN FWHM COLLIMATION
TIME RESOLUTION:	10 SEC
EFFECTIVE AREA:	3 DETECTORS . . . 60 CM ² EA (LARGE DETECTORS) 2 DETECTORS . . . 2.3 CM ² EA (THIN WINDOW DET.) 1 DETECTOR . . . 1 CM ² (SMALL FLARE DET.)
DYNAMIC RANGE:	> 10 ⁵
COMMENT:	3 COLLIMATED SYSTEMS (0°, ± 60° FROM VERTICAL) SCAN THE SUN TO PRODUCE SPECTROHELIograms.

2. SCOPE OF DATA

The data provided to Lockheed by the mission control center at Goddard consisted of two main varieties: quick-look and production. The quick look data differs from the production in that it offers less complete coverage and less adequate engineering data. In particular, it lacks information regarding the final aspect solution of the spacecraft, thereby admitting the possibility of some positional errors in the maps produced from it. Otherwise, the scientific content is very similar to that of the production data which later supersedes it.

2.1 Quick Look Data

The quick look data was received on the evening following its acquisition via a direct telephone link with Goddard Space Flight Center. Each transmission contained data from 1 to 4 orbits (out of the 16 which occur each day). Although there were frequent problems with the phone lines, some quick look data was eventually received for all but 31 of the 1196 days of orbital operation (nearly half the omissions occurred in December 1977). The data was recorded on magnetic tape, and stored until its analysis was completed.

2.2 Production Data

The production data was received by mail. Each tape contained the set of data dumps falling on a particular day, and was received, typically, about two months after their acquisition. Each tape received was cataloged, and entered into the Lockheed tape library in Sunnyvale, California, where it is preserved. Production tapes were eventually received for all but one day of orbital operations (March 10, 1978). In addition to the original tapes in the Sunnyvale tape library, an additional set of 485 copy tapes was made, each reel containing the data for approximately 2.5 days of operation. These copy tapes are stored at the computer facility in Palo Alto, and are used in the day-to-day analysis operations. Surplus quick-look tapes were used as the raw material.

2.3 Coverage

Both data sets cover the period June 23, 1975 through September 30, 1978, a period which included the trailing part of the last solar cycle, and

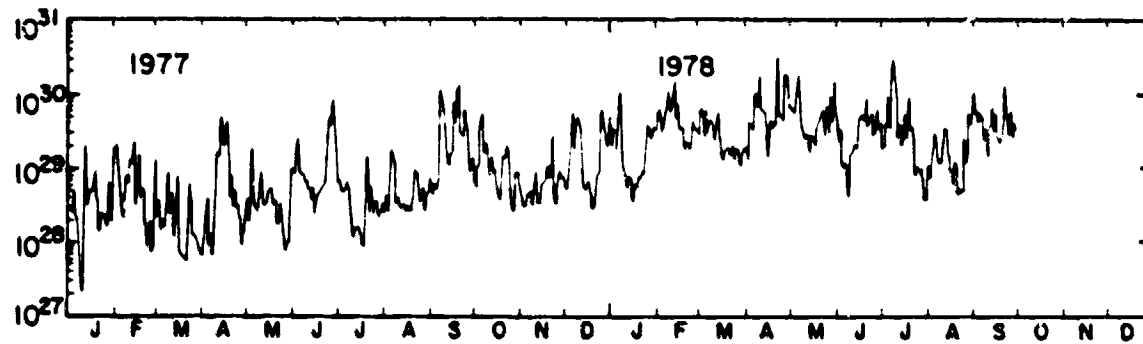
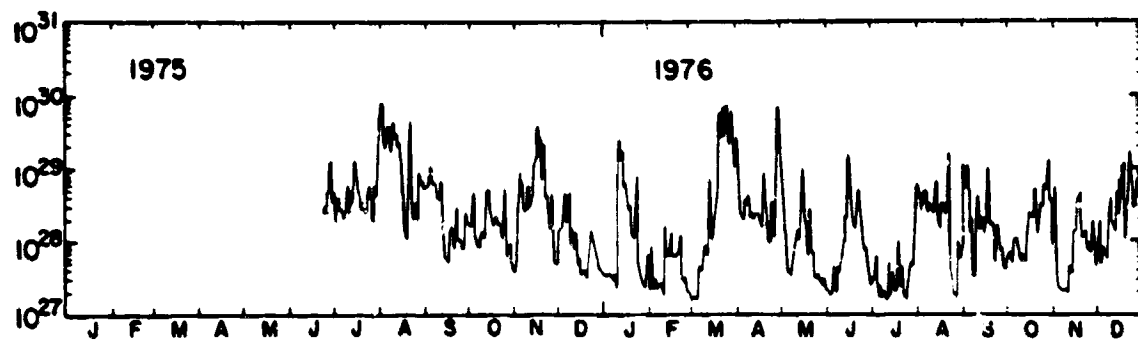


Figure 2.3-1: Daily total outputs of the full sun (in ergs) in the 1 - 8 μ band. Note the minimum in the first half of 1976.

the ascending part of the current one (see Figure 2.3-1). The first solar data were obtained on June 24th. With the exceptions noted in the Final Report to the operations phase (Wolfson, Acton, and Smith, 1978), the Mapping X-Ray Heliometer was operated in its solar data collecting mode for approximately 60 minutes (sunrise to sunset) out of every 90 minute orbit; but because of additional down time introduced by the South Atlantic Anomaly, the total coverage is only about 50% of each day. Also, some orbits are missing from the production tapes, particularly during the last months of operation.

3. SOFTWARE DEVELOPMENT

In the course of the activities undertaken under the current contract, a wide variety of computer programs have been developed for handling and manipulating the scientific data. Initially, the quick look tapes were processed on an HP-2116C mini-computer acquired during the instrument development phase of the project, and the production tapes on the main Lockheed computer system in Sunnyvale. Later, both functions were transferred to an HP-1000 computer, which was acquired under the present contract explicitly for the purpose of data analysis. This computer is equipped with two 9-track 1600 bpi tape drivers, an interactive CRT display terminal, and Versatec plotter/printer. Table 3.1 summarizes the most important software capabilities available for quick look and production data.

The most basic software capability is that of being able to extract from the tapes the engineering status information and the contents of the individual data memories. Figure 3-1 illustrates a typical printout of engineering status information. This is always available but seldom explicitly extracted, since the information required can generally be used internally by the other programs. Figure 3-2 shows the contents of a typical Mapping X-Ray Heliometer memory, which consists of a two-dimensional (32x16) array of numbers. Each number in the array is a proportional detector count. The thirty-two lines are the X-ray spectra observed in each of the positional area segments (the sixteen columns corresponding to the number of counts at different energies). The last line is used to record the background spectrum. In the particular example chosen, the peaks due to two separate sources are easily recognizable in area segments 14-19 and 25-29. Both show the maximum number of counts in the fifth energy channel.

Table 3.1 BASIC SOFTWARE CAPABILITIES

Function	Quick Look	Production
1. Printout engineering status information	X	X
2. Printout individual memories of data	X	X
3. Printout changes in engineering status	X	
4. Scan data for major intensity fluctuations	X	
5. Compute and printout orbital sums	X	X
6. Create and display histogram maps	X	X
7. Determine source coordinates	X	X
8. Plot light curves (intensity versus time) for selected area segments	X	X
9. Produce automated light curves for pre- selected source coordinates		X
10. Extract spectra for specified times and fit temperatures to them	X	X
11. Extract and plot time sequences of temperature and emission measure for specified locations		X
12. Determine expected location of an extra-solar source		X
13. Produce and display reference maps showing relative locations of McMath regions	X	X

23139109 ON 07/02/75 (DAY 183) 090 IN LITE & MXRH NITE SB
150 IN SUN? S YES
 time of MF V H+ S ON
 SA B+ S ON
 SB B+ S ON
 V HVC S ON
 SLA HVC S ON
 SLB HVC S ON
 V PHO S ON
 SLA PRD S ON
 SLB PRD S ON
 V SENS D/R S OFF
 SL SENS D/R S OFF
 FLARE FL/FP S ON
 LMSC FLARE? S NO
 V LO THRSII S 16
 V HI THRSII S 64
 SL LO THRSII S 4
 SL HI THRSII S 64
 V SENS MD S AUTO
 SLA SENS MD S AUTO
 SLB SENS MD S AUTO
 CMDND DAY? S NO
 CMDND NITE? S YES ← MXRH in nighttime mode.
 V ONLY MODE? S NC
 ALT D HOME S NC
 AZ COUNTS S 1126 ← C = azimuth offset command
 R.A. (DEG) = 253.042 = α right ascension & decl. of OSA-spin axis
 DEC. (DEG) = 64.990 = δ }
 RA A REF = 142.648 = α right ascension & decl. of Ref. Axis at UF.
 DECT A REF = 11.572 = δ
 PITCH (DEG) = -0.193 ← η = elevation of suncenter relative to wheel plane
 NULL (DCG) = 354.98
 SPIN (RPM) = 5.0002 ← w = spin rate
 T HIP 1 = 9.0430 ← at = time (in sec) from MF to 1st HIP.
 T HIP 2 = 19.7422 ← time to 2nd HIP
 T HIP 3 = 100.0000 ← time to 3rd HIP. (fill-in, in this case.)
 T SUN P 1 = 7.6561
 T SUN P 2 = 17.8499 } time from MF to 1st, 2nd, 3rd sunsensor
 T SUN P 3 = 100.0000 } pulses
 MMAT1 = 1.15723144-C1 = R1
 MMAT2 = 9.7142922-C1 = R2
 MMAT3 = 3.9471767-C1 = R3
 MMAT4 = 4.8054860-C1 = R4
 MMAT5 = -1.2484516-C1 = R5
 MMAT6 = -1.4145324-C1 = R6
 MMAT7 = 0.7306348-C2 = R7
 MMAT8 = -4.1766340-C1 = R8
 MMAT9 = -4.0623304-C1 = R9
 RELAY VOLT = 32.17
 MFGULTO 28V = 20.30
 UNREG POWER S OFF
 FOMMT GEN A S ON
 FOMMT GEN B S OFF

Figure 3-1: Sample printout of engineering information.

177777 FILE# 1 RECORD# 37
 0:28:28 ON 8/ 6/75 (DAY 218) ODN IN LITE & MORN DAY SA (NORM/COARSE) ET=122
 762 172 377 377

	1	2	3	4	5	6	7	8	9	10	11	12	13	14	15	16
	*	*	*	*	*	*	*	*	*	*	*	*	*	*	*	*
1*	0	0	0	0	0	0	0	0	0	0	0	0	0	0	0	0
2*	0	0	0	0	0	0	0	0	0	0	0	0	0	0	0	0
3*	0	0	0	0	0	0	0	0	0	0	0	0	0	0	0	0
4*	0	0	0	0	0	0	0	0	0	0	0	0	0	0	0	0
5*	0	0	0	0	0	0	0	0	0	0	0	0	0	0	0	0
6*	0	0	0	0	0	0	0	0	0	0	0	0	0	0	0	0
7*	0	0	0	0	0	0	0	0	0	0	0	0	0	0	0	0
8*	0	0	0	0	0	0	0	0	0	0	0	0	0	0	0	0
9*	0	0	0	0	0	0	0	0	0	0	0	0	0	0	0	0
10*	0	0	0	0	0	0	0	0	0	0	0	0	0	0	0	0
11*	0	0	0	0	0	0	0	0	0	0	0	0	0	0	0	0
12*	0	0	0	0	0	0	0	0	0	0	0	0	0	0	0	0
13*	0	0	0	0	0	0	0	0	0	0	0	0	0	0	0	0
14*	0	7	14	19	6	1	1	1	1	1	1	1	1	1	1	1
15*	0	3	15	36	39	24	32	19	3	3	3	3	3	3	3	3
16*	0	2	21	34	68	37	29	17	4	3	3	3	3	3	3	3
17*	0	4	19	48	42	28	27	14	1	1	2	2	2	2	2	2
18*	0	3	15	19	28	25	24	8	1	1	1	1	1	1	1	1
19*	0	2	3	4	10	9	2	1	1	1	1	1	1	1	1	1
20*	0	0	1	2	1	3	1	1	1	1	1	1	1	1	1	1
21*	0	0	0	0	0	0	0	0	0	0	0	0	0	0	0	0
22*	0	0	0	0	0	0	0	0	0	0	0	0	0	0	0	0
23*	0	0	0	0	0	0	0	0	0	0	0	0	0	0	0	0
24*	0	0	0	0	0	0	0	0	0	0	0	0	0	0	0	0
25*	0	2	8	18	17	15	19	2	0	2	1	0	0	1	0	0
26*	0	7	25	44	64	53	44	26	2	2	4	4	4	4	1	1
27*	0	4	39	56	65	61	58	26	3	1	0	1	1	1	1	1
28*	0	2	28	27	46	32	22	14	3	1	1	1	1	1	1	1
29*	0	2	0	10	23	15	12	3	1	1	0	0	0	0	0	0
30*	0	0	2	2	1	2	2	1	1	0	0	0	0	0	0	2
31*	0	1	0	1	2	0	1	1	0	0	0	0	0	0	0	0
32*	0	0	0	1	0	0	0	1	0	0	0	0	0	0	0	0

Figure 3-2: Printout of an MXRH memory showing counts from two sources (August 6, 1975; 0028:28 UT).

In order to interpret such memory data spatially, the rows are summed horizontally over a pre-selected set of energy channels (usually 2-13 or 2-15), and the results displayed in the form of a histogram map (Figure 3-3). The histogram map appears on a Tektronix CRT screen permitting the source locations to be selected in an interactive fashion. The computer converts the indicated source positions directly into heliographic coordinates, which are also included as a part of the display. The approximate temperature and emission measure of the plasma producing the intensity peaks can be determined by examining the underlying spectra. The computer contains in its memory a series of spectra corresponding to the response of each detector to a variety of Tucker and Koren (1971) like isothermal plasmas. From these the best fit is selected, and the chi-squared test is used as an indication of the goodness of fit (Figure 3-4).

Time variations of intensity can be studied by making a sequence of maps, but this is cumbersome. A more efficient technique is to use the light curve option (Figure 3-5), in which the count rate from each memory containing information regarding a particular detector-position swath is plotted as a function of time. This will normally provide a temporal resolution of about one point per twenty or forty seconds, depending on the detector. When sufficient counts are available (as during a flare), each intensity point can also be fit by a temperature and emission measure (Figure 3-6). If desired, the preflare spectral contribution can be subtracted so that only the flare plasma is analyzed.

Of these basic data reduction capabilities a number of special-purpose variations exist. One of the most powerful is the automated light curve production technique which was extensively exploited in our preparation of the archival data set for the National Space Science Data Center (see Section 5.3). In this mode, the coordinates of the positions to be monitored are selected in advance, and the data from all three collimator systems are used to place an automatic limit on the possible level of X-ray emission from each of these points at intervals of one minute in time. The full disk output of the sun is also monitored, and the results stored on tape.

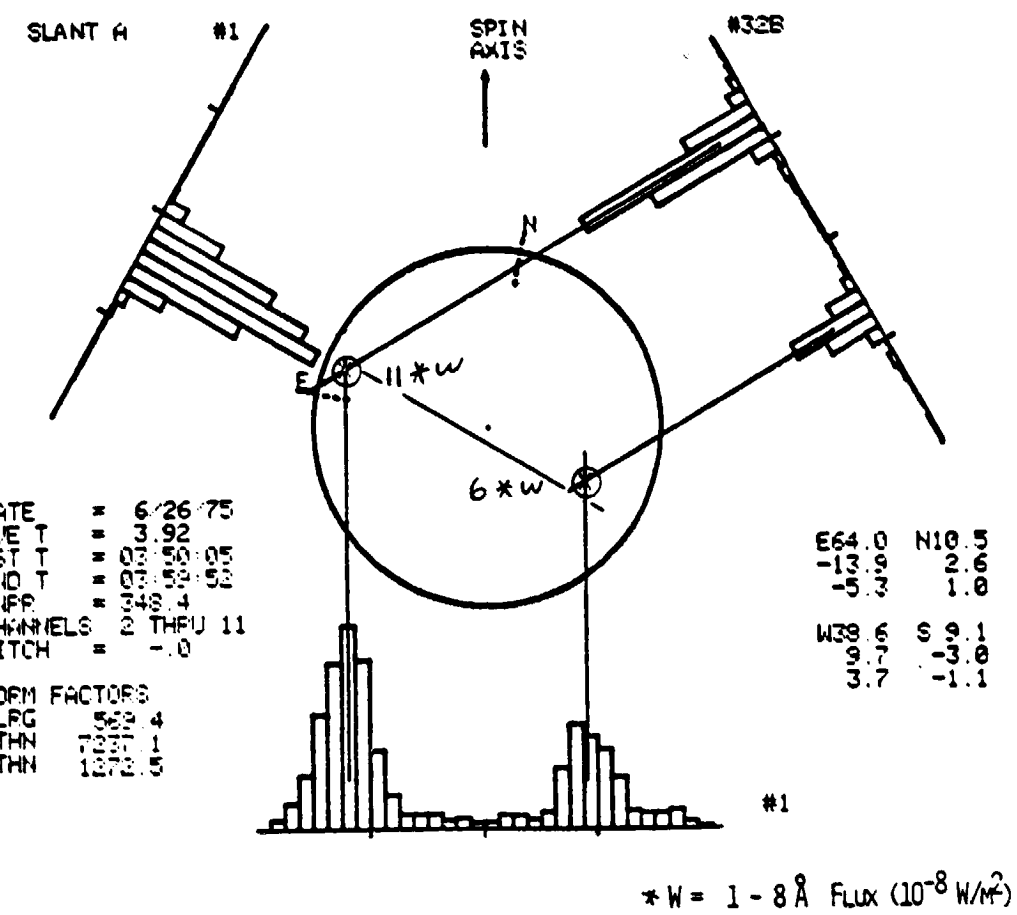


Figure 3-3: MXRH histogram map of the X-ray sun
(June 26, 1975; 0350:05-0359:52 UT).

DETECTOR=LV DATE 8/26/75 TIME 13:20:24
 AREA SEGMENTS 14 TO 19 PITCH .108
 COLCT= 1.859 AVERAGE TIME= 13.502 FOR 56 MEMORIES
 COUNTS= 835 1203 1739 719 267 94 62 24
 15 4 10 8 11 31 51 57
 BACKGR= 2945 34 34 30 34 33 43 70
 31 20 40 38 21 113 183 211
 COLLECTING TIME= 35.84 SEC

 BEST FIT PARAMETERS

 T6= 3.350
 EMISSION MEASURE= 22.794 PER AREA SEGMENT IN 6. AREA SEGMENTS
 CHISQ= 35.99 FOR 11 DEGREES OF FREEDOM

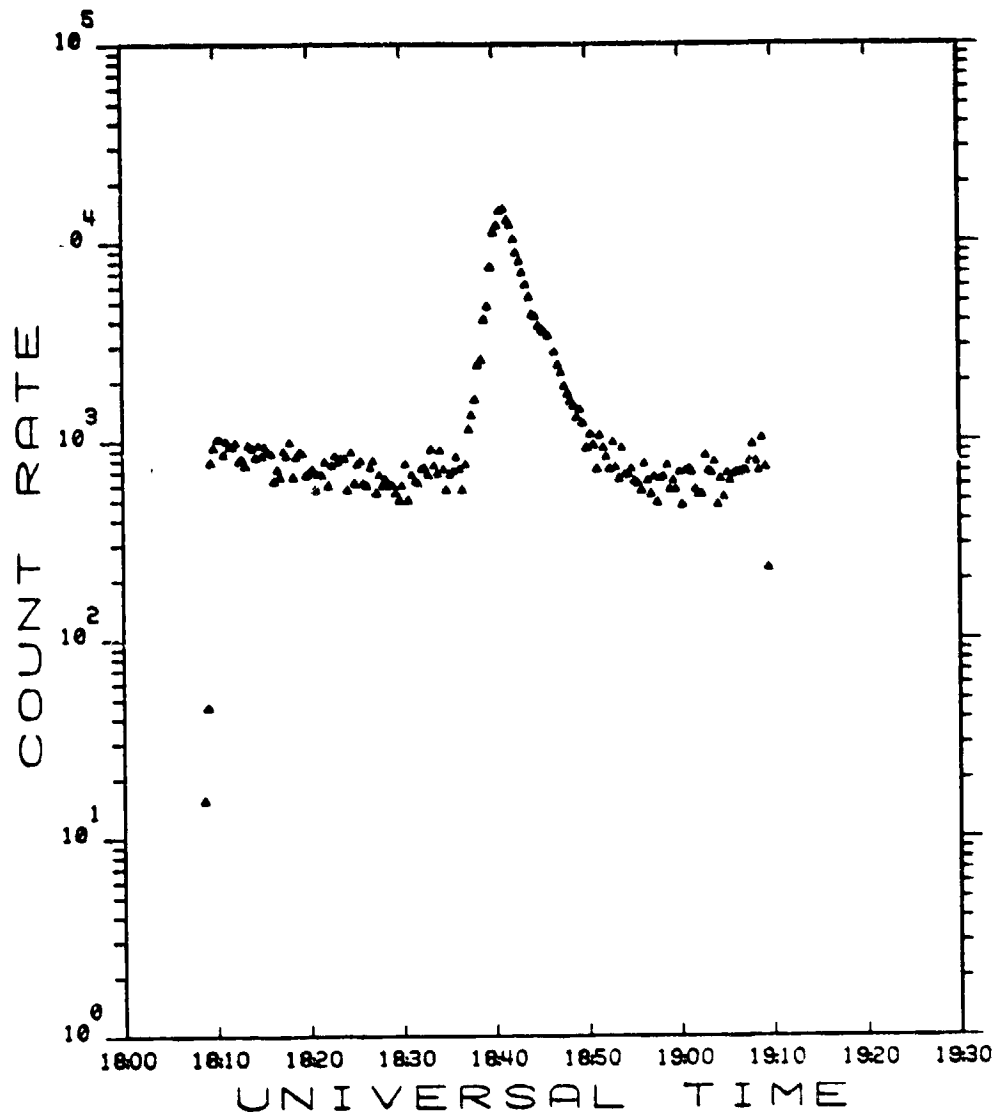
 CHANNEL ENERGY OBSERVED PREDICTED SIGMA CHISQ
 1 1.46 .106E+03 .104E+03 .309E+01 .3
 2 1.96 .153E+03 .148E+03 .371E+01 2.2
 3 2.54 .630E+02 .733E+02 .239E+01 18.6
 4 3.06 .227E+02 .227E+02 .148E+01 .0
 5 3.58 .742E+01 .656E+01 .907E+00 .9
 6 4.13 .439E+01 .183E+01 .771E+00 10.1
 7 4.82 .177E+00 .400E+00 .602E+00 .1
 8 5.80 .466E+00 .209E-01 .441E+00 1.0
 9 6.33 -.203E+00 .439E-02 .285E+00 .3
 10 6.83 -.229E+00 .946E-03 .422E+00 .3
 11 7.44 -.350E+00 .149E-03 .396E+00 .0
 12 7.96 .390E+00 .270E-04 .372E+00 1.1

 TOTAL SOURCE COUNTING RATE= 357.03 (BASED ON 4158 COUNTS)
 THE TOTAL BACKGROUND COUNTING RATE WAS 11.942
 LIVE EXPOSURE TIME= 11.269 TRIANGLE FACTOR= 1.00

Figure 3-4: Comparison of observed and predicted spectra in 12 energy channels.

ORBITING SOLAR OBSERVATORY - 8
LOCKHEED MAPPING X-RAY HELIOMETER EXPERIMENT

04 - 30 - 76



AREA SEGMENTS 8 THRU 9
PHA CHANNELS 2 THRU 13
* = VERTICAL SMALL FLARE
▲ = VERTICAL LARGE

PROCESSED ON: 7/16/79 AT 10:10:00

DTR

Figure 3-5: MXRH light curve (McMath 14179; April 30, 1976).

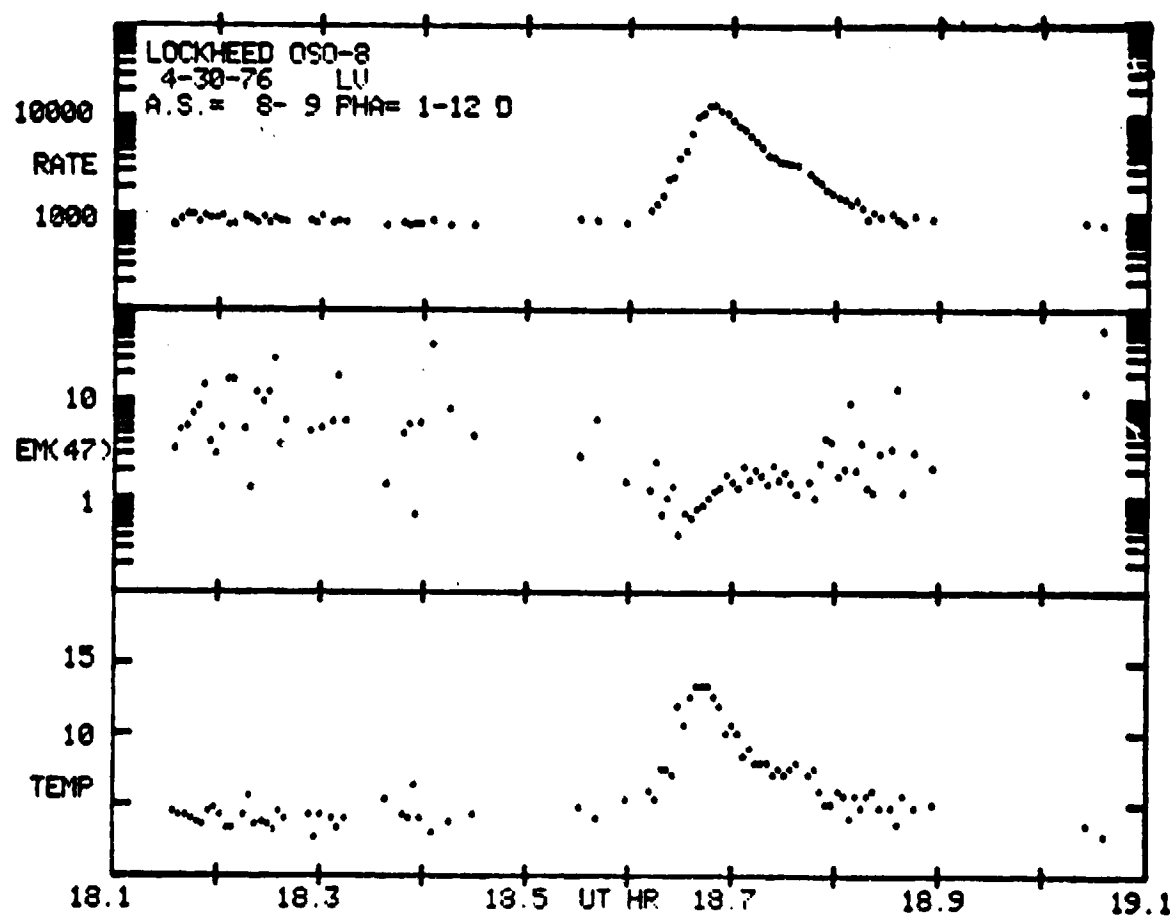


Figure 3-6: Resolution of intensity light curve into temperature and emission measure components.

4. EXTENT OF DATA ANALYSIS AND DOCUMENTATION

The extent to which the available data have been analyzed is summarized in Table 4.1. All quick look data and every production tape received has been examined. From either quick-look or production sources a characteristic X-ray map has been drawn for each day of operation. These are kept in a series of folders to which supplementary information may be added as appropriate. This would include spectra and, when significant intensity variations were noted, light curves and additional maps at the various event peaks. For the most part, this archive was produced in near real-time, using the telephone-transmitted quick look data. A separate complete set of quick look records of calibrations and engineering status is also maintained (as indicated in the Operational Phase final report, the instrument displayed very little variation in performance over the lifetime of the experiment).

The production tapes are already partially documented when received from Goddard, in the sense of being accompanied by a list giving the contents (i.e., date and times) of each data file. These records have been preserved, but for the most part, they are superseded by the more extensive (and more relevant) listings of solar X-ray coverage times prepared as part of our submission for the National Space Science Data Center (see Section 5.3 and Figure 5.3-1).

On the negative side, it would not be possible to say that the wealth of spectral data contained in the MXRH archives has been adequately investigated. The daily active region temperatures determined between August 1, 1975 and June 30, 1977 were a start in that direction, but detailed time-dependent spectral variations have been studied in only a few isolated events of special interest. The reason for this is that the extraction of temperatures is difficult and time-consuming, and does not lend itself easily to automation. Moreover, the results depend on the choice of detector and energy channels. The reduced data set prepared for the National Space Science Data Center has also not been adequately studied, and is the object of a follow-on Contract (NASS-25906).

Some potentially-interesting positional variations may have been overlooked as a result of the relatively low number of histogram maps which were produced out of the vast number potentially available. We have concluded, however, that to first order, with the resolution of the current

Table 4.1

EXTENT OF DATA PROCESSING

	Quick Look*	Production†
Histogram Map	at least one per day	as needed
Scan for flares	all	N/A
Automated light curves for National Space Science Data Center	N/A	every day
Active region temperatures	at least once per day through June 30, 1977	as needed
Orbital sums	one-fourth	one-third
Calibration	all	all not in quick look

* 1165 days available, average of 3 orbits per day

† 1195 days available, average of 16 orbits per day

experiment, the solar active regions tend to act as relatively stationary point sources in the 1-8 \AA band. The most important information is therefore to be found in their intensity variations, which we have studied in detail.

5. DISSEMINATION OF REDUCED DATA

The obligation to make reduced data from the experiment available to the scientific community in general was fulfilled in three major ways: contribution of inputs to the NOAA solar forecast center, publication of daily maps in Solar Geophysical Data, and submission of a specially-produced synoptic data set to the National Space Science Data Center. In addition, numerous special sets containing additional data related to specific times or events were prepared and mailed to investigators making requests.

5.1 Contributions to the NOAA Solar Forecast Center

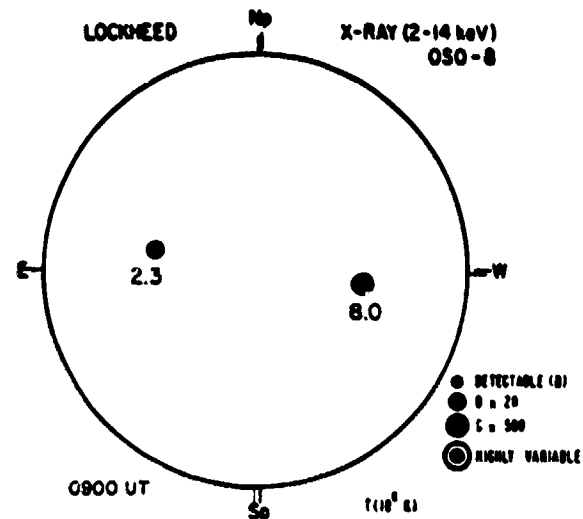
The NOAA Space Environment Research Laboratory in Boulder, Colorado has the duty of monitoring and reporting daily solar activity and of making forecasts of future activity for dissemination in near real-time. Their predictions are based on a combination of visual, magnetic, X-ray and radio observations. During the operational life of the Mapping X-Ray Heliometer experiment a preliminary daily quick-look histogram map (similar to Figure 3-3) was sent to the Forecast Center each morning by telecopier. These maps supplemented the full disk X-ray information available from NOAA's own SMS and GOES satellites by showing how the flux was distributed among the possible sources, a capability which greatly enhanced its predictive value. When quick look coverage was available, the MXRH data was also used to identify the locations of full-disk X-ray bursts whose locations could not be identified in the H-alpha patrols. Similar preliminary maps were also sent by telecopier to Columbia University and to the OSO-8 Pointed Instrument Control Center at the University of Colorado when requested for their mission planning.

5.2 Publication of Daily Maps by the World Data Center

At the end of each month, the quick-look folders for that month were assembled and a characteristic map prepared for each day. The approximate strength and location of each source is indicated and an additional notation is made if significant X-ray flaring was detected during the period of quick-look coverage. The resulting maps (Figure 5.2-1) were submitted by mail to World Data Center A in Boulder, Colorado, which published them as a part of

AUGUST 7, 1975 ($P = 12.92$, $B_0 = 6.17$, $L_0 = 287.90$)

Map giving temperature
(10^6 °K) and intensity
category.



SEPTEMBER 26, 1978 ($P = 25.56$, $B_0 = 6.93$, $L_0 = 281.54$)

Map giving intensity
only.

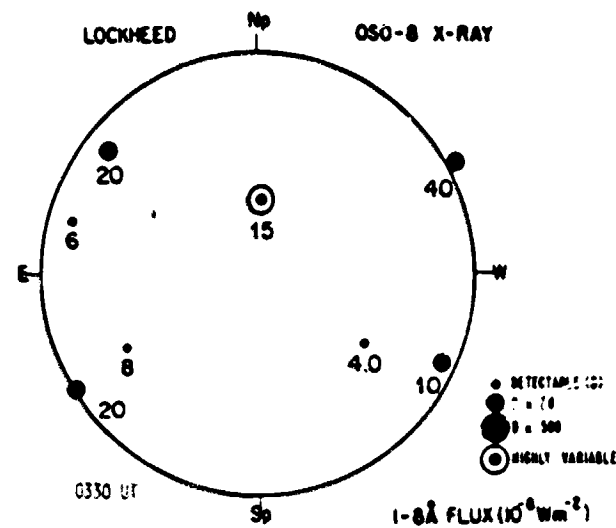


Figure 5.2-1: The two formats of daily map published in Solar Geophysical Data (Prompt Reports). Maps of the upper kind were provided from August 1, 1975 through June 30, 1977. Maps of the lower kind were provided for July 1, 1977 through September 30, 1978.

the pictorial section of its periodical Solar Geophysical Data (Prompt Reports). Approximately 1125 Mapping X-Ray Heliometer maps were published, each appearing in an issue dated two months after its acquisition. They cover the period August 1, 1975 through September 30, 1978. The director of the World-Data Center (Shapley, 1976) has indicated that Solar-Geophysical Data, which is the primary and most timely publication of its kind, has a regular readership in excess of 2500 persons, of which 60-70% have responded in polls that they use the X-ray maps.

5.3 Archival Data for the National Space Science Data Center

A special archival set of Mapping X-Ray Heliometer data was prepared for preservation on microfiche in the National Space Science Data Center (Mosher, 1980: Bull. Amer. Astron. Soc. 11, 710). The archival data serves two functions: it provides a definitive list of available solar data coverage times, and it presents in graphical form the probable intensity variation of every potentially interesting source on each day of coverage.

Figure 5.3-1 illustrates the format adopted for the tabulation of coverage times, and Figure 5.3-2 illustrates the graphical coverage for a typical day. The purpose of the graphical coverage is to indicate the disposition of the sources at one moment during the day (by means of a histogram map), to identify those sources in terms of the underlying McMath activity center numbers, and to display the probable intensity variation of each in the 1-8A intensity band at a resolution of 1 minute in time. Each light curve point is an upper limit on the possible level of X-ray emission emanating from the specified position. Depending on the level of activity, up to 14 different locations may be monitored on any one day (on the day illustrated in Figure 5.3-2, five potential sources were considered). The flux levels from the full disk and in the background directions are also indicated. The full disk values which we report have been found to be in good agreement with the more extensive full-disk measurements provided by NOAA's SMS/GOES satellites (Donnelly *et al.*, 1977), and extend to somewhat lower flux levels than they can monitor.

The complete Lockheed Mapping X-Ray Heliometer submission to the National Space Science Data Center consists of 19 microfiche pages of coverage time tabulations and 101 microfiche pages of reduced graphical data. In all, nearly 600 distinct regions were followed.

RECORD OF DATA COVERAGE OR IMAGE PRODUCTION DATA TAPE 398

PAGE 1

START OF DATA			END OF DATA			PITCH	SNPR
FILE	REC	TIME	FILE	REC	TIME		
2-22-78							
1	36	12:22:33	1	91	13:28:36	-.38	129.7
2	24	13:57:44	2	37	14:11:44	-.40	129.7
3	1	14:12:25	3	48	15: 1: 8	-.51	129.6
3	86	15:33:15	3	99	15:53: 4	-.47	129.7
4	1	15:53:25	4	34	16:27:26	-.50	129.6
4	75	17: 9:19	4	84	17:18:22	-.51	129.7
5	1	17:18:42	5	35	17:54:16	-.58	129.7
5	85	18:44:52	5	129	19:30:41	-.60	129.7
7	21	20:20:26	7	22	20:22: 9	-.64	129.7
7	23	20:25:14	7	32	20:34:58	-.61	129.7
7	32	20:35: 7	7	63	21: 8:49	-.61	129.7
7	111	21:55:41	7	137	22:22:43	-.66	129.7
8	1	22:23:13	8	22	22:43: 7	-.67	129.6
8	22	22:47:10	8	22	22:47:10	-.66	129.6
8	66	23:31:28	8	93	23:59:52	-.69	129.6
2-23-78							
8	94	0: 0:13	8	122	0:28:57	-.71	129.6
9	1	0:29:18	9	1	0:29:38	-.71	129.6
9	36	1: 7: 6	9	99	2: 9:44	-.73	129.5
10	31	2:42: 4	10	92	3:45:13	-.74	129.5
11	23	4:17:54	11	58	4:54: 0	-.82	129.5
12	1	4:54:21	12	27	5:20:33	-.84	129.5
12	60	5:53:36	12	126	6:56:24	-.89	129.5
13	1	7:33:22	13	58	8:31:56	-.91	129.5
13	90	9: 4:26	13	133	9:47:47	-.97	129.6
14	1	9:48:17	14	19	10: 7:18	-.98	129.6
14	81	10:40: 0	14	113	11:42:51	-1.04	129.6
15	30	12:10:34	15	92	13:18:25	-1.09	129.6
16	23	13:51: 8	16	39	14: 6: 1	-1.11	129.6
17	1	14: 6:22	17	42	14:48:51	-1.11	129.6
17	42	14:49: 1	17	47	14:53:59	-1.18	129.6
17	47	14:54:10	17	48	14:54:26	-1.15	129.6
17	79	15:26:42	17	94	15:41:37	-1.16	129.6
18	1	15:42:17	18	31	16:13:26	-1.19	129.6
18	79	17: 2: 7	18	80	17: 3:50	-1.23	129.6
19	1	17: 4:41	19	1	17: 4:41	-1.23	129.6
19	2	17: 5:43	19	23	17:27:26	-1.20	129.5
19	23	17:29:31	19	37	17:44: 3	-1.23	129.5
20	1	17:44:26	20	1	17:45:17	-1.23	129.5
20	53	18:37:43	20	82	19: 0:12	-1.26	129.5
20	83	19:10: 4	20	94	19:22: 5	-1.30	129.4
21	22	20:13:19	21	68	21: 0:37	-1.32	129.4
21	116	21:49:17	21	123	21:56:50	-1.33	129.4
22	1	21:57:20	22	41	22:39:10	-1.37	129.4
22	86	23:24:25	22	120	23:59:54	-1.43	129.4

Figure 5.3-1: Sample printout of solar coverage times from the National Space Science Data Center submission. Each line represents a continuous data sequence with no gap exceeding one minute.

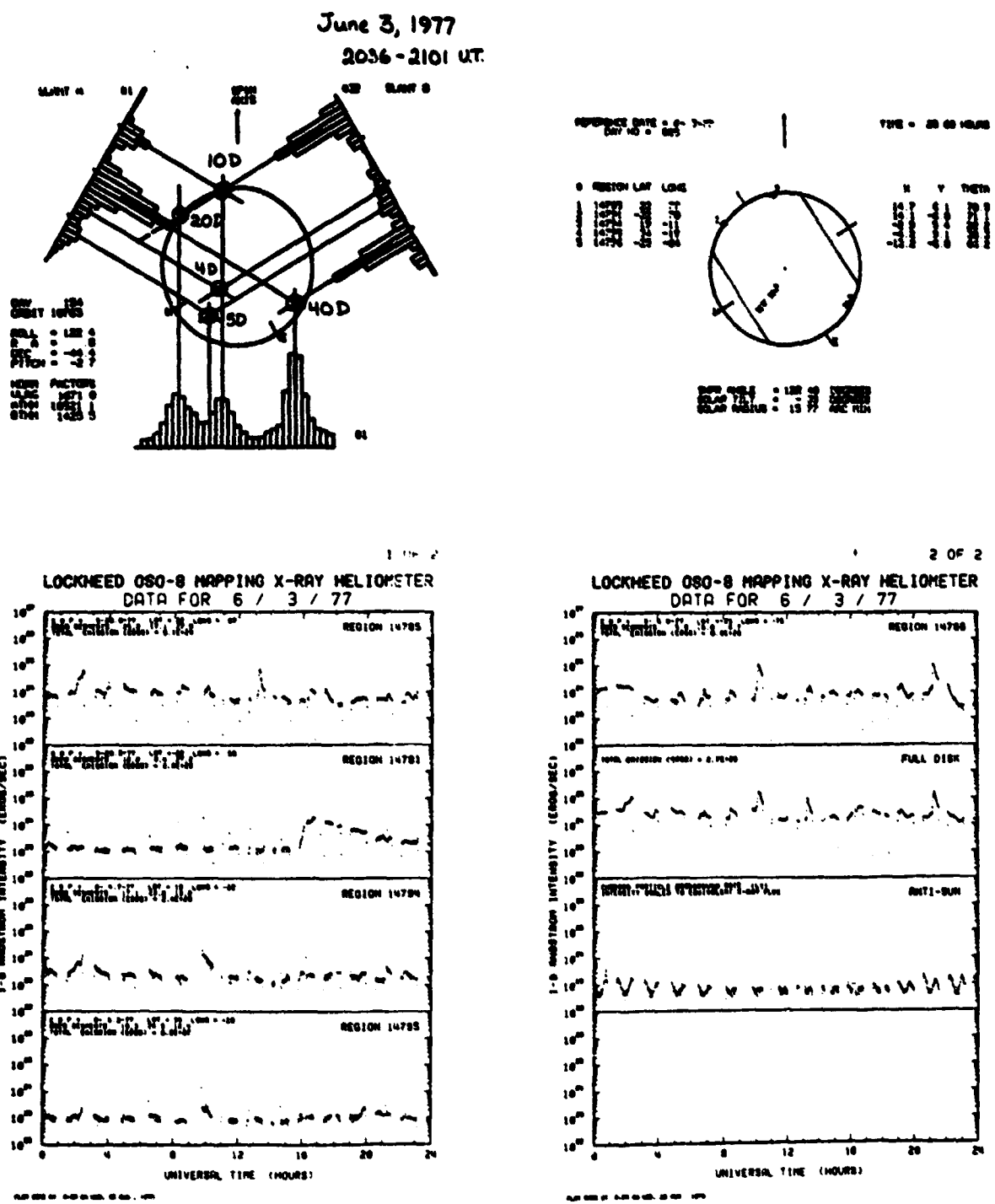


Figure 5.3-2 Sample "page" of daily data plots from the National Space Science Data Center Submission (June 3, 1977).

ORIGINAL PAGE IS
OF POOR QUALITY

5.4 Miscellaneous Distributions of Data

Appendix C gives a rough compilation of the special requests for specific data which were received and accommodated during the period of the current contract. Most of these were from astronomers desiring MXRH-type information to supplement their own observations. Most often, either the spatial distribution of X-ray emission or the behavior of a specific source was required. In both cases, the Lockheed experiment was the only instrument offering such a capability. A number of these requests led to collaborative investigations and publications (see Section 6, and Appendix A).

Not included in the present tabulation are the 11 rocket launches mentioned in the Final Report to the Operations Phase (Wolfson, Acton, and Smith, 1978) for which Lockheed provided real-time support in the choice of launch window and selection of targets.

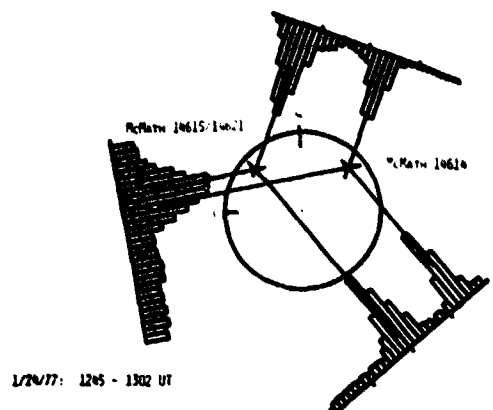
6. PRINCIPAL SCIENTIFIC RESULTS

The scientific results of the Mapping X-Ray Heliometer data analysis program are best described in the various publications which are listed in Appendix A. Copies of twelve of the most important of these have been included as Appendices D through O. The following is a brief summary of the conclusions reached therein. Also mentioned are a few as-yet unpublished results, including the somewhat negative ones from the extra-solar observational program.

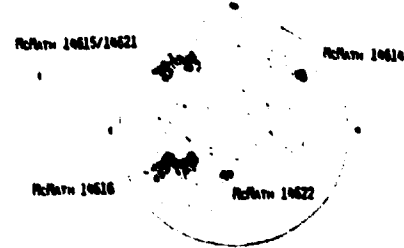
6.1 Evolution of Young Active Regions

By means of its normal observing mode involving frequent scans of the complete solar disk, the Mapping X-Ray Heliometer provided a rather unique opportunity for being able to go backwards in time, to trace the history of each X-ray emission source back to its earliest stages. As a result, a considerable effort has been and continues to be directed towards the study of this aspect of the data set. Preliminary conclusions based on the exhaustive study of one particularly well observed example have been reported in Wolfson, Acton, Leibacher and Roethig (1977, Appendix E). Perhaps the most surprising conclusion of that study was the discovery of the burstiness of the early X-ray emission, which was observed within three hours of the first indication of emerging magnetic flux. Such X-ray burstiness has subsequently also been observed at the birth of numerous other regions, which, on the average, appear to be more "flare"-rich (relative to their strength) in their earliest stages

X-RAY MAP (MXRH)



MT. WILSON MAGNETOGRAM



1/20/77: 1740 - 1923 UT

X-RAY LIGHT CURVES

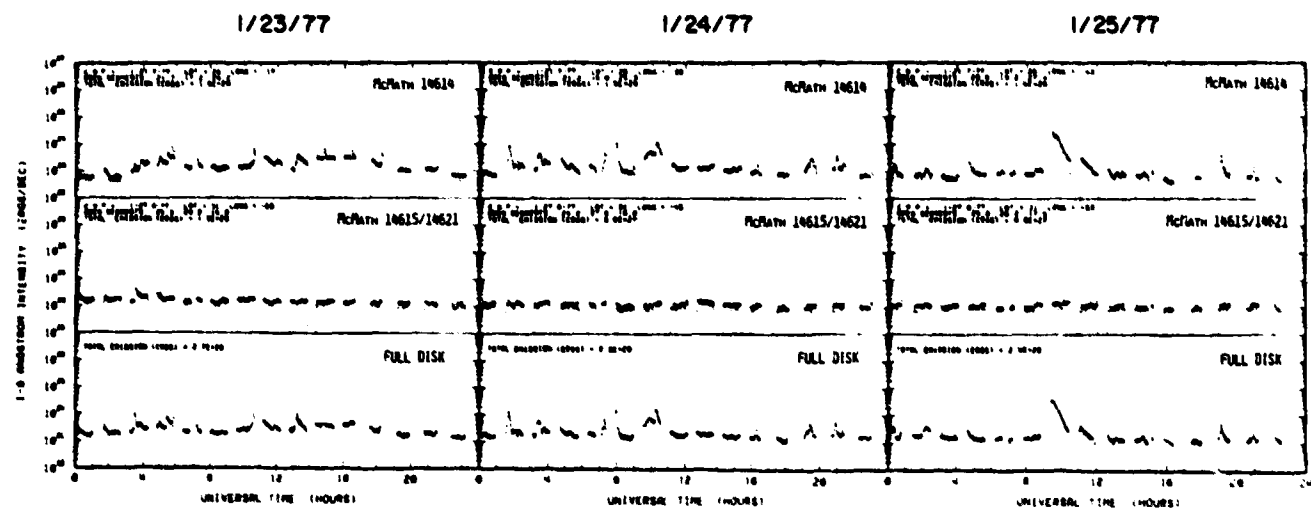


Figure 6.1-1: Light curves demonstrating the difference in flare activity between young (McM 14614) and mature (McM 14615/14621) regions with similar levels of non-flare emission.

than in their later history (see Figure 6.1-1). This strongly suggests that the magnetic configuration of a mature region is not required for the basic flare mechanism, although the increased energy available in that case may permit the events to assume a greater intensity. Another somewhat surprising result of this study was the detection, at least in this one case, of a relatively stable non-flare plasma having a temperature of about 3.5×10^6 °K. This component of the early X-ray emission was seen to grow in intensity through a slow and relatively steady increase in emission measure (i.e., quantity of emitting material), rather than through a change in temperature. The sudden intensity spikes of the flares, on the other hand, were seen as being due to temperature fluctuations at a relatively constant emission measure.

The collaborative study of Avery, Feldman, Gaizauskas, Roy, and Wolfson (1977), in which H-alpha, microwave, and X-ray observations were combined, likewise pointed to the importance of fluctuations in newly emerged regions. The particular event studied in that case is the smallest with which all three emissions are known to have been associated. The limited spatial resolving power of the Mapping X-Ray Heliometer was essential in determining the portion of the disk from which the X-ray emission originated.

6.2 Preflare Phenomena

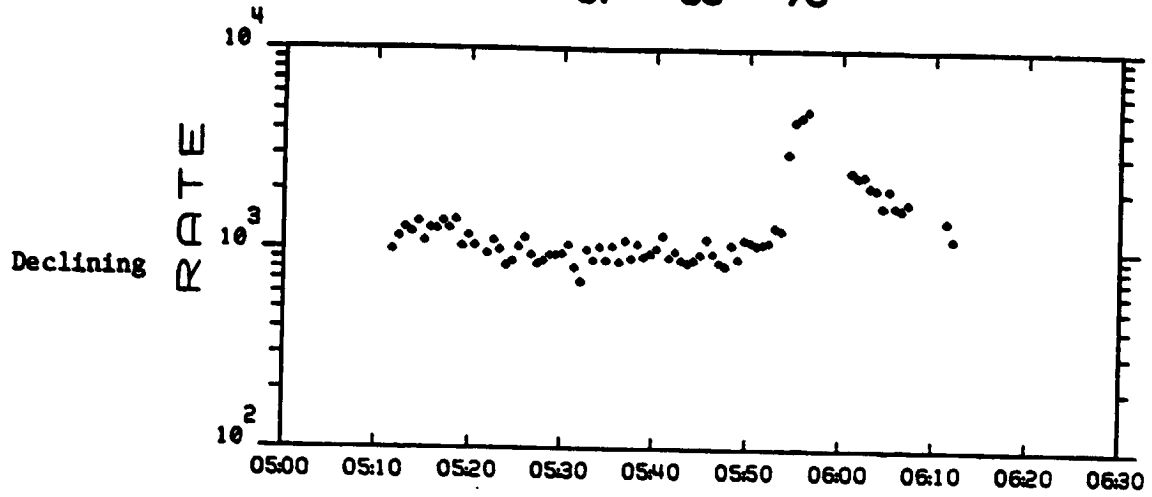
The comprehensive coverage provided by the Mapping X-Ray Heliometer likewise permits flaring regions to be studied before the event. Two important publications were generated in this regard.

The first, that of Wolfson, Acton and Leibacher (1978, Bull. Amer. Astron. Soc. 10, 456), dealt with the possibility of systematic intensity or spectral changes in the immediate preflare period (10-20 minutes). This study concluded that when a single region was isolated, no systematic variation in either temperature or intensity could be detected in the preflare period, and suggested that earlier suggestions of such an effect, based on full disk data, may have been due to confusion with the signals from other regions (see Figure 6.2-1).

The second study, that of Mosher and Acton (1980, Appendix 0), looked in greater detail at the association between X-ray emission and filament activity in the preflare period, but again found nothing of predictive value, at least for the normal small flares in young active regions. In the case of the

ORBITING SOLAR OBSERVATORY - 8
LOCKHEED MAPPING X-RAY HELIOMETER EXPERIMENT

07 - 08 - 75



Steady

Rising

Figure 6.2-1: Three sample light curves from the pre-flare study.

disparition brusque (sudden disappearing filament) type events in decayed regions, the filament eruption was confirmed, as had previously been observed on Skylab, to precede the rise of X-ray emission, which is essentially simultaneous with the H-alpha emission.

6.3 Postflare Relaxation

Flares themselves can be reasonably well studied on the basis of full disk measurements, since at their peaks they generally strongly dominate the X-ray emission from the whole sun. An important effect which appears to have been generally overlooked in the full-disk measurements is the apparent temporary suppression of flare activity in the period immediately following a major event. Wolfson, Acton, Roethig and Walt (1978, Appendix H) interpret this as being due to a general buildup and relaxation of the stressed flare configuration over a time scale of about one day.

6.4 Flare Geometries

Relatively little effort has been directed towards looking for evidence of geometric changes in association with flares, as this aspect of the problem can be better studied by photographic instruments, such as those on Skylab. We do, however, rather commonly detect slight rising motions, on the order of one arc minute, in the decay phase of major events (see Figure 6.8-1). Such motions are consistent with the photographic results (see, for example, Pallavicini *et al.*, 1977). We also see no direct evidence for a significant spatial extent to the emission source at the wavelengths we monitor, but this is again consistent with the photographic results considering our large instrumental width (see also Sec. 6.10).

6.5 Sympathetic Flares

The Mapping X-Ray Heliometer data set is a very reasonable one to investigate for the often-suggested possibility of "sympathetic" flares, that is, situations in which activity in one solar active region triggers activity in a different one. The preliminary studies of Wolfson (unpublished) suggest that "sympathetic" flares are not abnormally common in the OSO-8 data, and therefore not real, but the formulation and application of rigorous statistical tests is surprisingly difficult.

6.6 Spectral Observations

Considerable use has been made of the spectral information provided by the Mapping X-Ray Heliometer's proportional counter detectors, although, as previously noted, it has been possible to study only a very small portion of it in detail. The three most important publications dealing specifically with conclusions based on the spectral data are probably those of Datlowe (1977, Appendix G); Wolfson, Acton, and Datlowe (1978, Appendix K); and the collaborative article by Parkinson et al. (1979, Appendix L).

It had long been known that small flares tend to exhibit relatively low temperatures. Datlowe (1977) showed, however, that if the preflare emission is subtracted, the added portion which lights up during the flare is always found to have a high temperature, even if the event is very small. A threshold of about 10 million degrees Kelvin was found, and is thought to be characteristic of the instability giving rise to the flare.

Wolfson, Acton, and Datlowe (1978) addressed the assertion that the emission measure (i.e., the quantity of X-ray emitting material) decreases at the start of flares, and showed this to also be an artifact arising from trying to treat as a single mass the larger preflare region and the smaller injection of very hot flaring material (which dominates the response of the detectors). If the preflare portion is subtracted, the emission measure of the flare component by itself is always found to increase steeply from its first detectability.

The collaborative article by Parkinson et al. (1979) uses data from both the Mapping X-Ray Heliometer and the Columbia University Spectrometer to establish the origin of the 1.9 \AA feature in the flare spectrum. The MXRH observations permitted that feature to be followed farther into the post-flare period (and therefore to lower intensities) than was possible with the Columbia experiment. This assisted in the identification of the feature as being due to dielectronic recombination of ions in the range Fe XIX - Fe XXII.

Additional conclusions related to spectral observations from the Mapping X-Ray Heliometer were presented by Mosher at the Third Skylab Workshop Series on Energy Balance and Physical Conditions in Active Regions (Orrall, 1980). The temperatures of young active regions were found to provide no reliable indication of their future growth. In addition, the temperature characteristic of growing regions previously reported by Wolfson et al. (Sec.

6.1) was found to depend quite a bit on the choice of detector and energy band. Also discussed was the apparent discrepancy between flare temperatures indicated by the Large and Thin Window detectors -- the ones sensitive to harder X-rays tending to show much higher temperatures and greater intensity variations. It was shown that this implies that the fluctuating component in the flare must be even smaller and hotter than had previously been suspected.

6.7 Statistical Properties of Active Region X-Ray Emission

The articles of Mosher (1980, Appendix M; and 1980, Appendix N) deal in effect with statistical conclusions based on the average behavior of a large number of regions -- a kind of study for which the extensive Mapping X-Ray Heliometer data files are particularly well suited.

The first of these relates the average level of non-flare X-ray emission to the size of the underlying photospheric region as observed in white light. Both the number and area of the sunspots are found to be of about equal importance. The X-ray flux is most predictable if the product of area times count is used as the size parameter

The second interprets the average fall-off of X-ray intensity as a region passes behind the limb, which is related to the height structure of the source. The soft X-ray intensity is shown to increase exponentially down to the lowest observable layers, in contradiction of some earlier beliefs. The median height was found to be 20,000 km. A slight temperature gradient was also discovered, with the lower layers appearing hotter than the higher ones.

6.8 GRF's and Active Filaments

A considerable amount of effort was directed towards the investigation of gradual rise and fall (GRF) and eruptive filament events, only a portion of which has been published (Acton and Mosher, 1978; Appendix I) since it largely duplicates studies done by Skylab (Webb, et al, 1976). Figure 6.8-1 is a typical Mapping X-Ray Heliometer observation of a filament eruption associated limb flare (Mosher and Wolfson, 1978: Bul. Amer. Astron. Soc. 10, 460). The centroid of the X-ray emission is seen to move slightly outward at about 2 km/sec. In Figure 6.8-2, this motion is shown relative to the position of the earlier prominence eruption. The temperatures of such events are found to be relatively low (Figure 6.8-3). Finally, Figure 6.8-4 shows a model of the eruption and reformation of filaments with X-ray emission suggested by the work.

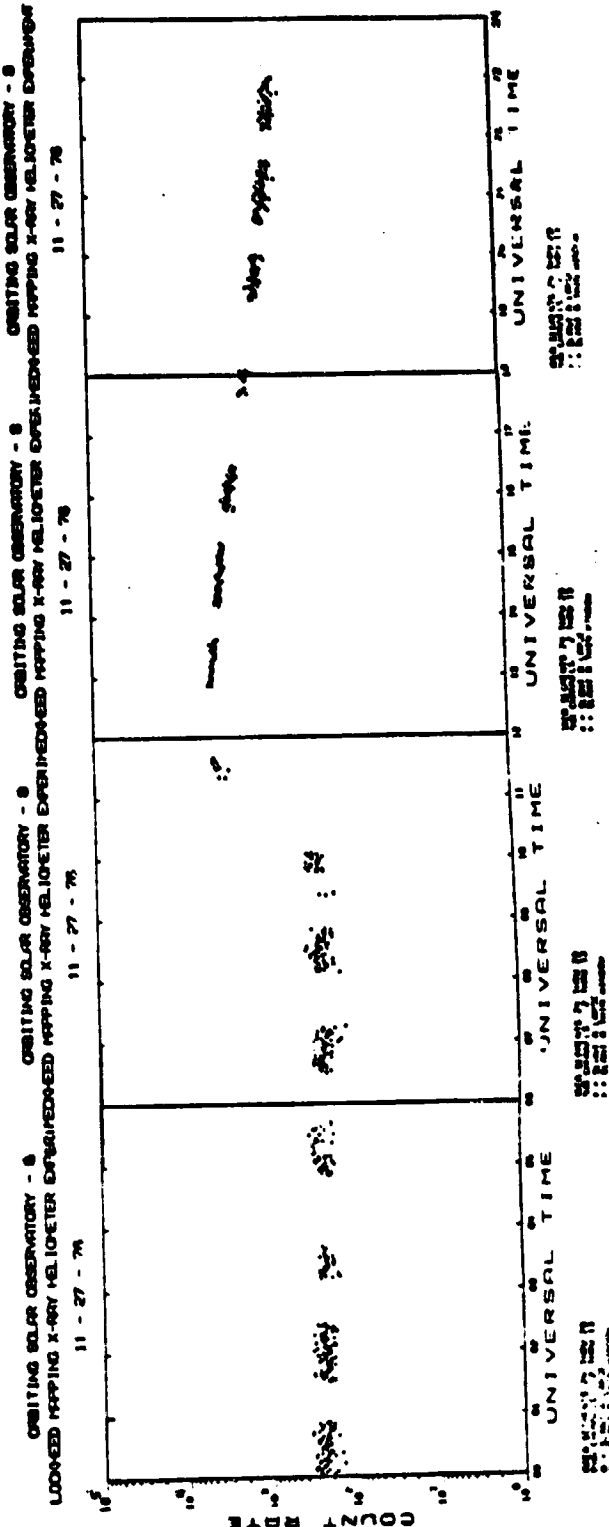
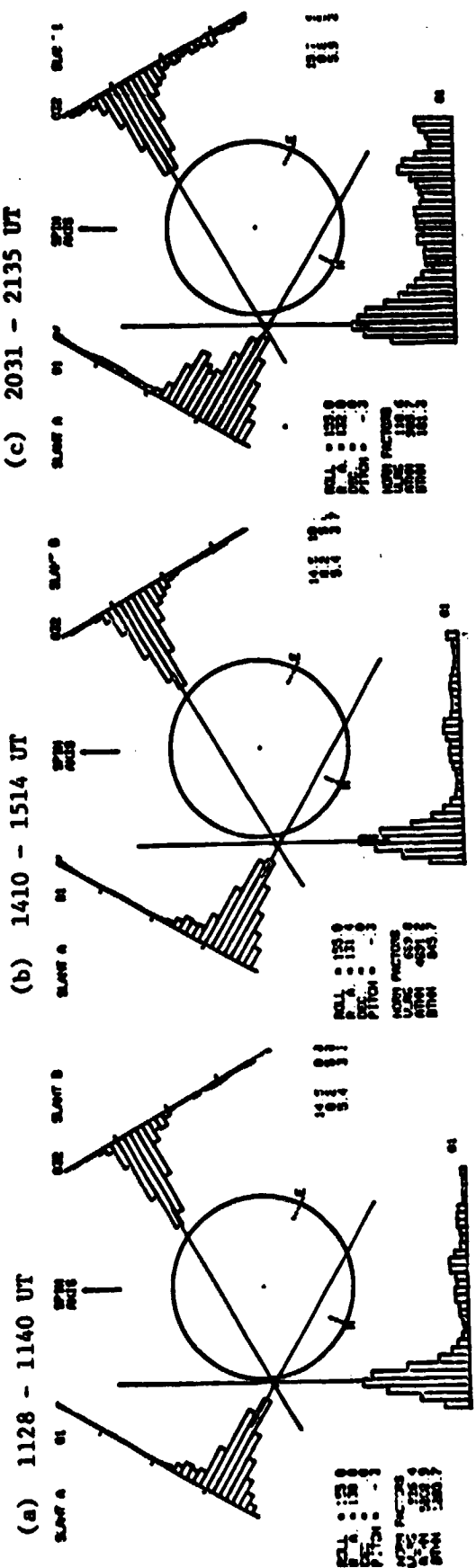


Figure 6.8-1: Maps and light curve of a flare associated with an eruptive prominence.

NOVEMBER 27, 1976

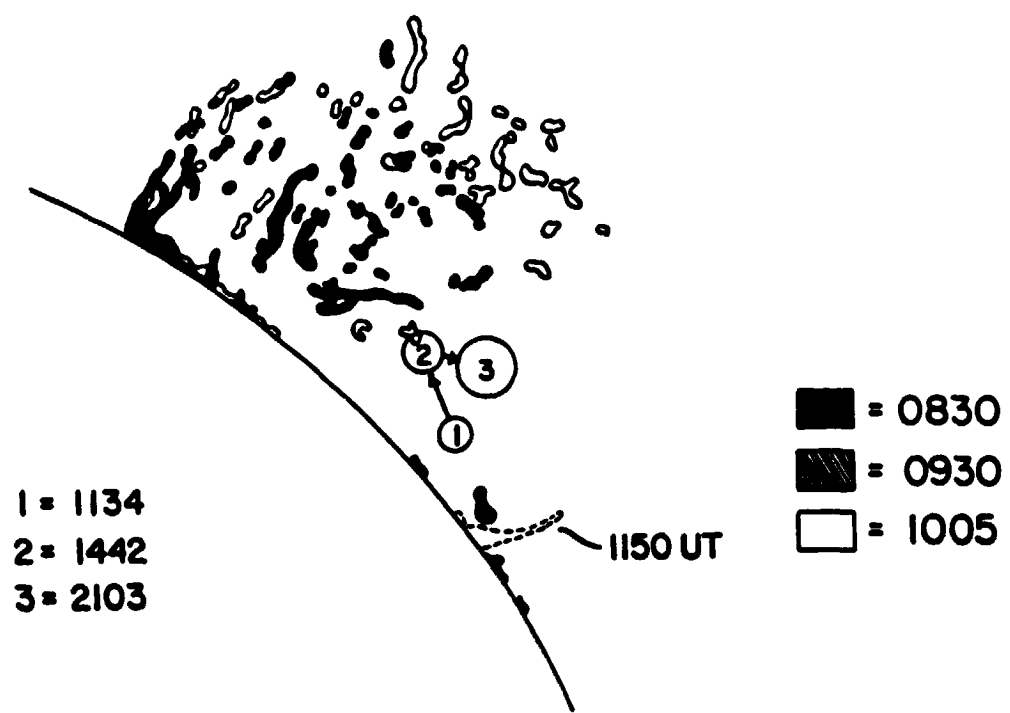
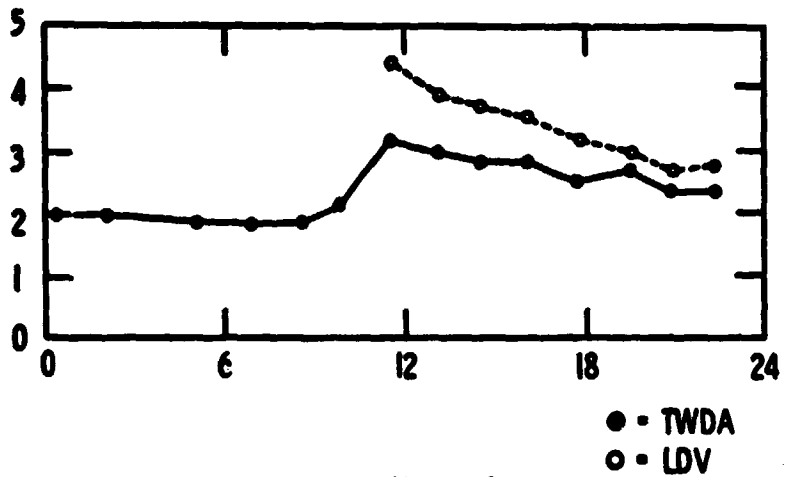


Figure 6.8-2: Location of the X-ray source relative to the earlier prominence eruption.

SPECTRAL OBSERVATIONS OF NOV. 27, 1976 EPL

(a) TEMPERATURE ($10^6 \text{ } ^\circ\text{K}$)



(b) EMISSION MEASURE (10^{48} cm^{-3})

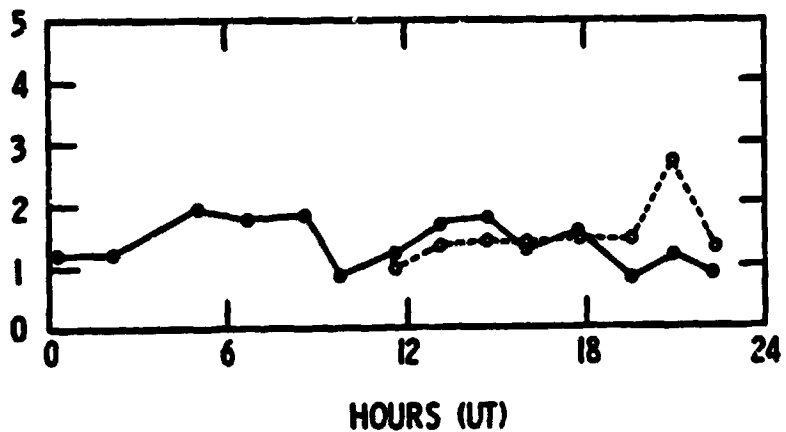


Figure 6.8-3: Interpretation of the event in terms of temperature and emission measure.

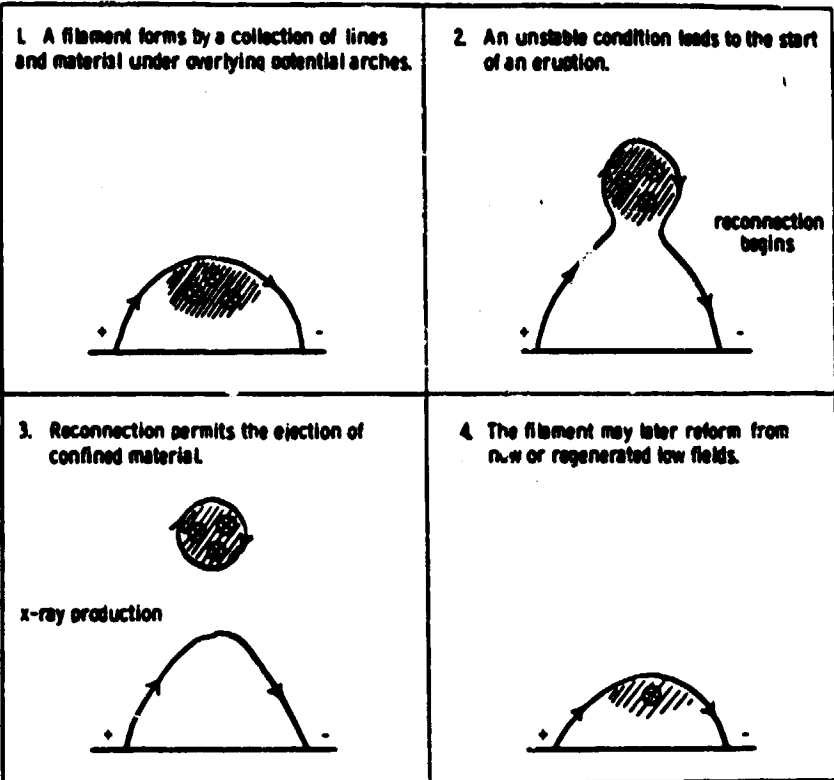
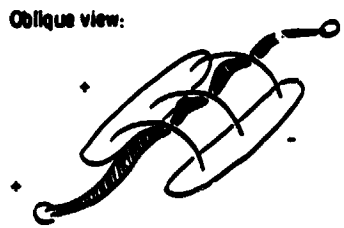


Figure 6.8-4: A possible model of the eruption and subsequent reformation of a filament with X-ray emission at the tops of the magnetic loops.

6.9 Ultraviolet Flashes

The results of a collaborative study with the University of Colorado, involving the comparison of MXRH measurements with simultaneous measurements of transient brightenings in the ultraviolet are described in the final report to Task II (Bruner, 1980). The work is published in Lites, Bruner and Wolfson (1980).

6.10 Eclipses

Partial eclipses of the sun were observed from OSO-8 in April and October of both 1976 and 1977. The variation of intensity with time as a source is covered by the lunar limb can, under favorable circumstances, permit its geometry to be studied with higher spatial resolution than is possible with the detectors alone. The best example was on October 12, 1977, in which case a size of about 2 arc-minutes, which is consistent with photographic results, was deduced (Wolfson, unpublished). The eclipses also provided evidence that the Thin Window A detector (which responds to the softest energies) sees a general haze of X-ray emission covering the disk (possibly from unresolved regions). The other detectors do not see this haze (Mosher, unpublished).

6.11 Radio Bursts

Several radio astronomers expressed interest in the Mapping X-Ray Heliometer observations and their relation to radio burst and interferometric observations. In addition to the collaborative study already mentioned in Section 6.1, that of Stewart, Wolfson, and Lemen (1978) is also notable. In it, the Mapping X-Ray Heliometer observations were used primarily to establish the relatively stationary character of the X-ray source associated with a moving Type IV burst. The X-ray source was found to be inadequate to sustain the radio emission. Marsh, Zirin, and Hurford (1979) similarly used temperatures and emission measures obtained by the MXRH to interpret the mechanism of radio burst emission in three flares. Finally, Benz, Jaeggi, Mosher and Nelson (1980) found a negative result, that is, they were unable to determine a definite relationship between the timing of Type I radio bursts and the behavior of the associated soft X-ray source.

6.12 Observations of Extra-Solar Sources

During nearly one-third of its operational life (i.e., for approximately 30 minutes out of every 90 minute orbit) the OSO-8 spacecraft was unable to observe the sun due to its occultation by the earth. During each of these periods (except during the last months of the experiment when the MXRH was turned off at night to conserve power) the Mapping X-Ray Heliometer was commanded to record and transmit data gathered in the general direction of an extra-solar source of interest and within range of the wheel plane. The MXRH is not well-suited for the observation of these extra-solar sources, which have much harder spectra than the solar active regions, and, not surprisingly, very little use has been made of them. Figure 6.12-1 is a typical map of Sco X-1, the strongest of the extra-solar sources; while Figure 6.12-2 shows the weaker but steadier Crab Nebula. By adding together the results from scans obtained on many night-time passes, it is possible to considerably improve the statistics of the Crab Nebula peak, and the underlying spectrum was used to verify and adjust the calibration of the instrument. Figure 6.12-3 summarizes the results of a brief effort to observe X-rays from Jupiter in November, 1976. Experimenters on OSO-3 had similarly been unable to detect emission from that potentially interesting source (Peterson et al., 1976).

7. NEW TECHNOLOGY

Due to the nature of the work no new technology was developed during the course of this effort.

July 13, 1975
23:13 - 23:33

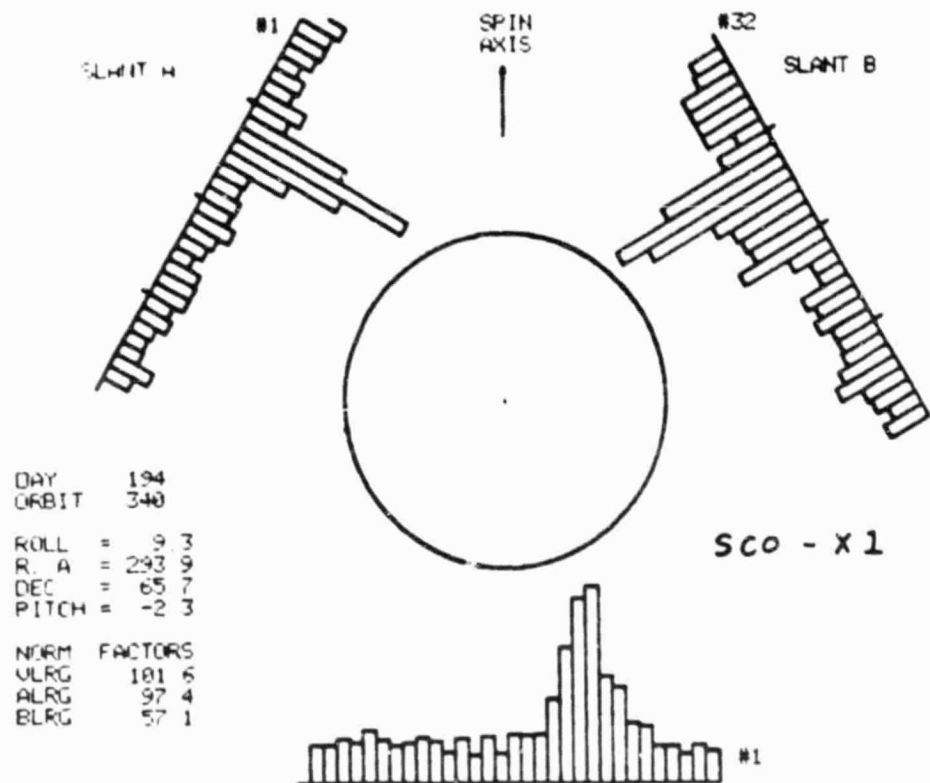


Figure 6.12-1: Map showing Sco X-1 (July 13, 1975; 2313-2333 UT).

(map made on a daytime pass
using COMMANDED NITE mode)

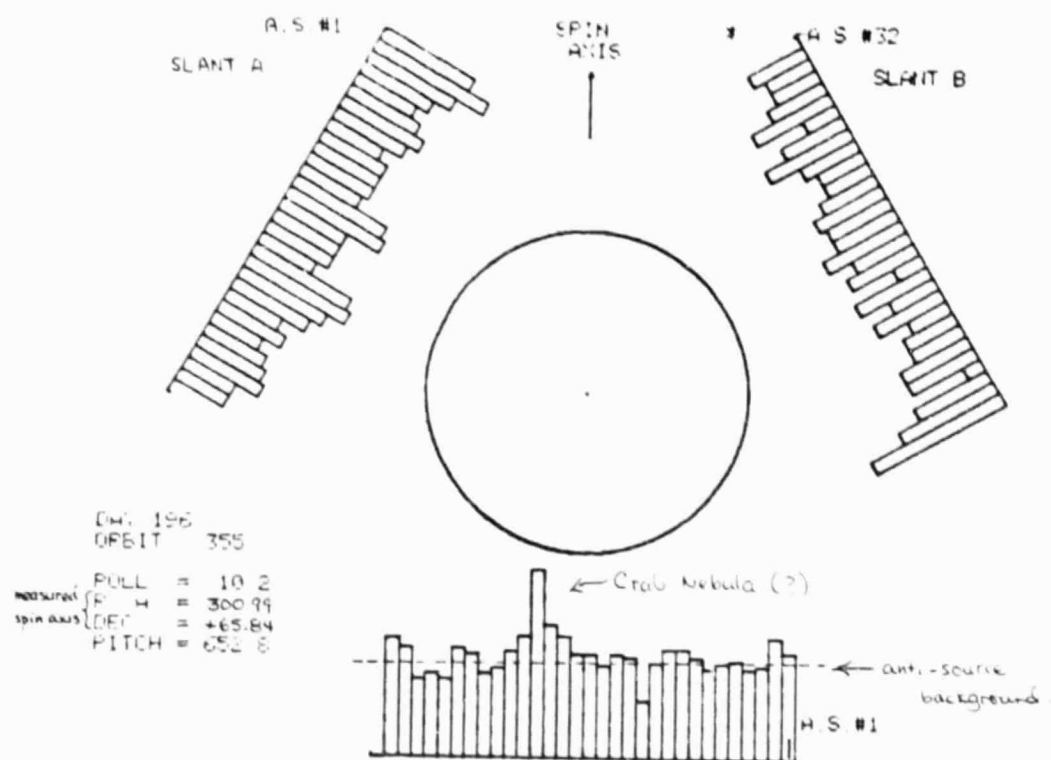


Figure 6.12-2: Map showing the Crab Nebula (July 13, 1975; 2313-2333 UT).

JUPITER
Nite

ROS 7808
Nov. 19, 1976
22:17 - 23:12
Z

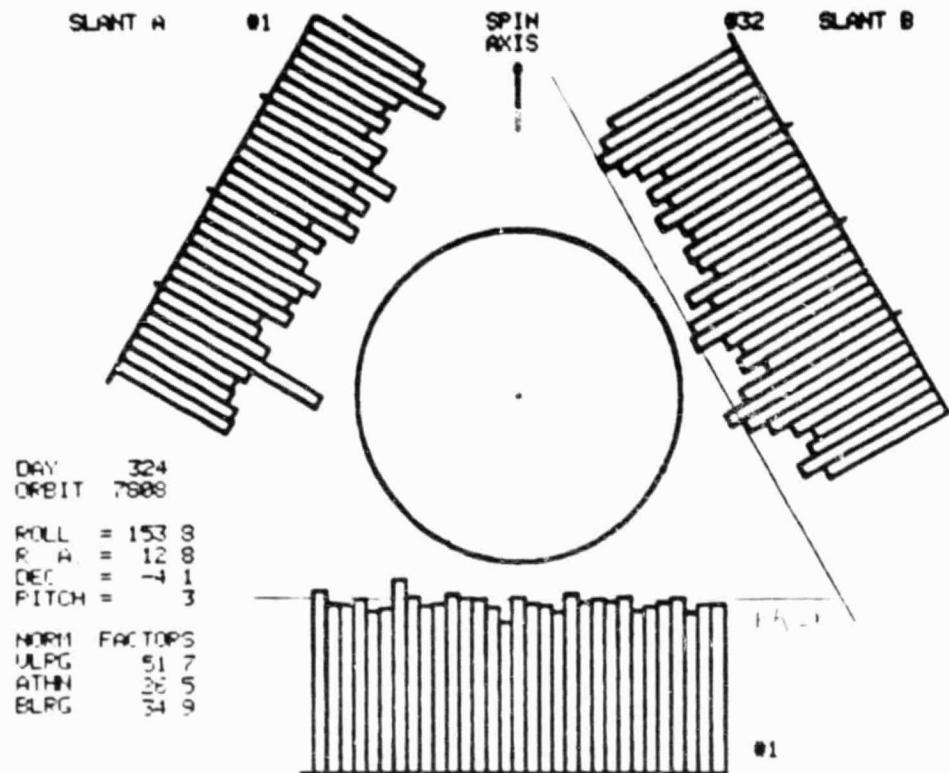


Figure 6.12-3: Map made looking in the direction of Jupiter (November 19, 1976; 2217-2312 UT).

Appendix A

PUBLICATIONS AND PRESENTATIONS OF THE
LOCKHEED OSO-8 DATA ANALYSIS PROGRAM
(Chronological Order)

I. Major Publications of Scientific Results from the MXRH Program

Smith, K.L., Acton, L.W., Mosher, J.M., and Wolfson, C.J. (July, 1975 - September, 1978): "Daily Solar X-Ray Maps," Solar-Geophysical Data Prompt Reports.

Wolfson, C.J., Acton, L.W., Roethig, D.T., and Smith, K.L. (1977): "2-30 keV X-Ray Data from OSO-8," in Collected Data Reports for STIP Interval II, (UAG Report 61, Coffey and McKinnon, eds.), 187.

Wolfson, C.J., Acton, L.W., Leibacher, J.W. and Roethig, D.T. (1977): "Early Evolution of an X-Ray Emitting Solar Active Region," Solar Physics, 55, 181.

Wolfson, C.J., Acton, L.W., Roethig, D.T. and Walt, M. (1978): "Evolution of the X-Ray Emitting Corona Preceding and After Major Solar Events," in Shea, Smart, and Wu, eds., Contributed Papers to the Study of Travelling Interplanetary Phenomena/1977. (Proceedings of COSPAR Symposium B, AFGL-TR-77-0307), 295.

Acton, L.W. and Mosher, J.M. (1978): "X-Ray Emission Associated with Filament Activity," in Physics of Solar Prominences (I.A.U. Colloquium #44, Jensen, Maltby and Orrall, eds.), 269.

Wolfson, C.J., Acton, L.W. and Datlowe, D.W. (1978): "Does the Emission Measure Decrease During the Start of a Soft X-Ray Flare?," Solar Physics, 59, 373.

Mosher, J.M. (1979): "The Height Structure of Solar Active Regions at X-Ray Wavelengths as Deduced from OSO-8 Limb Crossing Observations," Solar Physics, 64, 109.

Mosher, J.M. (1980): "Predictions of Solar X-Ray Fluxes Based on Sunspot Structure," in Solar-Terrestrial Predictions Proceedings, Vol. III: Solar Activity Predictions, R.F. Donnelly, ed., (U.S. Dept. of Commerce - NOAA), C159.

Mosher, J.M. and Acton, L.W. (1980): "X-Rays, Filament Activity, and Flare Prediction," Solar Physics, 66, 105.

II. Additional Publications Incorporating Results from the MXRH Program
(Partial Listing)

Avery, L.W., Feldman, P.A., Gaizauskas, V., Roy, J.R., and Wolfson, C.J. (1977): "A Search for Microwave Emission from Solar X-Ray Bright Point Flares," Astron. and Astrophysics, 56, 327.

Lites, B.W. and Hansen, E.R. (1977): "Ultraviolet Brightenings in Active Regions as Observed from OSO-8," Solar Physics, 55, 347.

Shea, M.A., Smart, D.F., and Coffey, H.E. (1977): "A Summary of Significant Solar-Initiated Events During STIP Intervals I and II," in Shea, Smart, and Wu, eds., Study of Travelling Interplanetary Phenomena/1977, 393.

Marsh, K.A., Zirin, H., and Hurford, G.J. (1979): "VLA Observations of Solar Flares, Interpreted with Optical, X-Ray and Other Microwave Data," Astrophys. J., 228, 610.

Parkinson, J.H., Veck, N.J., Ashfield, M.E.C., Culhane, J.L., Ku, W.H.-M., Lemen, J.R., Novick, R., Acton, L.W., and Wolfson, C.J. (1979): "An Investigation of the 1.9 \AA Feature in Solar Flare X-Ray Spectra," Astrophys. J., 231, 551.

Lites, B.W., Bruner, E.C. Jr., and Wolfson, C.J. (1980): "OSO-8 Observations of the Impulsive Phase of Solar Flares in the Transition Zone and Corona," Solar Physics, (in press).

III. Brief Presentations and Reports

Wolfson, C.J., "Recent Observations from the Lockheed X-Ray Experiment on OSO-8," presented at the Southern California Solar Neighborhood Meeting, 16 January 1976. No published abstract.

Wolfson, C.J., Acton, L.W., Newkirk, L.L., Roethig, D.T., and Smith, K.L., "X-Ray Bursts from a Young Active Region (McMath 13811) During August 19-22, 1975," presented at the U.S.-Japan Cooperative Seminar on High Energy Phenomena in Solar Flares, 10-13 May 1976. Extended Abstract published in Seminar Proceedings.

Avery, L., Feldman, P.A., Gaizauskas, V., Roy, J.-R., and Wolfson, C.J., "Search for Solar X-Ray Bright Points at Radio, Optical and X-Ray Wavelengths," presented at the Canadian Association of Astronomy, meeting, 16 June 1976. Abstract and paper published.

Wolfson, C.J., Acton, L.W., Newkirk, L.L., Roethig, D.T., and Smith, K.L., "The Early Evolution of X-Ray Producing Active Regions," presented at the American Astronomical Society Meeting, 22-25 June 1976. Abstract: Bull. Am. Astron. Soc., 8, 317.

Catura, R.C., Acton, L.W. and Wolfson, C.J., "Highlights of the First Year of Operation of the Lockheed OSO-8 Instrument," presented at the IAU Sixteenth General Assembly, 31 August 1976. No published abstract.

Datlowe, D.W., Participant in the Second Skylab Solar Workshop ("Solar Flare"), 1976, 1977. Contributions incorporated in the proceedings.

Ishiguro, M., "OSO-8 Mapping X-Ray Heliometer Image Forming," presented at the Symposium on Image Forming and Intensity Measurements, Spring, 1977.

Datlowe, D.W., "OSO-8 Solar X-Ray Bursts" presented at the Southern California Solar Neighborhood Meeting, 15 April, 1977.

Datlowe, D.W., "OSO-8 Solar X-Ray Burst Observations," presented at the American Astronomical Society Meeting, 12-15 June, 1977. Abstract: Bull. Am. Astron. Soc., 9, 298.

Wolfson, C.J., Acton, L.W., and Roethig, D.T., "Evolution of the X-Ray Emitting Corona Preceding and After Major Solar Events," presented at the L.D. DeFeiter Memorial Symposium on Study of Travelling Interplanetary Phenomena (part of XX th COSPAR Meeting), 7-11 June, 1977. Abstract and paper published.

Mosher, J.M., "The Height Structure of X-Ray Active Regions from OSO-8 Limb Crossing Observations," presented at the Southern California Solar Neighborhood Meeting, 18 July 1977.

Datlowe, D.W., "Does the Instability which Produces the Soft X-Ray Flare Plasma Require a Minimum Temperature?," presented at the Southern California Solar Neighborhood Meeting, October 1977.

Bruner, E.C., Jr., Lites, B.W. and Datlowe, D.W., "Mass Motions in Impulsive Flare-Like Brightenings as Observed by OSO-8," presented at the OSO-8 Workshop, 7-10 November 1977. Paper published in Proceedings, pp. 218-243.

Datlowe, D.W., "OSO-8 Observations of the Soft X-Ray Continuum in Solar Flares", presented at the OSO-8 Workshop, 7-10 November 1977. Summary published in Proceedings, pp. 277-278.

Mosher, J.M., "The Height of the X-Ray Emitting Plasma," presented at the OSO-8 Workshop, 7-10 November 1977. Paper published in Proceedings, pp. 123-133.

Mosher, J.M. and Wolfson, C.J., "Observations of a Moving X-Ray Source Associated with an Eruptive Prominence at the Limb," presented at the American

Astronomical Society Meeting, 26-28 June 1978. Abstract: Bull. Amer. Astron. Soc., 10, 460.

Wolfson, C.J., Acton, L.W., and Leibacher,, J.W., "Soft X-Ray Observations During the Preflare Phase of the Solar Flare Phenomenon," presented at the American Astronomical Society Meeting, 26-28 June 1978. Abstract: Bull. Amer. Astron. Soc., 10, 456.

Mosher, J.M., Participant in the Third Skylab Solar Workshop ("Energy Balance and Physical Conditions in Active Regions"), 1978, 1979. Contributions incorporated in the proceedings.

Acton, L.W., and Mosher, J.M., "X-Ray Emission Associated with Filament Activity," presented at IAU Colloquium #44, 14-18 August 1978. Presentation published in Proceedings.

Stewart, R.T., Wolfson, C.J., and Lemen, J.R., "Evidence from X-Ray and Radio Observations for Electron Acceleration in the Source Region of a Moving Type IV Solar Radio Burst," presented at the IAU Asian-South Pacific Regional Meeting 5-8 December 1978. Extended abstract published in the proceedings.

Mosher, J.M., Acton, L.W., Wolfson, C.J., "Reduced Solar X-Ray Data from OSO-8," presented at the American Astronomical Society Meeting, 13-18 January 1980. Abstract: Bull. Amer. Astron. Soc., 11, 710.

Benz, A.O., Jaeggi, M., Mosher, J., and Nelson, G.J., "On the Spatial and Temporal Correlation of Type I Bursts with Soft X-Rays," presented at the Workshop on Radio Noise Storms, March, 1980. Paper published in the proceedings.

Appendix B

ADDITIONAL COLLABORATORS IN THE DATA ANALYSIS PROGRAM

In addition to the persons given as authors of the present report, the following made important contributions to the program of analysis of Mapping X-Ray Heliometer data for which this is partial acknowledgement:

Consultants

J.L. Culhane
J.W. Leibacher
L.L. Newkirk

Student Assistants*

C. Bednar
G. Bruner
M. Damron
P. Damron
T. Farrand
R. Jong
N. Lin

* (Affiliated with the Exploratory Experiences Program of the Palo Alto Unified School District, Palo Alto, California).

Appendix C

TABULATION OF REQUESTS FOR LOCKHEED X-RAY DATA

The following is a partial listing of requests for specialized Mapping X-Ray Heliometer Data sets which were received and honored during the contract period. It gives the name and affiliation of the person making the request and specific area of his or her investigation:

G. Artzner and A. Jouchoux (Laboratoire de Physique Stellaire et Planetaire, Paris): Ultraviolet observations of flares.

M.E.C. Ashfield (Mullard Space Science Lab, University College, London): Comparison of MXRH and Columbia X-Ray Data from OSO-8, resulting in a collaborative publication (Appendix L).

L.W. Avery, J.R. Roy, and P.A. Feldman (Herzberg Institute, National Research Council of Canada): Search for microwave and X-ray emission from bright point flares, resulting in a collaborative publication (Appendix F).

A.O. Benz (Radio Astronomy Group, ETH, Zurich): Type I radio bursts, leading to a collaborative publication in progress.

R.C. Canfield (Sacramento Peak Observatory, University of California at San Diego): Bright point flares.

I.J.D. Craig and A.N. McClymont (University of Glasgow): Testing of dynamic, multithermal flare models.

J.P. Delaboudiniere (Laboratoire de Physique Stellaire et Planetaire, Paris): Support data for ultraviolet observations made by the D2B satellite.

J.E. Evans (Lockheed): Spectrum of ionizing radiation incident on the earth's atmosphere during solar flares.

V. Gaizauskas (Herzberg Institute, National Research Council of Canada): Oscillating microwave sources.

D. Gurnett (University of Iowa): Stereoscopic radio measurements.

E.R. Hansen and B.W. Lites (Laboratory for Atmospheric and Space Physics, University of Colorado): Sudden ultraviolet brightenings. A collaborative article is given in the Final Report for Task II.

E. Hiei (Tokoyo Astronomical Observatory): Limb flares.

G. Hurford, K. Marsh, and H. Zirin (Hale Observatories, Owens Valley Radio Observatory, Caltech): Support of VLA radio interferometric observations and interpretation of 10 GHz bursts. Results published.

- M. Ishiguro (Toyokawa Radio Observatory, Research Institute for Atmospheric Sciences, Nagoya, Japan): Image formation and deconvolution.
- S.R. Kane (University of California, Berkeley): Correlations with hard X-ray burst observations.
- P. Kaufman (CRAAM, Brazil): Statistical comparison of radio and X-ray time sequences.
- A.S. Krieger (American Science and Engineering): Support of rocket solar X-ray data with MXRH light curves.
- W.H.-M. Ku (Columbia University): Support data for Columbia X-Ray Spectrometer observations
- B.J. LaBonte (Big Bear Solar Observatory, Caltech): Search for ephemeral regions in X-rays.
- P.S. McIntosh (NOAA Space Environment Research Lab, Boulder): Slow X-ray events, disappearing filaments, and flare prediction.
- J.H. Parkinson (Columbia University & Mullard Space Science Lab): Temperature and emission measure changes during flares.
- E. Schmal (University of Maryland): VLA microwave observations.
- P.R. Sengupta (Pennsylvania State University): Models of Oxygen V in the earth's atmosphere.
- D.S. Spicer (Naval Research Lab, Washington): Flare spectra.
- R.T. Stewart (Division of Radio Physics, CSIRO, Australia): Moving Type IV radio bursts, leading to a collaborative publication in progress.
- R.G. Teske (University of Michigan): Early evolution of active regions.
- J.C. Vial (Laboratoire de Physique Stellaire et Planetaire, Paris): Ultraviolet observations of eruptive prominences.
- M. Weisskopf and K. Long (Marshall Space Flight Center and Columbia University): Support of extra-solar X-ray observations.
- H. Wiehl (University of Berne): Radio flare observations.

2-30 KEV X-RAY DATA FROM OSO-8

C.J. Wolfson, L.W. Acton, D.T. Roethig
and K.L. Smith

Reprinted from Coffey and McKinnon, eds.

Collected Data Reports for STIP Interval II
(UAG Report 61) (1977),
pp. 187-194

2-30 keV X-Ray Data From OSO-8

by

C. J. Wolfson, L. W. Acton, D. T. Roethig, and K. L. Smith
Lockheed Palo Alto Research Laboratory
Palo Alto, California 94304 U.S.A.

Introduction

This report presents key examples of data obtained during the STIP Interval II from the Lockheed Mapping X-ray Heliometer (MXRH) instrument on the NASA Orbiting Solar Observatory-8 (OSO-8) satellite. The MXRH responds to solar X-rays in the 1.5-30 keV energy range and has a spatial resolution of about 2 min of arc. Investigators are invited to contact the Lockheed group for additional MXRH data for this or other periods. The MXRH became operational 24 June 1975. Daily Daily MXRH maps of the sun have been published in *Solar-Geophysical Data - Prompt Reports* since August 1975.

Instrument Description

The MXRH looks radially outward from the rotating wheel of the OSO-8 satellite. It contains three detection systems, each collimated in one dimension with Oda-type mechanical collimators [Bradt et al., 1968; Oda, 1965]. The collimators have a FWHM of 2.0 arc min, although other instrumental effects broaden the instrument response function to about 4 arc min under some conditions. Each field of view is tilted 120° from the others. These systems are called Vertical, Slant A, and Slant B, with the Vertical system field of view parallel to the satellite spin axis. As the wheel rotation sweeps these fields of view past the sun, one obtains three one-dimensional distributions which can be unfolded to locate and isolate emitting X-ray regions. Each spatial distribution consists of 31 successive strips, or Area Segments, parallel with a system's field of view. Examples of these distributions are shown in Figures 3, 5 and 8. The wheel rotates at approximately 6 revolutions per min and, under normal operation, 4 revolutions are required to form a complete set of three distributions.

The instrument includes different types of proportional counter detectors which combine to provide spectral information from approximately 1.5 to 30 keV. The lower value is established by the thinnest Be window (75 μ m) and the practical upper value is determined by the solar spectrum - a limit often much lower than 30 keV. Spectral information is obtained by analyzing the proportional counter signals with 15-channel pulse height analyzers.

Medium sensitivity detectors (called Large Detectors) are situated behind each of the three collimated systems along with detectors of other sensitivities: a more sensitive detector is Thin Window Detector-B (TWD-B) in the Slant B system, the most sensitive detector is TWD-A, and the least sensitive detector is Vertical Small. Switching between pairs of these detectors provides a dynamic range of $>10^3$. For example, in Figure 4 there is an automatic switch from Vertical Large to Vertical Small Detector on the rise of the X-ray burst near 2245 UT and a switch back on the decay. Since the Vertical Small Detector has less detection area and a different spectral response than Vertical Large, both the amplitude (by a factor of from 4-12) and profile of the light curve change when the detectors switch.

Effective areas as a function of energy for three of the detectors are shown in Figure 1. The observation time for a point source is about 0.02 s per solar scan because the data are integrated over 27 of the collimator fan beams. Details of the instrument, its subsystems, and its operational modes are given in the Technical Manual for the Mapping X-ray Heliometer instrument on OSO-8 [Wolfson, Acton, and Gilbreth, 1975].

General Observations

The active region selected by the MONSEE Steering Committee for study under STIP Interval II was observed by the MXRH instrument for four solar rotations. X-rays from this region were first detected early on 6 March at approximately S05 W40, and the region continued to emit detectable X-rays until it was significantly behind the west limb on 11 March. The plage was named McMath 14118 during this rotation.

For both rotations 2 and 3, which occurred during the specified STIP interval, the region (first designated McMath 14143 and then 14179) was continuously emitting relatively intense X-radiation. Specific observations during these two rotations will be presented in the next section. Rotation 4 (McMath 14215) began in X-rays on 17 May with the last significant X-ray flux observed on 23 May when the region was near disk center. Calcium plage was reported until the region rotated over the west limb. There was no rotation 5 in X-rays or calcium plage.

It is impractical to present all of the MXRH data for the two disk transits included in STIP Interval II. Instead, a synopsis of the available data is presented in Figure 2 (the gaps principally result from periods when the satellite was behind the earth or in the South Atlantic Anomaly radiation belt). We will be happy to provide data on particular periods to anyone requesting it. Data near the events specifically

listed in MONSEE Bulletin No. 8 are discussed in the following section and are representative of the MXRH data.

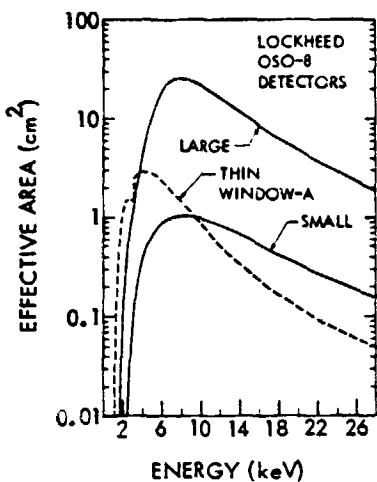


Fig. 1. Calculated effective areas of MXRH detection systems as a function of energy for normally incident photons.

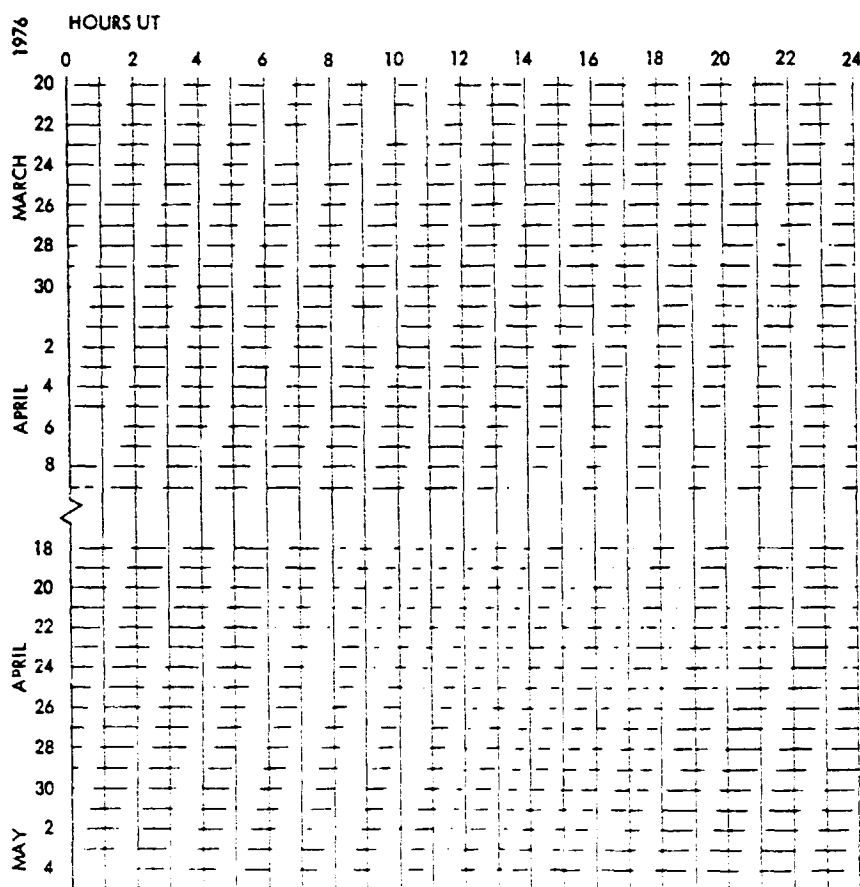


Fig. 2. A chart indicating the times of MXRH X-ray data during the intervals 20 May - 9 April and 18 April - 5 May 1976 when McMath Regions 14143 and 14179 were observable.

Specific Observations

A. 20 March

Type II radio bursts at the east limb were reported by Culgoora at 0205 and 2257 UT. A possible source was McMath 14143 which was approximately $54-43^\circ$ behind the east limb. Figure 3 shows the X-ray sun for both of these times and shows no X-ray emission at the east limb for either time. A modest X-ray emitting region (McMath 14127) is located at approximately N07 W15

To observe the temporal behavior of a particular region, a spatial Area Segment from a system in which the emitting X-ray region is not confused by other regions is selected and the count rate versus time is plotted. Light curves such as these for McMath 14127 during the two periods of interest are shown in Figure 4 where the 18th Area Segment of the vertical system is used. During these time periods, McMath 14127 was undergoing moderate activity which to a full disk monitor might be mistakenly associated with the east limb radio events. However, during these intervals, no east limb activity was observed in excess of the background rate of 15-120 counts/s.

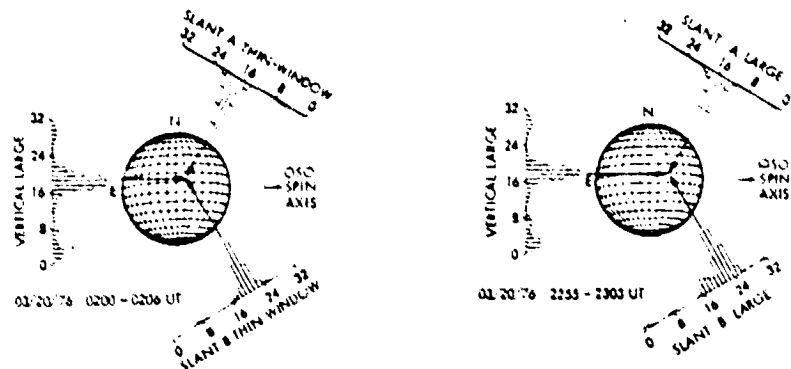


Fig. 3. The X-ray sun for the times when Type II radio bursts were observed at the east limb. Data are collected and displayed in terms of the 32 numbered Area Segments, 1.3 arc min in width. Each histogram is normalized to the peak intensity for that detection system. The arrows converge on the position of McMath 14127.

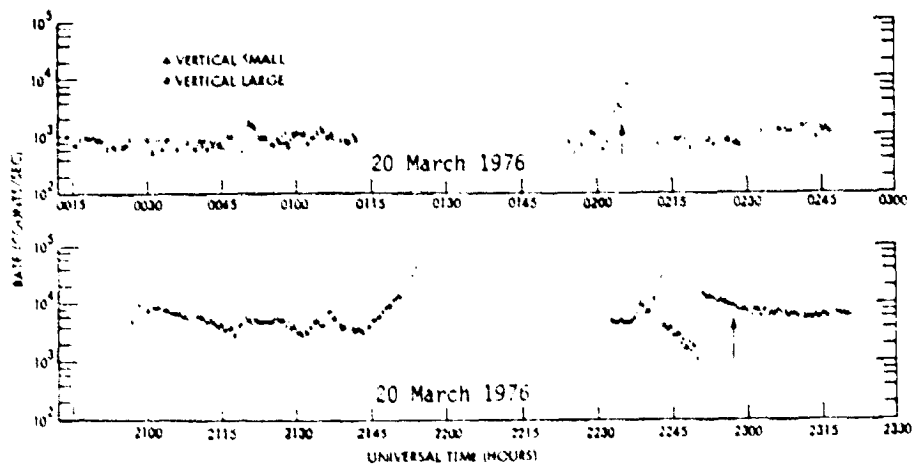


Fig. 4. Light curves of the X-ray emission from McMath 14127. The arrows at 0205 and 2257 UT mark the observations of the Type II radio events at the east limb. Automatic switching between the Vertical Large Detector and the less sensitive Small Detector occurs at 2241 and 2248 UT.

B. 23 March

The MONSEE Committee selected the period from 0840 to 1900 UT based on reported full disk X-ray enhancement, H_α loops at the east limb (1100 UT), and a Type IV radio burst at 0842 UT. McMath 14143, slightly behind the east limb, was judged the probable source. Although McMath 14127 continued to dominate the X-ray disk on the 22nd, significant X-ray emission from the east limb was observed by the MXRH instrument by mid-day; the map in Figure 5 is typical. A strong east limb X-ray burst occurred between 0404 and 0450 UT on the 23rd (a period missed due to orbit night and the South Atlantic Anomaly), making McMath 14143 the major source by 0450 UT. A spacecraft malfunction caused loss of data between 0601 and 0927 UT. By the time the malfunction was corrected, the region was in the decay phase of a large burst which peaked at about 0850 UT in the GOES-1 X-ray data. Figure 6 shows more than 10 hours of this smooth decay. Source characteristics determined by fitting the observed pulse height spectrum at 0950 UT to that expected from an isothermal plasma as described by Tucker and Koren [1971] were temperature = 10×10^6 K and emission measure = $2 \times 10^{49} \text{ cm}^{-3}$. This implies a 1 - 8 Å flux of 0.02 ergs/cm²s and a 0.5 - 4 Å flux of 0.002 ergs/cm²s.

McMath 14127 was easily observable throughout this decay period but, although three optical flares were observed, it was never the dominant source. Its maximum contribution was at 1647 UT when it emitted 25% of the full disk X-ray flux. By 2115 UT, McMath 14127 and McMath 14143 had approximately equal intensities.

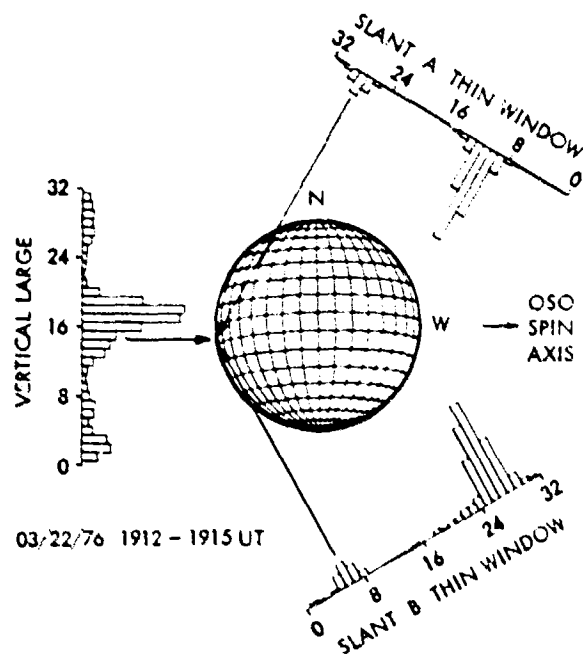


Fig. 5. The typical X-ray sun during the latter part of 22 March. Although McMath 14143 is about 20 degrees behind the east limb, the X-ray emitting plasma is high enough to produce a significant unocculted flux. The arrows indicate the position of this emission.

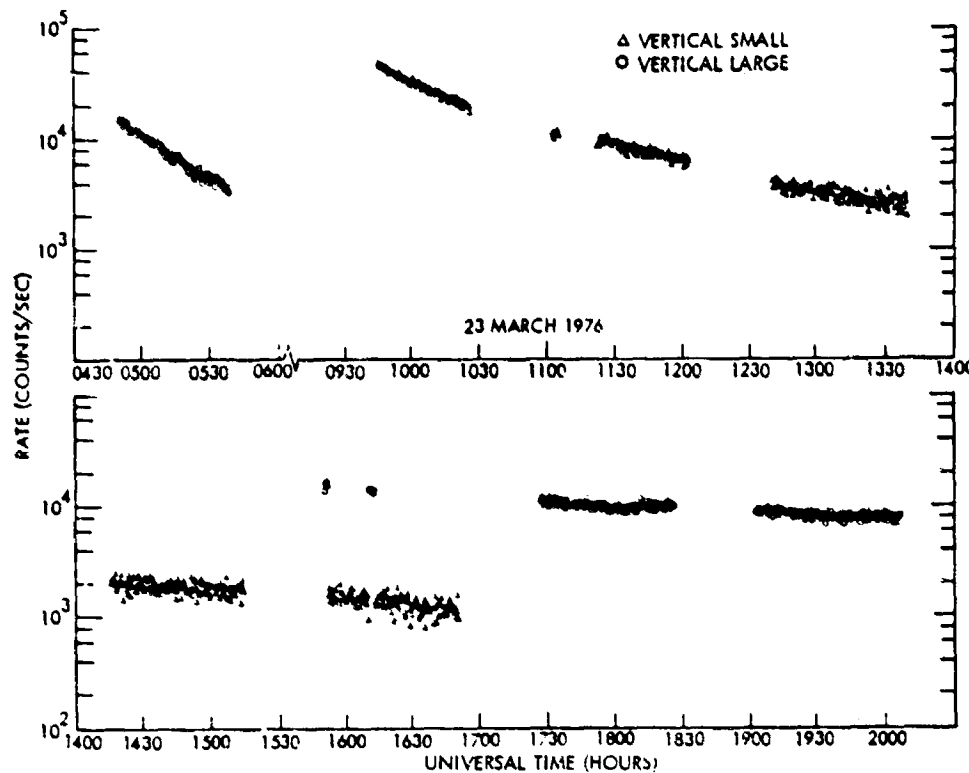


Fig. 6. X-ray light curve of McMath 14143 including 10 hours of the decay from an intense burst which occurred about 0900 UT on 23 March. The large data gap (0600 - 0930 UT) is a result of a spacecraft malfunction.

C. 28 March

Many H_α flares and radio bursts were reported from McMath 14143 between 1840 and 2400 UT. McMath 14127 had by then rotated behind the limb and was undetectable in X-rays while McMath 14146, McMath 14147, and McMath 14143 were on the disk and emitting detectable signals. McMath 14143 was dominant throughout this period. The intensity prior to the large event around 1840 UT was gradually decreasing with many superimposed enhancements (Figure 7). Several of these enhancements appear to be the sum of two or more bursts. For example, the event at 1840 UT seems to be the sum of a burst having a fast rise and a fast decay with a burst having a slow rise and a slow decay.

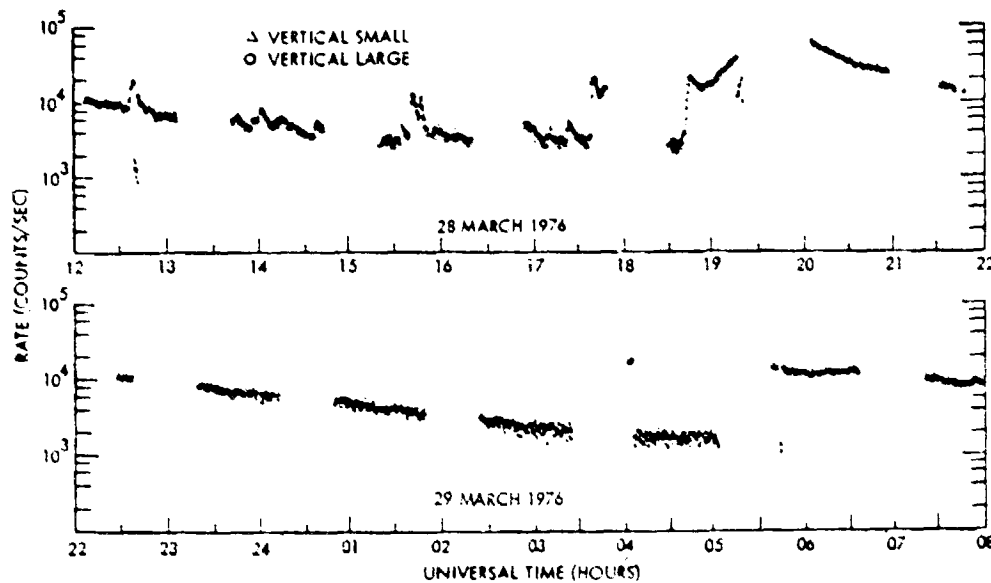


Fig. 7. The light curve for McMath 14143 on 28 and 29 March 1976.

D. 31 March

From 0730 to 1100 UT on 31 March, both McMath 14146 (on the west limb) and McMath 14143 (near disk center) were fairly stable and emitted nearly equal X-ray fluxes of about 500 counts/s in the Vertical Large Detector. The typical X-ray map for this period is shown in Figure 8. By the time the satellite came out of orbit eclipse at 1146 UT, McMath 14143 was more than 20 times as strong as McMath 14146 and continued to dominate the emission at least throughout the next day. Figure 9 shows the event which peaked around 1213 UT and then decayed for the next several hours. It should be noted that there was some additional enhancement during the orbit eclipse from 1248 to 1322 UT.

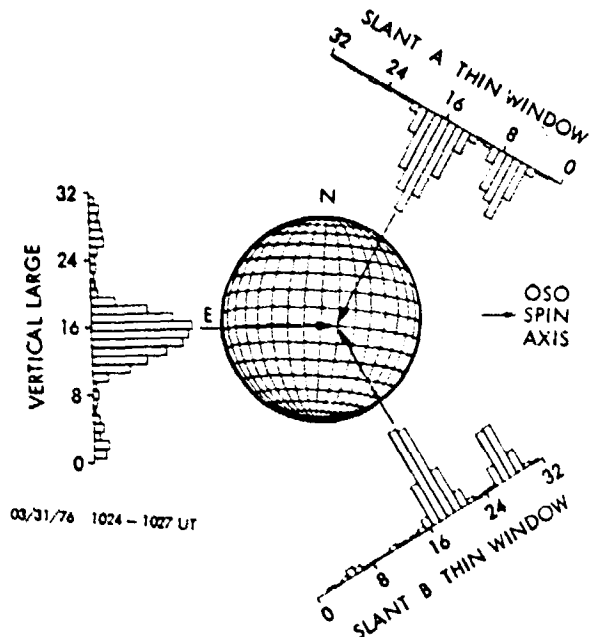


Fig. 8. The X-ray sun 90 min before the large enhancement of McMath 14143 near disk center.

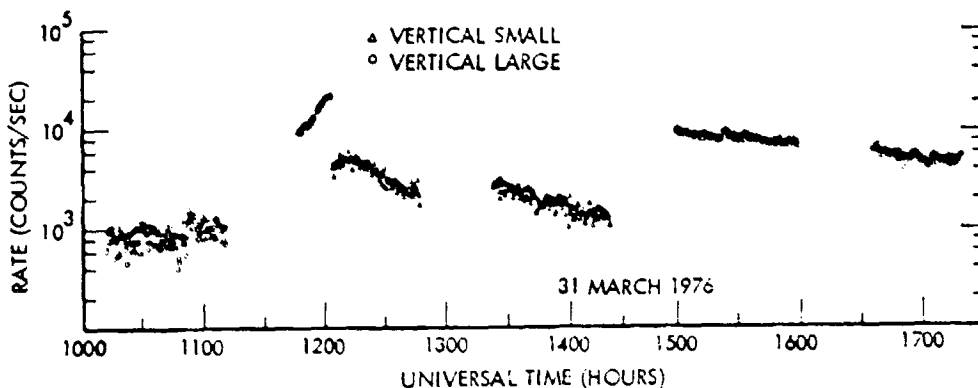


Fig. 9. The X-ray light curve for McMath 14143 on 31 March 1976. The peak emission was at approximately 1213 UT.

E. 30 April

As noted above, the region of interest, now on its third rotation, was redesignated McMath 14179. On 30 April many HI, X-ray, and radio events were reported along with a ground level solar cosmic ray event. Although McMath 14185 (~NO3 E16) was producing a detectable flux, McMath 14179 (~SO8 W32) completely dominated the solar X-ray emission throughout this period. Figure 10 displays more than a 24-hour period for this region. The proton producing event appears to have maximized some time prior to the start of orbit day at 2121 UT. Plasma parameters which result from interpreting the data at 2122 UT as the

emission from an isothermal plasma are temperature = 15×10^6 K, emission measure = 2×10^{49} cm $^{-3}$, 1 - 8Å flux = 2×10^{-2} ergs/cm 2 s, and 0.5 - 4Å flux = 4×10^{-3} ergs/cm 2 s.

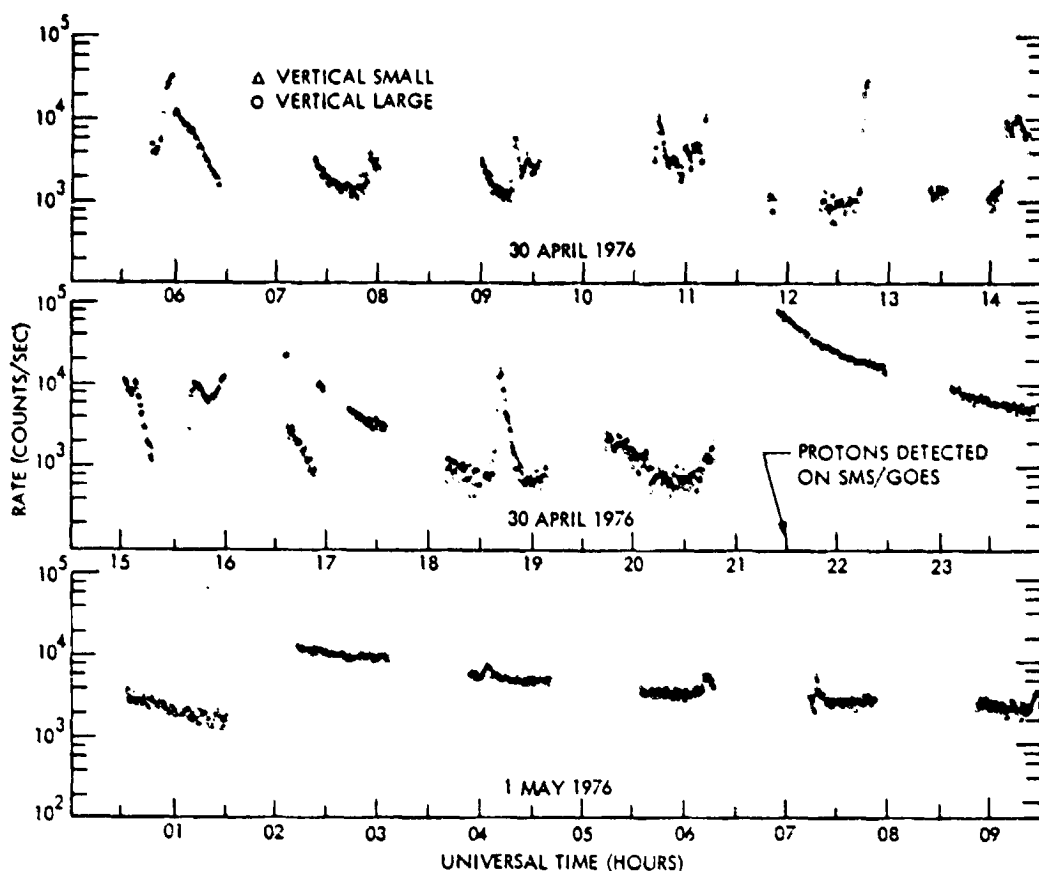


Fig. 10. The X-ray light curve for McMath 14179. The provisional time of the first 6 - 10 MeV proton detection is shown by the arrow at 2130 UT.

One immediately notes the large contrast in variability before and after this event. The visible impact is of course biased because the pre-event baseline is lower than the post-event baseline. However, examination of the counting rates establishes that bursts like these occurring during the 14 hours before the proton event would have registered well above the smooth post-event baseline after 0400 UT on 1 May.

Summary

We have presented six examples of the solar X-ray emission during STIP Interval II as observed with the Lockheed Mapping X-ray Heliometer instrument on the OSO-8 satellite. These data are representative of the data we have for the entire period. The major source of X-ray emission during STIP Interval II was a complex active region designated McMath 14143 on its second rotation and McMath 14179 on its third rotation. Other strong sources, however, were usually present also. The spatial resolution of the MXRH instrument enables one to separate clearly the emission from these different regions. Investigators desiring data not presented here, or a further reduction of these data, are encouraged to request it from the authors.

Acknowledgments

The authors wish to acknowledge the team that conceived, designed, and fabricated the MXRH instrument; especially Co-Investigators J. L. Culhane and R. C. Satura and Project Engineer, C. W. Gilbreth. Our thanks are extended to the personnel of GSFC who control OSO-8 and distribute the data. This work was supported by the National Aeronautics and Space Administration under contract NAS5-22411 and by the Lockheed Independent Research Program.

REFERENCES

- | | | |
|---|------|--|
| BRADT, H.,
G. GARMIRE,
M. ODA,
G. SPADA, and
B. V. SREEKANTAN | 1968 | The Modulation Collimator in X-ray Astronomy, <i>Space Science Reviews</i> , 8, 471. |
| ODA, M. | 1965 | High Resolution X-ray Collimator With Broad Field of View for Astronomical Use, <i>Applied Optics</i> , 4, 143. |
| TUCKER, W. H. and
M. KOREN | 1971 | Radiation From a High-Temperature, Low-Density Plasma:
The X-ray Spectrum of the Solar Corona, <i>The Astrophysical Journal</i> , 168, 283. |
| WOLFSON, C. J.,
L. W. ACTON, and
C. W. GILBRETH | 1975 | Mapping X-ray Heliosphere for Orbiting Solar Observatory-8, Final Report, NASA-CR-144710. |

Appendix E

EARLY EVOLUTION OF AN X-RAY EMITTING
SOLAR ACTIVE REGION

C.J. Wolfson, L.W. Acton, J.W. Leibacher,
and D.T. Roethig

Reprinted from Solar Physics (1977)
Vol. 55, pp. 181-193

EARLY EVOLUTION OF AN X-RAY EMITTING SOLAR ACTIVE REGION

C. J. WOLFSON, L. W. ACTON, J. W. LEIBACHER,
and D. T. ROETHIG

Lockheed Palo Alto Research Laboratory, 3251 Hanover Street, Palo Alto, Calif. 94304, U.S.A.

(Received 18 May, 1977)

Abstract. The birth and early evolution of a solar active region has been investigated using X-ray observations from the Lockheed Mapping X-Ray Heliometer on board the OSO-8 spacecraft. X-ray emission is observed within three hours of the first detection of H α plage. At that time, a plasma temperature of 4×10^6 K in a region having a density of the order of 10^{10} cm $^{-3}$ is inferred. During the fifty hours following birth almost continuous flares or flare-like X-ray bursts are superimposed on a monotonically increasing base level of X-ray emission produced by plasma with a temperature of the order 3×10^6 K. If we assume that the X-rays result from heating due to dissipation of current systems or magnetic field reconnection, we conclude that flare-like X-ray emission soon after active region birth implies that the magnetic field probably emerges in a stressed or complex configuration.

1. Introduction

The purpose of this paper is to investigate the birth and early evolution of a solar active region as observed at X-ray wavelengths. X-rays provide the most definitive indication of energetic processes and high temperature plasma. However, instrumental limitations have prevented previous studies (Dodson and Hedeman, 1956; Born, 1974; Glackin, 1975) from adequately evaluating these aspects of the earliest phases of active region formation. The X-ray data to be discussed in this paper were obtained with the Lockheed Mapping X-Ray Heliometer (MXRH) on the NASA Orbiting Solar Observatory-8 (OSO-8) spacecraft.

To put the X-ray observations into perspective, it is appropriate to review briefly current ideas on the birth and early development of active regions. When observing in H α or Ca-K, the first indication of active region birth is a pair of small bright plages (often called focii until they are large enough to be called plages) connected by Arch Filament Systems (AFS) (Bruzek, 1967, 1969; Weart, 1970). These young regions emerge at, or very quickly drift to, the border of supergranules (Bumba and Howard, 1964; Born, 1974). Associated with the developing plage is a bipolar magnetic field structure (Harvey and Martin, 1973) that is growing at about 10^{16} Max s $^{-1}$ (Mosher, 1976). Slowly rising magnetic arches, identified with flux tubes, would account for the photospheric magnetic feature and the AFS. These rising tubes carry some photospheric material upward which subsequently flows down the legs of the arches under gravity. An individual arch emerges, rises and becomes optically invisible in approximately 30 min. About ten arches (the AFS) are visible at any instant, and the general pattern is maintained for a few days. The high, invisible arches contribute to the total magnetic flux of the region.

The growth of a region usually terminates within a day or two of birth and the region begins to dissipate. However, a few regions continue to enlarge in plage area, magnetic complexity, flare productivity, etc. Roughly speaking, the probability of reaching any specified intensity in these indices varies inversely with the magnitude of the intensity. Eventually, all regions disintegrate.

X-ray observations, when studied within the context of active region formation discussed above, provide information on formation and evolution at coronal levels, especially the formation of the active region coronal condensation. However, no previous X-ray instrument could provide continuous long term coverage of the full disk with spatial resolution adequate to separate a new weak region from the other regions on the disk. Good temporal and spectral resolution are also required to interpret the conditions in the evolving plasma.

In the next section we will describe briefly the MXRH instrument which provides these capabilities and with which we have now observed more than a dozen active region births. We will concentrate on one particular region, McMath 13811, which was born in late August 1975. This region was chosen by selecting from the data for the last half year of 1975 all regions which were born within 60° of the central meridian and developed into major centers of activity before crossing the west limb. Four regions were found and of these the data available for McMath 13811 were the most complete. Though each region evolved differently in detail, the characteristics that apply to McMath 13811 generally apply to the other three regions so the evolution described here appears to be typical.

This study of McMath 13811 encompasses 50 hr beginning at 1400 UT on 19 August 1975. For the 32 hr following our study interval, the X-ray region showed a generally increasing average intensity, number of flares and peak flare emission until limb obscuration on 22 August. The region (redesignated McMath 13831) was inactive during its second disk passage.

2. The Mapping X-Ray Heliometer

The MXRH was activated in orbit on June 22, 1975. The instrument responds to X-rays in the 1.5-30 keV energy range, has a spatial resolution of about 2 min of arc, and maps the entire solar disk every 40 s. Longer integration times are required to detect regions of weak emission.

The instrument looks radially outward from the rotating wheel of the OSO-8 satellite. It contains three detection systems, each collimated in one dimension with Oda-type mechanical collimators (Bradt *et al.*, 1968; Oda, 1965). The collimators have a full width at half maximum transmission of 2 min of arc, although other instrumental effects broaden the instrument response function to about 4 min of arc under some conditions. Each field-of-view is tilted 120° from the others. These three systems are called Vertical, Slant A and Slant B, with the Vertical system field-of-view parallel to the satellite spin axis. As the wheel rotation sweeps these fields-of-view past the Sun, three one-dimensional count rate distributions are obtained.

These distributions permit the location and isolation of emitting X-ray regions. Each spatial distribution consists of 31 successive strips, or area segments, parallel to a system's field-of-view. Examples of these distributions are shown later in Figure 4. The wheel rotates at approximately 6 rpm and, under normal operation, four revolutions are required to form a complete set of three distributions.

The instrument includes different proportional counter detectors which combine to provide spectral information from approximately 1.5 to 30 keV. The low energy limit is established by the thinnest Be window ($75 \mu\text{m}$) and the effective high energy limit is determined by the solar spectrum and intensity and is usually substantially lower than 30 keV. Spectral information is obtained by 15 channel analysis of the proportional counter signals.

Identical medium sensitivity detectors (called Large Detectors) are situated behind each of the three collimated systems along with detectors of other sensitivities. A more sensitive detector is Thin Window Detector B (TWD-B) in the Slant B system, the most sensitive detector is TWD-A, and the least sensitive detector is Vertical Small. Automatic detector switching provides a sensitivity range of $>10^5$. Effective areas as a function of energy for three of the detectors are shown in Figure 1. The observation time for a point source is about 0.02 s per wheel rotation.

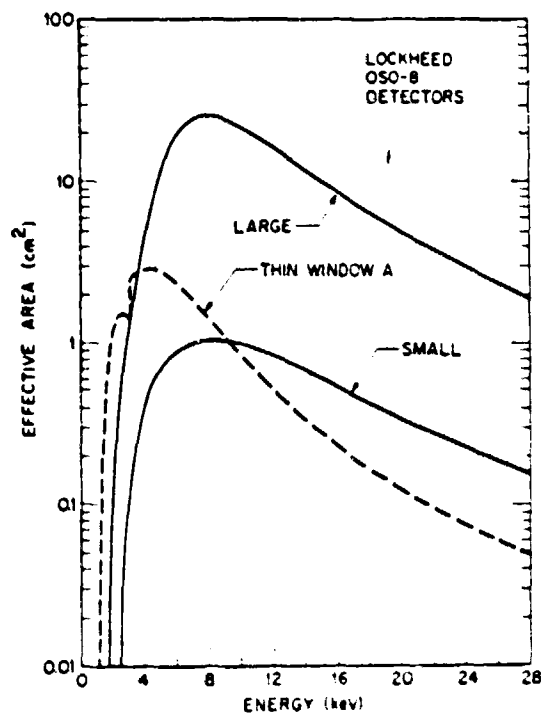


Fig. 1. Calculated effective areas of MXRH detection systems as a function of energy for normally incident photons.

The instrument response to the solar X-ray emission is shown in Figure 2 where total counts which will be collected from a point source in one solar scan are plotted as a function of plasma temperature. The X-ray spectrum which was folded through the instrument response to produce these curves was computed by a code which is an

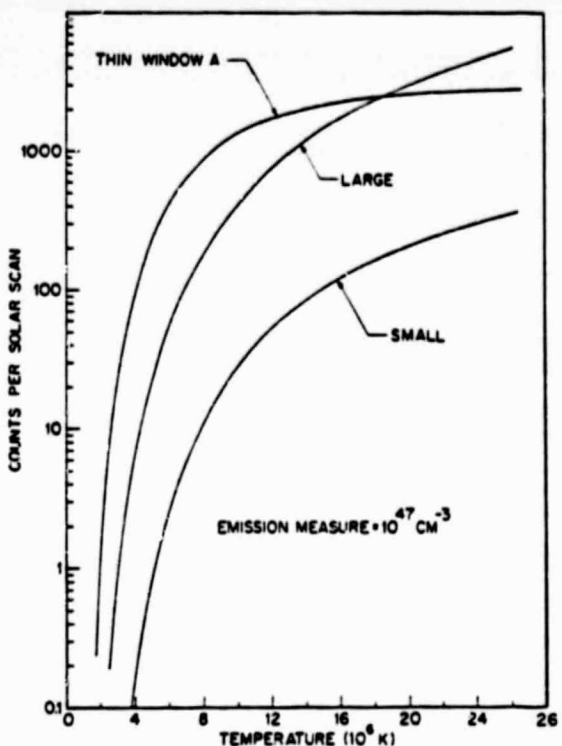


Fig. 2. Predicted total counts in MXRH detectors for one solar scan in response to a plasma with an emission measure of 10^{47} cm^{-3} . The prediction is based on an updated Tucker and Koren (1971) formulation for the X-ray emission from a low density plasma.

updated version of the formulation developed by Tucker and Koren (1971) for the X-ray emission from a low density plasma. Further details of the instrument, its subsystems, and its operational modes are given by Wolfson *et al.* (1975).

3. Observations

Figure 3 shows the birth of McMath region 13811 as observed in H α . These prints were made from full disk patrol movies obtained at the Big Bear Solar Observatory. The arrows are placed in identical locations on each print to assist in observing the plage birth at arrow C. When actually viewing the film, we first identify the plage at $1545 \pm 0015 \text{ UT}$ where the uncertainty results from the subjectivity of the viewer

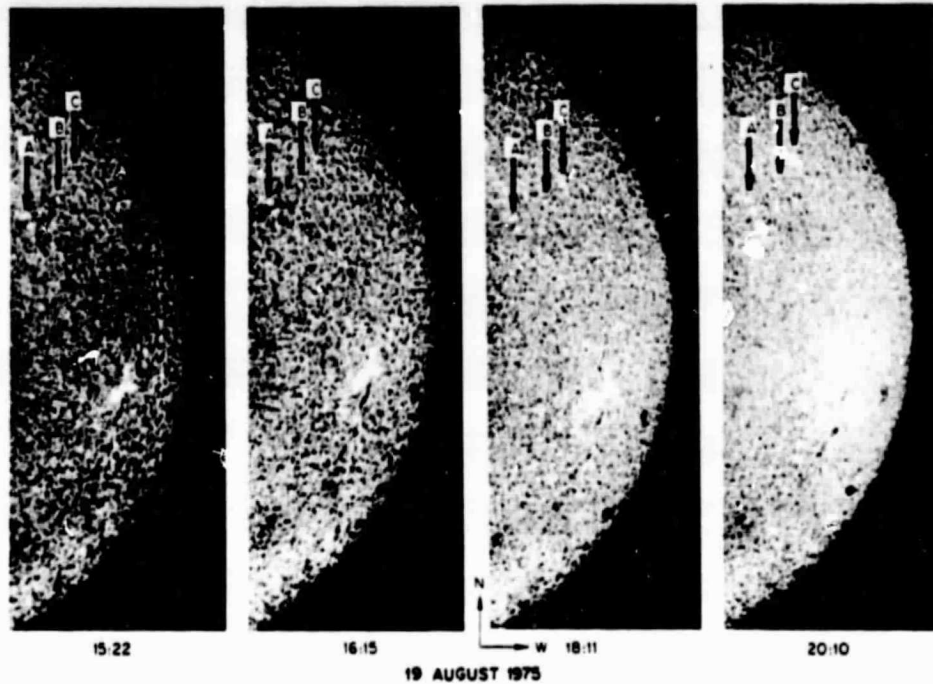


Fig. 3. H_α images of the western solar disk at four times during the latter part of 19 August. The three arrows are located identically on each photo to aid in observing the formation of McMath 13811 below arrow C. Photographs are courtesy of the Big Bear Solar Observatory.

and the variable spatial resolution (seeing limited to 2–4") of the full disk image. By the time (1820 UT) X-rays are first detected with the Vertical Large Detector, the region consists of two bright and one weak plage, each approximately 12 000 km wide, and the entire region falls within a circle of approximately 32 000 km diameter.

The X-ray Sun at three times during this early evolution is shown in Figure 4. Note that McMath 13811 dominates the X-ray disk at 0100 UT on 20 August. Moving backward in time, the region is easily detectable at 1830 UT on 19 August, but not detectable at 1640 UT. These three maps also show that McMath 13808 was in line with McMath 13811 as viewed by the more sensitive TWD-A system. For this reason the detailed analysis has primarily utilized data from the vertical system. This makes the threshold for detectability roughly an order of magnitude higher than if we had been able to use TWD-A.

We have limited the study of the early evolution of McMath region 13811 to the first 50 hr. The data for this period is displayed in Figure 5 where we have selected 10 min as a standard summation interval to produce maps (similar to Figure 4) wherever possible throughout the 50 hr period. Each point is the 10 min average count rate for the Vertical Large Detector after background subtraction. Typical statistical (one sigma) error bars are indicated. Data points which are truly adjacent in time are connected by solid lines while those which have a data gap either due to

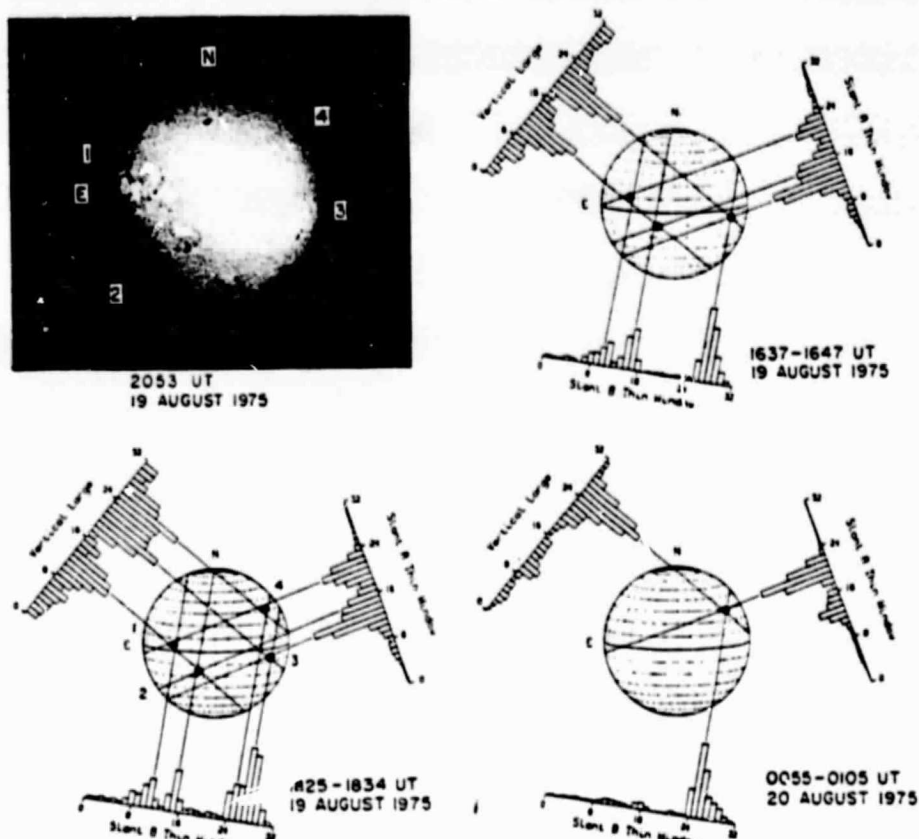


Fig. 4. The Sun as seen in X-rays and H α during the early evolution of McMath 13811. The MXRH X-ray data are collected and displayed in terms of 32 numbered Area Segments, each 1.3' in width. Each histogram is normalized to the peak intensity for that detection system. The four principal X-ray emitting active regions are labeled: (1) McMath 13808, (2) McMath 13807, (3) McMath 13796, and (4) McMath 13811. The H α photograph is courtesy of the Sacramento Peak Observatory.

satellite eclipse or the South Atlantic Anomaly are connected by a dashed line. This distinction is made since some variations of less than 30 min will be lost due to these data gaps.

Optical observations are indicated along the top of Figure 5. H α birth is taken from the Big Bear Observatory movies as described earlier, while the H α flare activity is taken directly from *Solar-Geophysical Data* (1976a) with the arrows marking flare maxima. Periods of no flare patrol are also indicated.

We have also examined the 50 hr period with 20 s time resolution. A sample of these data taken during the first half day of the existence of the region is shown in Figure 6. The background rate, as shown, is well below the solar signal. These observations demonstrate conclusively that the early evolution of this region at these energies is highly structured, or 'bursty', on time scales of minutes.

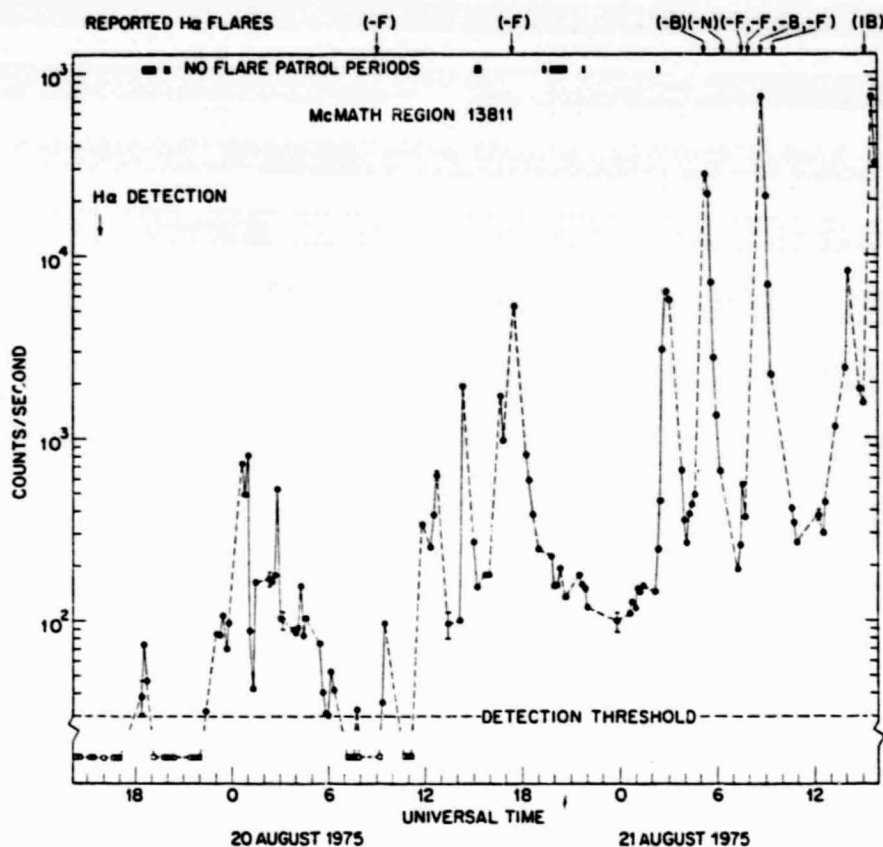


Fig. 5. A two day light curve for the X-ray emission from McMath 13811 as observed by the MXRH Vertical Large Detector after background subtraction. Representative error bars are shown. Each point is a 10 min average, with solid lines connecting continuous data sets and dotted lines connecting interrupted data sets. Rates in excess of $10000 \text{ counts s}^{-1}$ were obtained with the less sensitive Vertical Small Detector and normalized for display.

A word is in order concerning the meaning of the sensitivity threshold of the MXRH. Even for a fixed summation time the criteria for detection varies with the varying background intensity. We have selected a conservative value of 30 counts s^{-1} as the detection threshold rate for the entire time period. For the X-ray emission from an optically thin plasma at 4 million degrees, this threshold rate corresponds to an emission measure, $\int n_e^2 dV$, of $8 \times 10^{46} \text{ cm}^{-3}$. For comparison with other X-ray data this threshold is equivalent to $6 \times 10^{-6} \text{ erg cm}^{-2} \text{ s}^{-1}$ in the 1–8 Å bandpass; the nominal SMS/GOES 2 threshold is $10^{-4} \text{ erg cm}^{-2} \text{ s}^{-1}$ (*Solar-Geophysical Data*, 1976b). The threshold count rate can, of course, be obtained by other combinations of temperature and emission measure. Examples are presented in Table I. The flux values of Table I include both continuum and line emission although in this

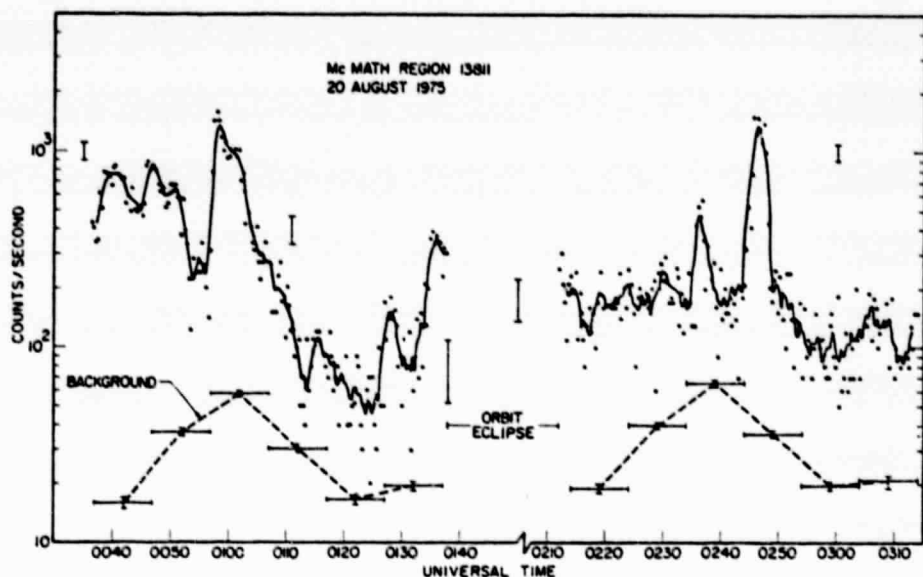


Fig. 6. A light curve of the X-ray emission from McMath 13811 for a three hour period during the first half day of the region's development. Each data point is the average rate for area segments 24–26 over a 20 s interval. Statistical error bars (one sigma) are indicated. The solid curve displays a 5 point running average of the individual data points.

temperature range the contribution to the large detector count rate due to line emission is never more than 25%.

TABLE I
Combinations of emission measure and temperature which produce a detectable signal in the MXRH Vertical Large Detector

\log_{10} emission measure (cm ⁻³)	Temperature (10 ⁶ K)	1–8 Å flux (erg cm ⁻² s ⁻¹)
44	26	2×10^{-7}
46	5.9	3×10^{-6}
48	2.8	1×10^{-5}

4. Discussion

Four experimental facts concerning the formation of McMath 13811 should be noted:

- (1) X-ray emission is detectable within 3 hr of the first detectable H α plage.
- (2) The overall X-ray intensity of the region shows a gradual increase with many large amplitude spikes superimposed on the upward trend.

(3) When observed with 20 s time resolution, there are many flare-like X-ray bursts (more than a factor of two increase in intensity in a minute or less) even during the first day after plage appearance.

(4) X-ray bursts and H α flares, as reported in *Solar Geophysical Data* (1976a) and augmented by direct examination of H α films, show some strong correlations as well as other equally clear examples of lack of correlation.

The time relationship between the appearance of the chromospheric and coronal counterparts of an active region is quite important in interpreting the birth phenomena. We have inferred above that the X-ray birth for McMath 13811 came about 2½ hr after the H α birth. Such a conclusion is dependent upon the sensitivities of both observing instruments. The H α photographs are full disk, so to be identified as a plage the area must be about $5 \times 5''$ or larger. The H α plage grew quite rapidly so the error in H α birth is probably less than 15 min. For determining the X-ray birth we have only about 45% time coverage, so although the X-ray intensity certainly crossed the detector threshold within 2½ hr of H α appearance, we may have missed seeing earlier emission. The fact that the early X-ray emission is very bursty makes it relatively unlikely to catch the earliest emission.

Let us picture the region at 1830 UT as a simple bipolar system with a semi-toroidal flux tube arched above the photosphere. The cross sectional area and the length along the centroid of the tube can be estimated as $1.1 \times 10^{18} \text{ cm}^2$ and $3.0 \times 10^9 \text{ cm}$ respectively by assuming the two brighter spots on the H α photo of 1811 UT are the footpoints of the tube. An independent method of estimating these parameters is to use the Mt. Wilson magnetograph map at 1700 UT on 20 August as given in the *Solar Geophysical Data* (1975) and using the formulation of Mosher (1976) to work backward on a growth curve for similar regions. This technique yields similar magnitudes and these values are consistent with the observations of Ephemeral Active Regions (Harvey and Martin, 1973). The tube volume is thus estimated at $3 \times 10^{27} \text{ cm}^3$.

For a 30 min period centered around 1830 UT, the average X-ray count rate is 50 counts s $^{-1}$, the temperature is $4.0 \times 10^6 \text{ K}$, and the emission measure is $1.1 \times 10^{47} \text{ cm}^{-3}$. For a volume of $3 \times 10^{27} \text{ cm}^3$ this yields an rms electron density of $6 \times 10^9 \text{ cm}^{-3}$. Such a density is about an order of magnitude higher than 'quiet', large scale, coronal features, and roughly the same as non-flaring active regions (Vaiana *et al.*, 1975). Therefore, within 3 hr of the chromospheric birth at least one small, dense, coronal feature has been formed. This feature was detectable by the MXRH because of its transitory, elevated temperature.

The trend of general increase in X-ray intensity for 50 hr either represents an increase in effective temperature, an increase in the amount of emitting material, or a combination of the two. To investigate this further, we have determined the parameters of the isothermal coronal plasma which most closely reproduces the pulse height distribution for each data point in Figure 5. Although the isothermal assumption is an oversimplification, most of the fits to the data were reasonable and the effective temperatures obtained in this manner are physically meaningful, especially for comparative purposes.

The resulting variation of temperature and emission measure with time are shown in Figure 7. The temperature is quite variable but appears to consistently return to a baseline value of approximately three million degrees, even though the intensity (as seen in Figure 5) increases by more than an order of magnitude. Correspondingly, the emission measure shows a monotonic upward trend with an *e*-folding time of about 18 hr. Thus, a reasonable model for the developing coronal condensation involves an increasing amount of material at a relatively stable temperature of $\sim 3.0 \times 10^6$ K with superimposed injections or transitory *in situ* creations of hotter material. The multi-thermal analysis of this model is beyond the scope of the present work.

The superimposed enhancements seem to occur in groups which are separated by about 14 hr (around 0200 UT on the 20th, 1600 UT on the 20th, and 0600 UT on the 21st). This may be merely a coincidence, or may be related to spatial or temporal periodicities imposed by the mechanisms which determine how new flux emerges.

Figure 6 displayed a small portion of the region's early evolution with high time resolution. The frequency of X-ray bursts in this sample is above average but very seldom is the light curve smooth. We observed 10 bursts of more than a factor ten increase during the initial 50 hr period, with the median increase being a factor of 25. The *e*-folding rise times of these bursts vary from 22 s to 4.5 min and the fall times vary from 2 to 23 min. To the extent of our data coverage ($\sim 55\%$), all are consistent with flare-like temperature and emission measure profiles; i.e. both the temperature and emission measure increase to account for the increased X-ray emission. The many flare-like bursts seen in these high time resolution data add to our general evolutionary model by suggesting that throughout the entire developmental period impulsive heating is taking place in a manner similar to that for regular flares. This is not surprising, since X-ray bright points are known to flare (Golub *et al.*, 1974) and a very young active region is probably synonymous with an X-ray bright point. The existence of flares does not, therefore, distinguish the few young regions that will continue to develop fully from the multitude of X-ray bright points which last only a day or less.

Figure 5 shows relatively poor detailed correlation between X-ray bursts and reported H α flares and subflares. An in-depth analysis of specific examples is not part of this study, but careful comparison of MXRH and H α records for this and other data sets reaffirms the fact that some X-ray bursts have little or no counterpart H α emission and *vice versa*. The nearly pure X-ray events (e.g. 1415 UT on 20 August) are especially interesting because they may imply localized energy release and strong containment of the thermal energy in the corona. Such a phenomena is hard to understand in terms of a simple arched flux tube model of the active region.

5. Summary and Conclusions

The Mapping X-Ray Heliometer instrument on OSO-8 has observed the birth and early evolution of the X-ray features associated with several active regions. One of

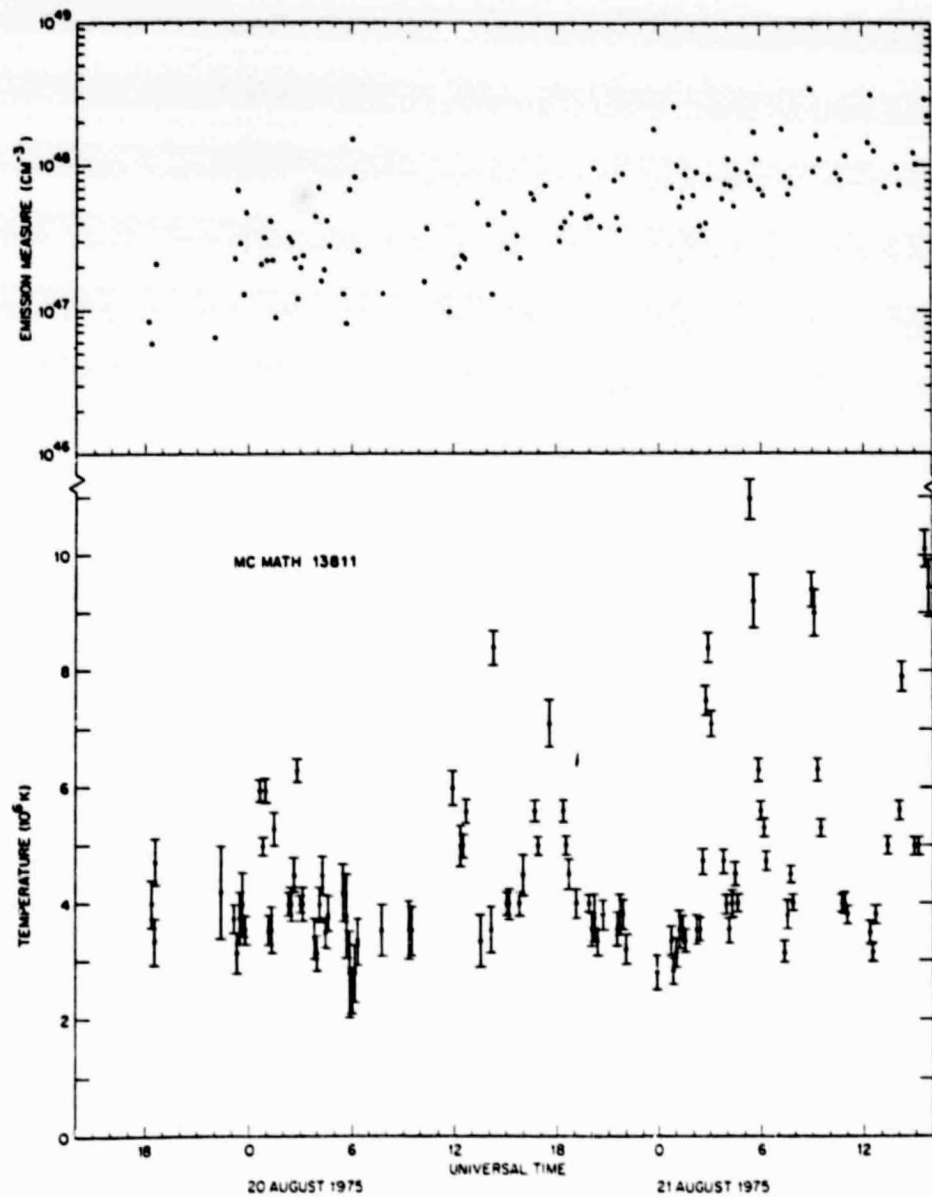


Fig. 7. The temperature and emission measure of McMath 13811 as a function of time during the region's development. The parameters were obtained by comparing the observed pulse height distributions for the 10 min data sets displayed in Figure 5 to predicted distributions for isothermal coronal plasmas. The error bars represent the larger of either: (a) the one sigma variations that result when the spectra are perturbed by counting statistics, or (b) the step size of the temperature grid used in the numerical computations. Such errors are meaningful for relative comparison but underestimate for the absolute values.

these (McMath 13811) has been studied in detail, and for it we find that soft X-ray emission is detectable within 3 hr of the first $H\alpha$ detection. The X-ray intensity is seen to generally increase for the two days after birth with many bursts superimposed upon this upward trend.

On the basis of this study we suggest that very early in the history of the active region a discrete volume of the order of 10^{27} cm^3 with a density of about 10^{10} cm^{-3} was formed. The first detectable X-ray emission resulted from impulsive heating of this pre-existing volume to $\sim 4 \times 10^6 \text{ K}$. The subsequent temporal evolution suggests that there is a gradually increasing amount of material at a relatively stable temperature of $\sim 3 \times 10^6 \text{ K}$ combined with many transient inputs of hotter material. Even during the first half day some of the transients are so rapid as to require impulsive heating similar to the flares observed in older and presumably more complex regions.

We do not have adequate optical or magnetic coverage to do detailed correlations with the X-ray evolution of this region. Previous observations (Weart, 1970; Glackin, 1975; Frazier, 1972) suggest that individual flux arches are continually emerging and rising into the corona and that the growth of an active region means the number of arches existing simultaneously is increasing. The observed increasing X-ray baseline may well correspond to an increasing number of arches with effective temperature of $\sim 3 \times 10^6 \text{ K}$. In addition, any single arch or combination of arches may flare, resulting in the observed X-ray bursts. This study has shown that flaring processes (at least as inferred from X-ray emission) begin almost at once after magnetic flux emergence. This precedes the generally accepted period of development of magnetic field complexity which may be indicative that the field emerges in a stressed or complex configuration.

Acknowledgements

The authors wish to acknowledge the team that conceived, designed, fabricated and presently operate the MXRH instrument; especially Project Engineer, C. W. Gilbreth and ground station scientist, K. L. Smith. Numerous useful scientific discussions with R. C. Catura, J. L. Culhane, D. W. Datlowe, J. Mosher and L. L. Newkirk are gratefully acknowledged. We thank R. L. Moore for several discussions concerning the interpretation of the $H\alpha$ films and the associated X-ray data. Among the many people who have worked with us through the years to make the OSO-8 program a success, we express special thanks to J. Donley, W. Worrall and R. Thomas of NASA and J. Buterbaugh of Hughes Aircraft Corporation. This program has been supported by the National Aeronautics and Space Administration under Contract NAS5-22411, NAS5-11360, and by the Lockheed Independent Research Program.

References

- Born, R.: 1974, *Solar Phys.* **38**, 127.
Bradt, H., Garmire, G., Oda, M., Spada, G., and Sreekantan, B. V.: 1968, *Space Sci. Rev.* **8**, 471.

- Bruzek, A.: 1967, *Solar Phys.* **2**, 451.
Bruzek, A.: 1969, *Solar Phys.* **8**, 29.
Bumba, V. and Howard, R.: 1964, *Astrophys. J.* **141**, 1492.
Dodson, H. W. and Hedeman, E. R.: 1956, *Monthly Notices Roy. Astron. Soc.* **116**, 427.
Frazier, E. N.: 1972, *Solar Phys.* **26**, 130.
Glackin, D. L.: 1975, *Solar Phys.* **43**, 317.
Golub, L., Krieger, A. S., Silk, J. K., Timothy, A. F., and Vaiana, G. S.: 1974, *Astrophys. J. Letters* **189**, L93.
Harvey, K. L. and Martin, S. F.: 1973, *Solar Phys.* **32**, 389.
Mosher, J. M.: 1976, California Institute of Technology, Ph.D. Thesis.
Oda, M.: 1965, *Appl. Optics* **4**, 143.
Solar-Geophysical Data: 1975, No. 374, Part I, U.S. Dept. of Commerce (Boulder, Colorado, U.S.A.).
Solar-Geophysical Data: 1976a, No. 378, Supplement, U.S. Dept. of Commerce (Boulder, Colorado, U.S.A.).
Solar-Geophysical Data: 1976b, No. 378, Part II, U.S. Dept. of Commerce (Boulder, Colorado, U.S.A.).
Tucker, W. H. and Koren, M.: 1971, *Astrophys. J.* **118**, 283.
Vaiana, G. S., Krieger, A. S., Timothy, A. F., and Zombeck, M.: 1976, *Astrophys. Space Sci.* **39**, 75.
Weart, S. R.: 1970, *Astrophys. J.* **162**, 987.
Wolfson, C. J., Acton, L. W., and Gilbreth, C. W.: 1975, *Mapping X-Ray Heliometer for OSO-8, Final Report*, NASA-CR-144710.

A SEARCH FOR MICROWAVE EMISSION FROM
SOLAR X-RAY BRIGHT POINT FLARES

L.W. Avery, P.A. Feldman, V. Gaizauskas,
J-Rene Roy, and C.J. Wolfson

Reprinted from Astronomy and Astrophysics (1977)
Vol. 56, pp. 327-331

A Search for Microwave Emission from Solar X-ray Bright Point Flares

L. W. Avery¹, P. A. Feldman¹, V. Gaizauskas¹, J.-René Roy¹ and C. J. Wolfson²

¹ Herzberg Institute of Astrophysics, National Research Council of Canada, Ottawa, Canada K1A 0R6

² Lockheed Palo Alto Research Laboratory, Palo Alto, California 94304, USA

Received September 20, 1976

Summary. An attempt was made to detect 9.4-cm radio emission from flaring X-ray bright points with the 46-m telescope at the Algonquin Radio Observatory. Observations from the X-ray heliometer aboard OSO-8 were combined with optical and magnetic data to substantiate possible events. Reduction of 52 h of radio data has revealed one event which is a candidate for radio emission from a flaring X-ray bright point.

Key words: Solar activity — solar X-rays — solar radio emission

I. Introduction

Solar X-ray bright points are compact emitting regions which are distributed over the entire solar disc, in intimate association with small, bipolar magnetic regions. Their properties have been discussed by Golub et al. (1974), who suggest that bright points represent a new type of X-ray phenomenon, with a formation mechanism different from that of active regions.

Among the more interesting properties of these features is that 5–10% are claimed to undergo abrupt and intense X-ray flaring during their lifetime ($\langle \mathcal{T} \rangle \sim 8$ h). Such flaring occurs at all latitudes (Golub et al., 1974). Corresponding brightenings have been reported in chromospheric lines (Golub et al., 1975), but little else is known about these flaring bright points. In particular, no observations of their radio counterpart have been made. Because of the possibility that these events are the manifestation of the solar flare process in its simplest, most rudimentary form, we believe their study is potentially important for understanding the basic flare mechanism. Accordingly, we have undertaken a joint study of bright point flares in an attempt to supplement the X-ray data by means of microwave and optical observations.

In this paper we report on our attempt to detect the microwave counterpart of flaring X-ray bright points.

Send offprint requests to: L. W. Avery

II. Observing Procedure

The joint observations were carried out at 9.4 cm with the 46-m telescope of Algonquin Radio Observatory (ARO)¹, in Hz at the Ottawa River Solar Observatory (ORSO) and in X-rays (1.5–30 keV) with the Lockheed Mapping X-ray Heliometer (MXRH) on OSO-8.

For our observations at 9.4 cm we utilized a solid-state noise source as a "hot load" to balance the solar signal. We adopted Virgo A (3C 274) as a calibration source at a flux density of 100 Jy². The telescope beam (HPBW = 8.6') was switched back and forth at one minute time intervals between two positions on the Sun. The two positions were chosen close to the limb, and in quiet parts of the disc near the heliographic poles, to avoid confusion with ordinary activity. Figure 1 illustrates the beam size and the positions used on 10 March 1976.

This observing procedure had several advantages: by observing near the limb the number of bright points in the beam was maximized due to foreshortening; and, by switching between two positions, the solar area monitored for bright-point flares was doubled. In addition, changes in receiver gain and/or the atmosphere, being common to the observations of both positions, could be distinguished from real, localized solar events. Such a procedure results in a minimum detectable flux density of about 500 Jy for events of less than an hour in duration. By contrast, the ARO solar patrol threshold is $\sim 10^4$ Jy.

During all our observations simultaneous whole-disc coverage at 10.7 cm from the ARO solar patrol was available. These observations were invaluable in distinguishing between occasional solar bursts in the side-lobes and the much weaker activity which we were seeking within the main beam of the 46-m telescope.

Optical Hz observations with the 25-cm photoheliograph at ORSO were coordinated with the ARO effort. The optical telescope was programmed to scan the same parts of the Sun being observed at ARO. The

¹ The Algonquin Radio Observatory is operated by the National Research Council of Canada as a national radio astronomy facility

² 1 Jy = 10^{-26} W m⁻² Hz⁻¹ = 10^{-4} solar flux unit

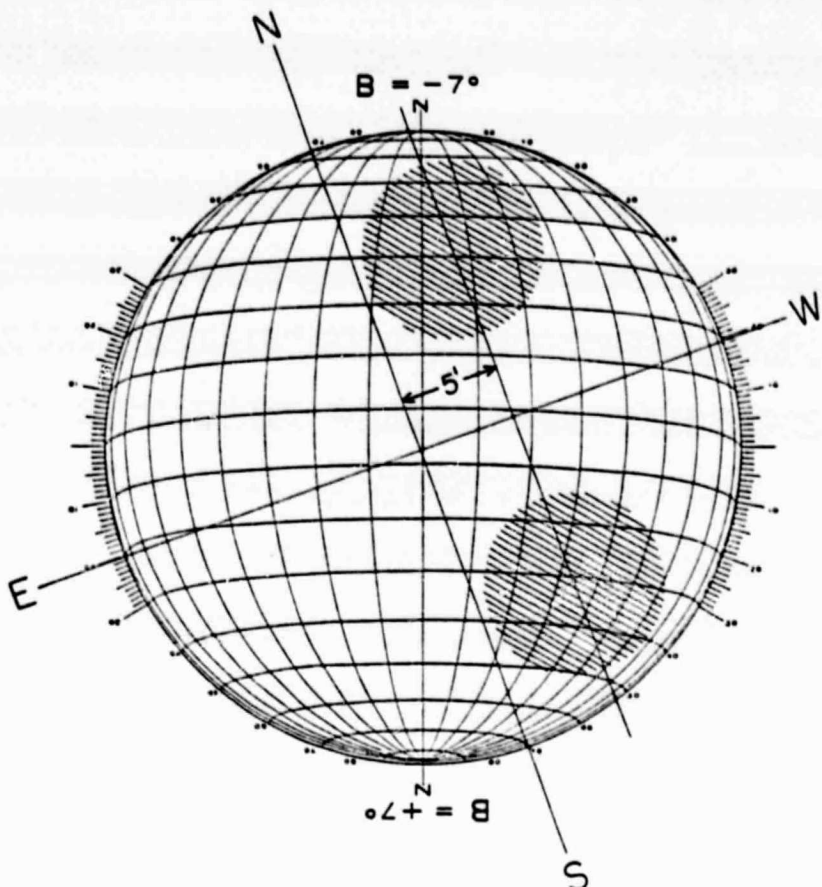


Fig. 1. Positions between which the 8.6' beam of the ARO 46-m telescope was switched at one-minute intervals on 10 March 1976

combined radio and optical observations, being of high sensitivity and high spatial resolution ($1 \text{ mm} = 15''$), respectively, constituted a powerful tool for the study of the low intensity and highly localized activity of interest to us.

The X-ray heliometer on OSO-8 consists of three one-dimensional collimators ($\text{FWHM} = 2'$) with relative orientations of 120° . The Sun is scanned in three directions every 40 s, and matching observations at different orientations enables the location of X-ray sources on the disc. The detector elements are proportional counters of differing types in order to achieve a dynamic range of 10^5 . The MXRH spectral response is approximately 1.5–30 keV with maximum efficiency for photons of about 3–6 keV. This energy range is substantially higher than that used for the Skylab observations of Golub et al. (1974).

III. Results

Observations were made of the Sun in February, March and April 1976. Reduction of the resulting 52 h of radio data has revealed only one event which is a suitable candidate for radio emission from a flaring X-ray bright point. The radio event occurred with the beam centered at S 30° W 30° on 10 March 1976, the most quiet of the

three observing periods. The 9.4-cm radio burst started at 2150 UT, reached a peak flux density of about 1200 Jy at 2157 UT and subsided sometime after 2210 UT (Figure 2a, b) when we had to stop observing. The time evolution of this event is typical of that exhibited by flaring X-ray bright points (Golub et al., 1975). The absence of any detectable flux increase in the whole-disc solar radio patrols at both Ottawa (A.P.O.) and Penticton (DRAO) (Bell, 1976) assures us that the burst we observed did not occur in a side-lobe of the 46-m telescope. In addition, no observable radio events of any type were recorded by the swept-frequency receivers at Ft. Davis (Maxwell, 1976) and Boulder (Warwick, 1976).

The available optical data give credence to the reality of this small radio event. Because of cloudy conditions at ORSO, we had to rely on whole-disc Hz filtergrams from NOAA. No sunspots were present in the area. Simultaneously with the radio burst, a small $\sim 5'' \times 10''$ Hz brightening (Fig. 3a) occurred at S 30° W 32° in a tiny plage (McMath 14119) which appeared on 7 March and was gone by 11 March. The event took place above a photospheric bipolar magnetic feature visible on Kitt Peak magnetograms obtained on 8, 9 and 11 March (see Fig. 3b). There was no data on 7 and 10 March. The bipolar magnetic feature closely resembles the "ephemeral active regions" (ER) described by Harvey

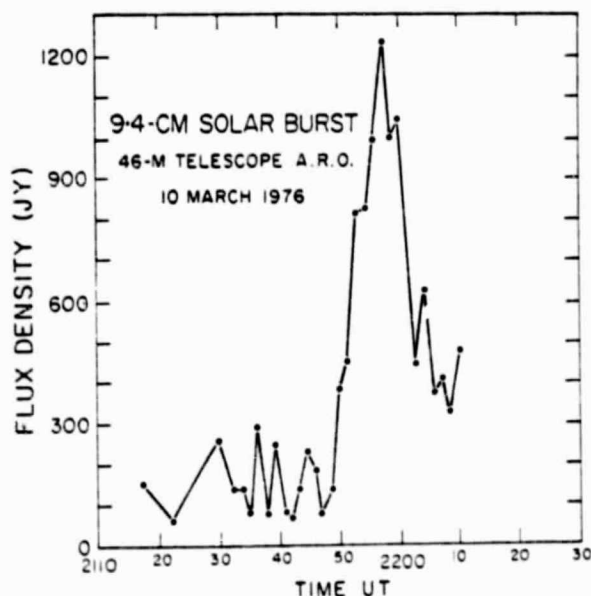
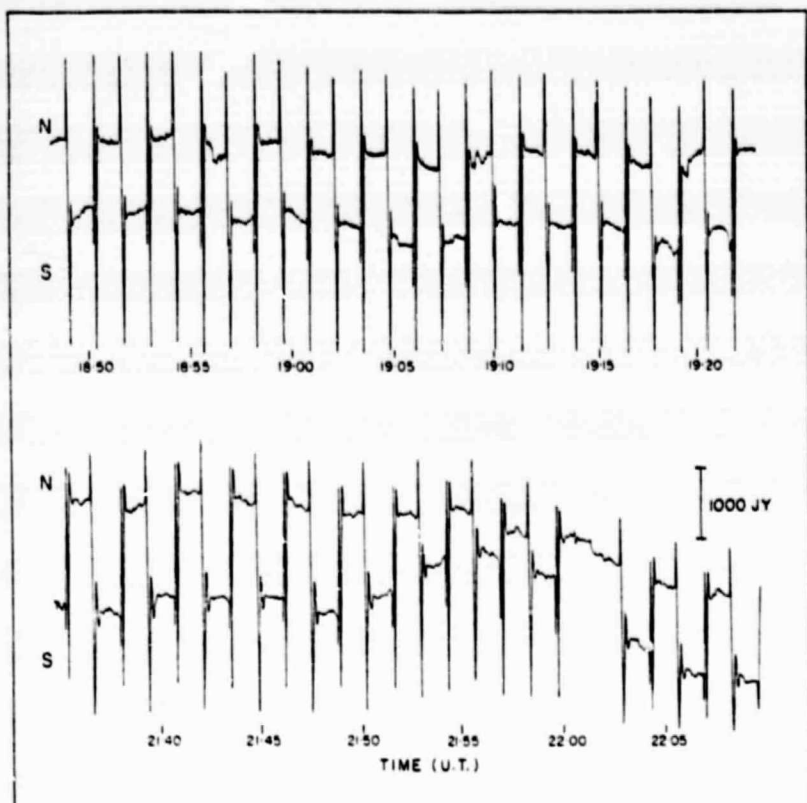


Fig. 2. **a** Signal obtained by the chart-recorder at ARO during a quiet period of the observations on 10 March 1976 (top). The northern hemisphere appears hotter than the southern one. The event shows up (bottom) as a decrease of the differential flux density due to heating in the southern position of the beam. The sharp spikes in the record are transients produced when the beam is moved

b Reduced observations showing the radio burst at 2150 UT

and Martin (1973) and Harvey et al. (1975). The magnetic feature had disappeared on 12 March, but this may in part be due to the center-to-limb effect on the longitudinal component of the field.

The emergence of OSO-8 from the Earth's shadow took place at 2201 UT on 10 March shortly after peak flux was recorded for our radio event. Figure 4 gives the

X-ray map during a period corresponding to the decay phase of the radio burst. The S 30°W 36° location corresponds to a weak source producing peaks of about 50 cts s^{-1} against a background of 12 cts s^{-1} as seen by the Slant B thin window detector and 145 cts s^{-1} against a background of 11 cts s^{-1} as seen by the more sensitive Slant A system. Similar X-ray maps for periods im-

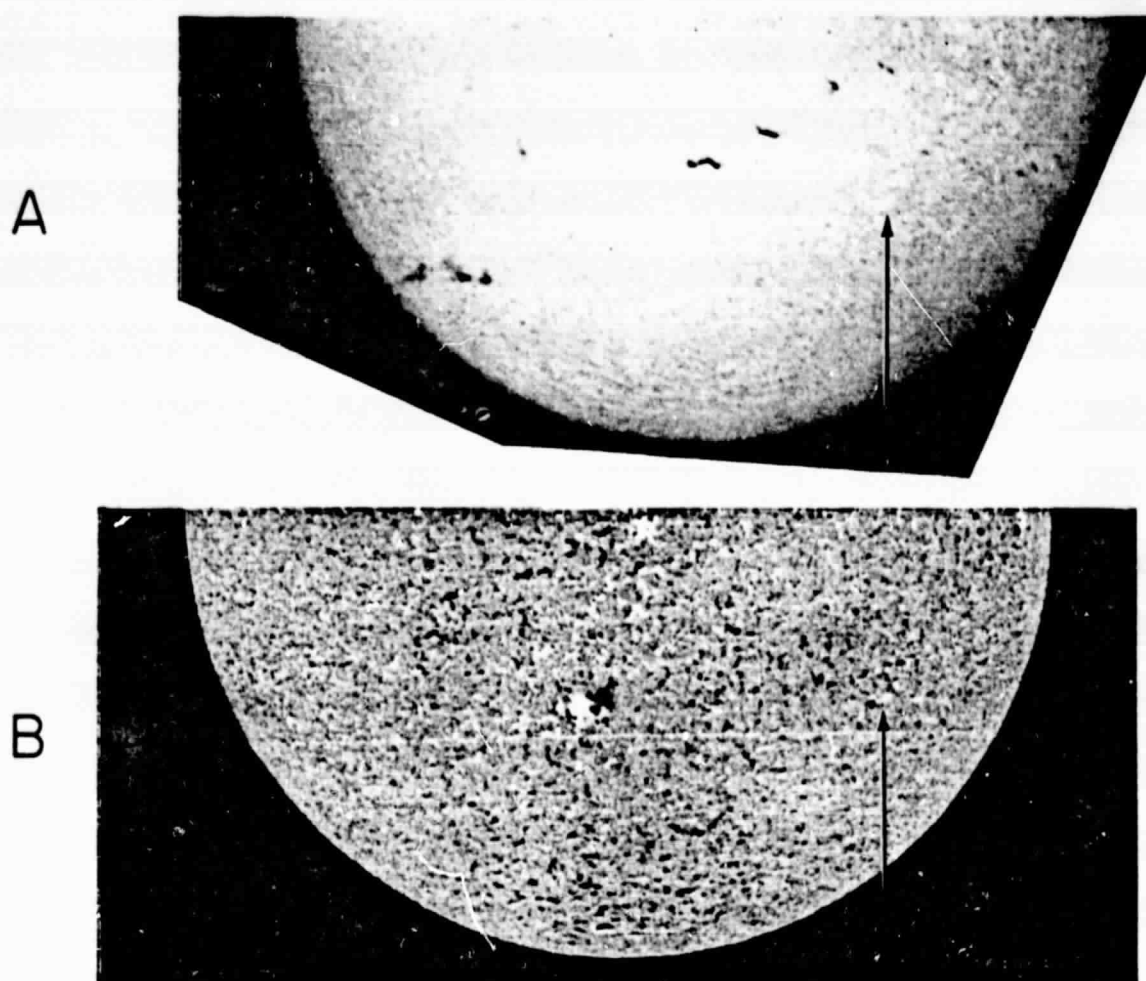
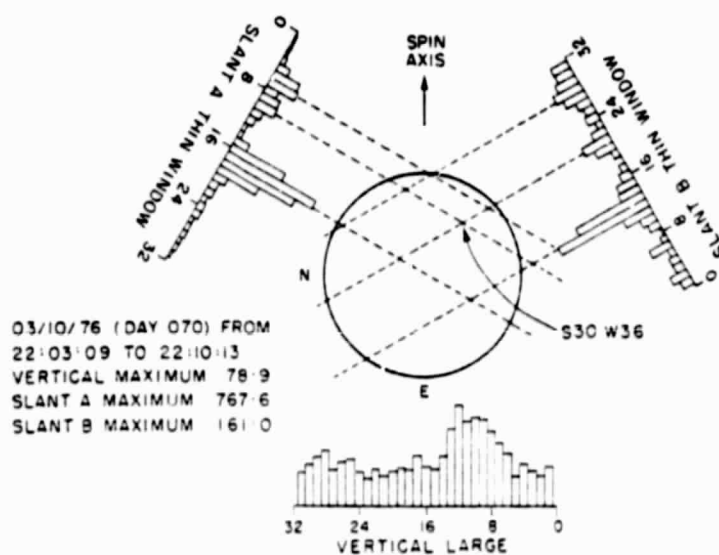


Fig. 3. **a** Southern half of a whole-disc Hz filtergram of the Sun on 10 March 1976 at 2157:27 UT. The transient brightening indicated at S30 W32 occurs within the southern positions of the radio beam as shown in Figure 1. **b** Magnetogram obtained on 11 March 1976 at about 1606 UT showing the bipolar magnetic feature (arrow) corresponding to the activity in the above filtergram (courtesy of Kitt Peak National Observatory)

OSO-8 LOCKHEED X-RAY MAPPING HELIOMETER



ORIGINAL PAGE IS
OF POOR QUALITY

Fig. 4. Scans of X-ray intensities obtained by the MXRH. When the small peaks in the counting rate distributions of Slant A and Slant B systems are matched, one of the three resultant sources corresponds to the location of the Hz brightening within acceptable positional errors

mediately after 22:10 show little or no signal. There were no indications of the source on a map made just prior to entering satellite eclipse (1930—1936 UT). Therefore, we conclude that transient, weak X-ray emission occurred during at least part of the radio burst, and that these X-rays originated from a location coincident with the Hz brightening within acceptable position errors.

IV. Discussion

Unfortunately, the X-ray data over the time period corresponding to the radio burst are not complete, but they do indicate the occurrence of an X-ray burst coincident with our radio event. However, the question of whether the site of the burst was a long-lived (>50 h) X-ray bright point (as described by Golub et al., 1976) or simply a tiny active region (assuming there is a difference) cannot be answered with the limited data available.

We were surprised that we observed only one event in 52 h of radio observation. If our feature was a typical X-ray bright point flare, we should have seen six times as many events according to the statistics of Golub et al. (1974). However, Harvey et al. (1975) and Golub et al. (1975) have pointed out the one-to-one correspondence of solar X-ray bright points and ephemeral magnetic regions (ER). Since the number of ER varies with the solar cycle in the same way as regular activity (Harvey et al., 1975), one might expect one-third as many X-ray bright points in March 1976. Furthermore, other events may be hidden in the fluctuations due to side-lobe effects from strong radio events in region McMath 14179 during our April observing period.

In summary, we are faced with the following alternatives. The event of 10 March 1976 was not a typical flaring X-ray bright point but was rather a microwave burst from a fairly young, tiny bipolar magnetic region which correlates with an Hz brightening and with

enhanced X-ray emission. If this is the case it is the weakest solar flare yet observed over such a broad electromagnetic spectrum. Alternatively, if we accept this event as the flaring of a *long-lived* X-ray bright point, we can address the question of whether X-ray bright points represent a distinct class of solar activity. No peculiar properties set our event apart from the wide variety of larger solar flares which occur generally in regions characterized by larger amounts of magnetic flux. Golub et al. (1976) have found that the longer-lived X-ray bright points generally reach larger sizes than is normal and, like our event, tend to occur within 30° of the equator. Such long-lived, bigger bright points may produce stronger flares than is typical. This would be consistent with our failure to see other radio bursts corresponding to shorter-lived X-ray bright points.

Acknowledgement. We thank D. M. Rust for bringing the importance of solar X-ray bright points to our attention. We also acknowledge the help of H. P. Gagnon and M. B. Bell in providing solar patrol radio data and of R. L. Moore for coordinated Hz observations at Caltech. Special thanks are due to A. Groen at ORSO and to R. Stefanik and the receiver group at ARO for technical assistance. A. Kryworuchko and G. Robinson assisted with reduction of the data. One of us (CJW) acknowledges support by NASA contracts NAS5-11360 and NAS5-22411, and by the Lockheed Independent Research Program.

References

- Bell, M. B.: 1976, private communication
- Golub, L., Krieger, A. S., Silk, J. K., Timothy, A. F., Vaiana, G. S.: 1974, *Astrophys. J. Letters* **189**, L 93
- Golub, L., Krieger, A. S., Silk, J. K., Timothy, A. F., Vaiana, G. S.: 1975, in *Solar Gamma-, X-, and EUV Radiation*, IAU Symposium 68, ed. S. R. Kane, p. 23
- Golub, L., Krieger, A. S., Vaiana, G. S.: 1976, in press
- Harvey, K. L., Martin, S. F.: 1973, *Solar Phys.* **32**, 389
- Harvey, K. L., Harvey, J. W., Martin, S. F.: 1975, *Solar Phys.* **40**, 87
- Maxwell, A.: 1976, private communication
- Warwick, J.: 1976, private communication

OSO-8 OBSERVATIONS OF THE SOFT X-RAY
CONTINUUM IN SOLAR FLARES

D. Datlowe

Reprinted from Hansen and Schaffner, eds.,
Proceedings of the November 7-10, 1977
OSO-8 Workshop (1977), pp. 277-278

OSO-8 OBSERVATIONS OF THE SOFT X-RAY CONTINUUM IN SOLAR FLARES

Dayton Datlowe

Lockheed Palo Alto Research Labs
3251 Hanover Street
Palo Alto, California 94304

SUMMARY

The soft X-ray continuum in solar flares is thermal bremsstrahlung from hot coronal plasmas. The heating of this plasma is one of the principal forms of energy release in flares. Results from the SKYLAB mission have emphasized the importance of arch structures in the morphology of this plasma.

This paper is a study of the temperature and emission measure evolution of the hot flare plasma as observed in 24 events by the Lockheed OSO-8 Mapping X-ray Heliometer (MXRH). Previous studies of the evolution of these plasma parameters include Culhane and Phillips (1970), Kahler and Kreplin (1971), Horan (1971), Datlowe *et al.*, (1974), and Pallavicini, Serio, and Vaiana (1977). The Lockheed instrument is a modulation collimator system which images the sun with 2 arc minute resolution. Photons from 2-15 keV are analyzed into 14 pulse-height channels. The instrument has 3 proportional counters with an effective area of 25 cm^2 at 8 keV, and one system has a 1 cm^2 effective area counter which is automatically switched in by high counting rates during flares. Because the instrument can isolate the X-ray flux from a particular active region and reject the remainder of the solar background, it is more sensitive than the non-imaging systems used in earlier studies.

To determine the temperature and emission measure during an event, observed pulse-height distributions are compared with a set of model spectra to find the minimum chi-squared. The source spectra are computed according to the methods of Tucker and Koren (1971), including line emission, free-free, and free-bound bremsstrahlung. These spectra have been folded through the detector response to give a set of comparison spectra.

The principal features of the evolution of these soft X-ray flares are the exponential growth of emission measure during the rising phase of the event, and the slow decrease in the emission temperature throughout all but the very

beginning of the event. These features have been well documented previously. As compared with sets of events studied before, the OSO-8 events are typically smaller. The time required to reach maximum emission measure is characteristic-
ically longer for these small events. The MKRH can easily measure temperatures as low as 3×10^6 K for active region studies. Nonetheless, peak flare temperatures less than 10×10^6 K were not observed even in the smallest of the 24 events. There is a sharp cutoff in the distribution of peak temperatures at 10^7 K, indicating temperatures above 10^7 K are required for these subflares to occur.

References:

- Culhane, J.L. and Phillips, K. 1970: Solar Physics 11 117.
Kahler, S.W. and Kreplin, R.W. 1971: Astrophysical Journal 168 531.
Horan, D.M. 1971: Solar Physics 21 188.
Datlowe, D.W., Hudson, H.S. and Peterson, L.E. 1974: Solar Physics 35, 193.
Pallaivicini, R., Serio, S. and Vaiana, G.S. 1977: Astrophysical Journal
216 108.
Tucker, W.H. and Koren, M. 1971: Astrophysical Journal 168 283.

This work was supported by National Aeronautics & Space Administration contracts NAS5-22411 and NAS5-11360.

EVOLUTION OF THE X-RAY EMITTING CORONA
PRECEDING AND AFTER MAJOR SOLAR EVENTS

C.J. Wolfson, L.W. Acton, D.T. Roethig
and M. Walt

Reprinted from Shea, Smart, and Wu, eds.,
Contributed Papers to the Study of Travelling
Interplanetary Phenomena/1977 (1978),
pp. 295-305

Evolution of the X-ray Emitting Corona Preceding and After Major Solar Events

C. J. Wolfson, L. W. Acton, D. T. Roethig, and M. Walt
Lockheed Palo Alto Research Laboratory
3251 Hanover Street
Palo Alto, CA 94304, USA

Abstract

Soft X-ray emission from the sun during STIP Interval II, observed with the Lockheed Mapping X-ray Heliometer on the NASA OSO-8 satellite, is presented. In examining the emission versus time for extended intervals around the times of the Class 1B flare on March 28, 1976, and the Class 1B flare on April 30, 1976, we find significantly more low level flare activity prior to the major flares than after. Twelve modest X-ray bursts are investigated and no compelling case of a preflare brightening phase is observed. Preliminary correlations with the time history of emitted solar particles are discussed.

1. INTRODUCTION

This study examines the condition of the solar corona prior to, during, and following two large solar flares which occurred during STIP Interval II. The principal observations which will be used are at X-ray wavelengths, and therefore provide an indication of the processes taking place in the high temperature plasma. Correlations with other related phenomena, to the extent presently available, will also be used to elucidate the entire flare phenomena.

The X-ray observations were obtained with the Lockheed Mapping X-ray Heliometer (MXRH) on the NASA Orbiting Solar Observatory-8 (OSO-8) satellite. The MXRH became operational on June 24, 1975, and obtained data through STIP Intervals I, II and III. A brief description of the MXRH instrument, the data coverage during STIP Interval II, and several sets of data for periods of major activity during this interval will be published in the UAG Special Report on the Retrospective World Interval 20 March to 5 May 1977 (Wolfson, Acton, Roethig, and Smith, 1977). That article will hereafter be referred to as Paper I and information in Paper I will in general not be restated in this paper.

The MXRH instrument responds to X-rays in the 1.5 - 30 keV energy range although the effective high energy limit for solar observations is usually substantially lower than 30 keV due to the steepness of the solar spectrum.

The instrument looks radially outward from the rotating wheel section of the OSO-8 satellite. It contains three detection systems, each collimated in one dimension with mechanical collimators. The collimators have a full width at half maximum transmission of 2 minutes of arc, although other instrumental effects broaden the instrument response function to about 4 minutes of arc under some conditions. Each field-of-view is tilted 120° with respect to the others. These three systems are called Vertical, Slant A and Slant B, with the Vertical system field-of-view parallel to the satellite spin axis. As the wheel rotation sweeps these fields of view across the sun, three one-dimensional count rate distributions are obtained. These distributions permit the location and isolation of emitting X-ray regions. Each spatial distribution consists of 31 successive strips, or area segments, parallel to a system's field-of-view.

An example of these distributions is shown in Figure 1, where the map for 1521-1524 UT on March 28 is presented. This example demonstrates how active regions which are overlapping in one detection system may be clearly resolved in a different system. The instrument maps the entire solar disk every 40 seconds. Longer integration times are required to detect regions of weak emission. Temporal information is obtained by monitoring the intensity versus time for selected area segments. Spectral information is obtained by 15 channel analysis of the proportional counter signals.

A more complete description of the MXRH may be found in Paper I and detailed information is given in the Technical Manual for the Mapping X-ray Heliometer Instrument on OSO-8 (Wolfson, Acton, and Gilbreth, 1975). Daily MXRH maps of the sun since August 1975 have been published in Solar Geophysical Data (SGD). It is anticipated that the MXRH will continue operation until at least October 1978.

The three largest solar flares observed by the MXRH between July 1975 and January 1977, as defined by either the magnitude of the resultant geomagnetic storm or the maximum intensity of the soft X-ray emission, occurred during STIP Interval II. In this paper we will study the time periods around the flare which occurred near 1930 UT on March 28 and the flare near 2115 UT on

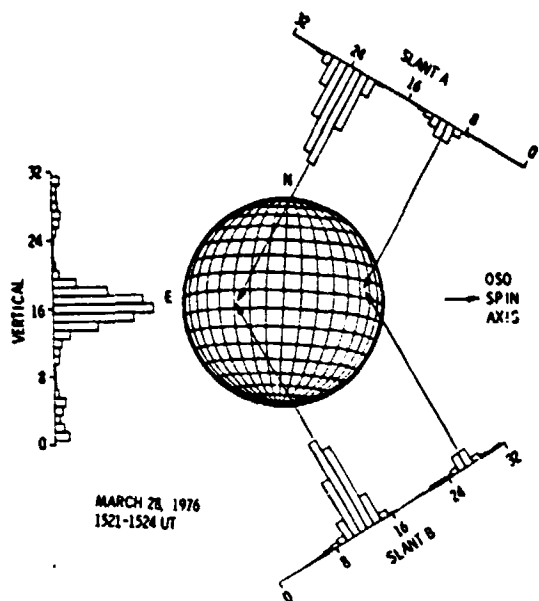


Figure 1. The X-ray Sun Prior to the Large Flare of McMath 14143 Near 1930 UT. The MXRH data are collected and displayed in terms of 32 numbered area segments, each 1.3 arc minutes in width. Each histogram is normalized to the peak intensity for that detection system. The arrows converge on McMath 14143 (\sim S7 E28) and McMath 14146 (\sim NS W55).

April 30. These two events were chosen in preference to the event near 0900 UT on March 23 since these two flares occurred well away from the solar limb thereby increasing the likelihood of the correlation with data from other observing instruments. The event of March 23 was at, or slightly behind, the visible east limb.

2. EVOLUTION OF X-RAY EMISSION

Figures 2 and 3 show soft X-ray intensity light curves for extended intervals around the times of the two major flares. The solid portion of the curve is a normalized MXRH count rate from the region which produced the major flare. OSO-3 views the sun for approximately 60 minutes out of every 90 minute orbit. Additionally, data losses result when the satellite is in the high background environment of the South Atlantic Anomaly radiation zone. We have drawn dashed curves through the MXRH data gaps based on the NOAA 1-8 \AA full sun X-ray observations (Donnelly, private communication, 1977). Minor variations, and variations known to be from a different region by optical observations, were eliminated from the NOAA data. Reported (SGD) optical flares and subflares are also indicated. Except for the two class 1B flares, one on March 28 and one on April 30, all of the H α enhancements were classified as subflares. Some higher time resolution data may be seen in Paper I.

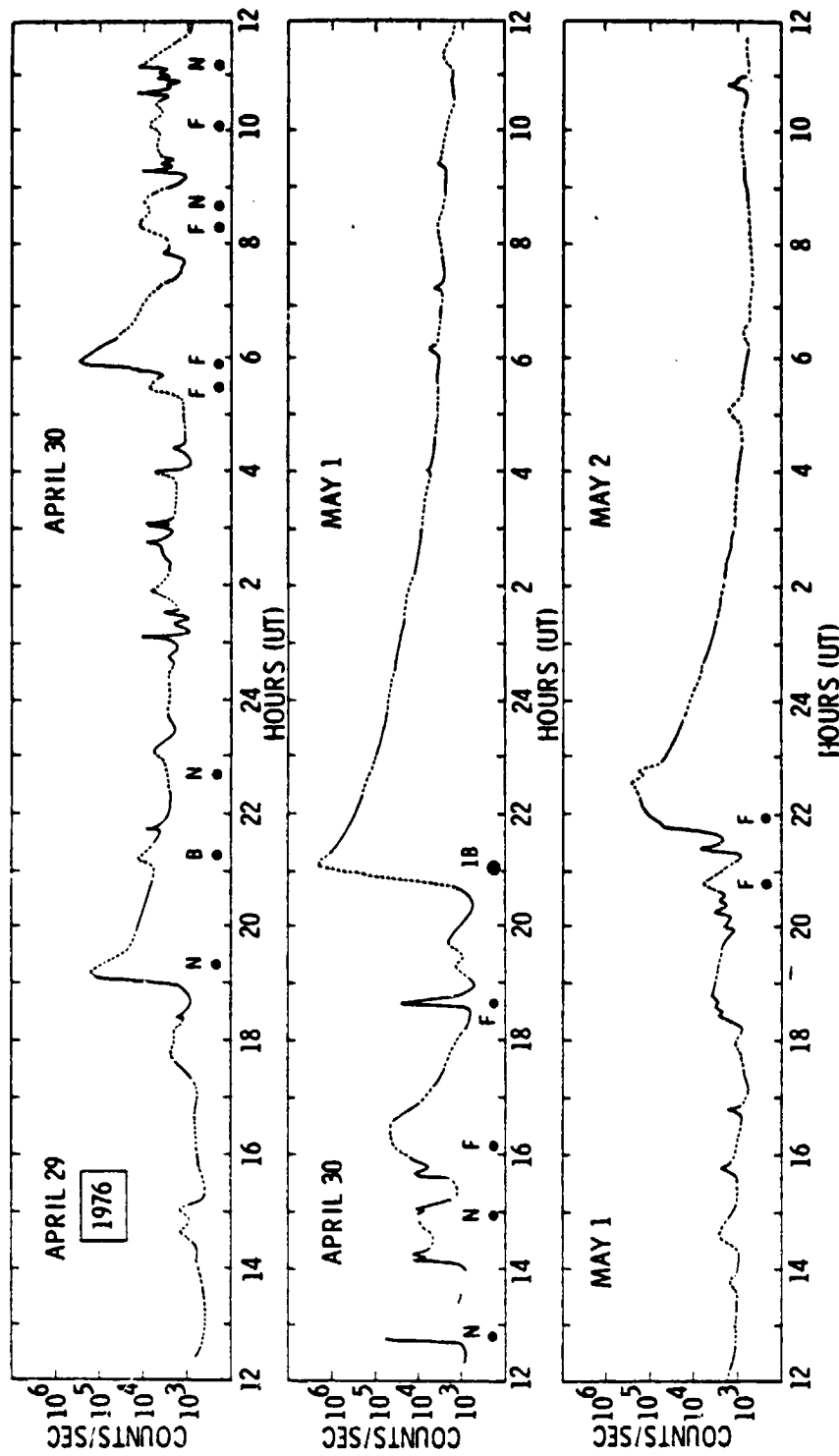


Figure 2. Light Curve of X-ray emission from McMath 14179. The data were collected from various MGRH detectors and normalized to the equivalent rate for the Vertical Large detector. The gaps in the MGRH data have been sketched-in based on data from the NOVA full sun X-ray monitors. Optical flares and subflares, as reported in Solar Geophysical Data, are also indicated.

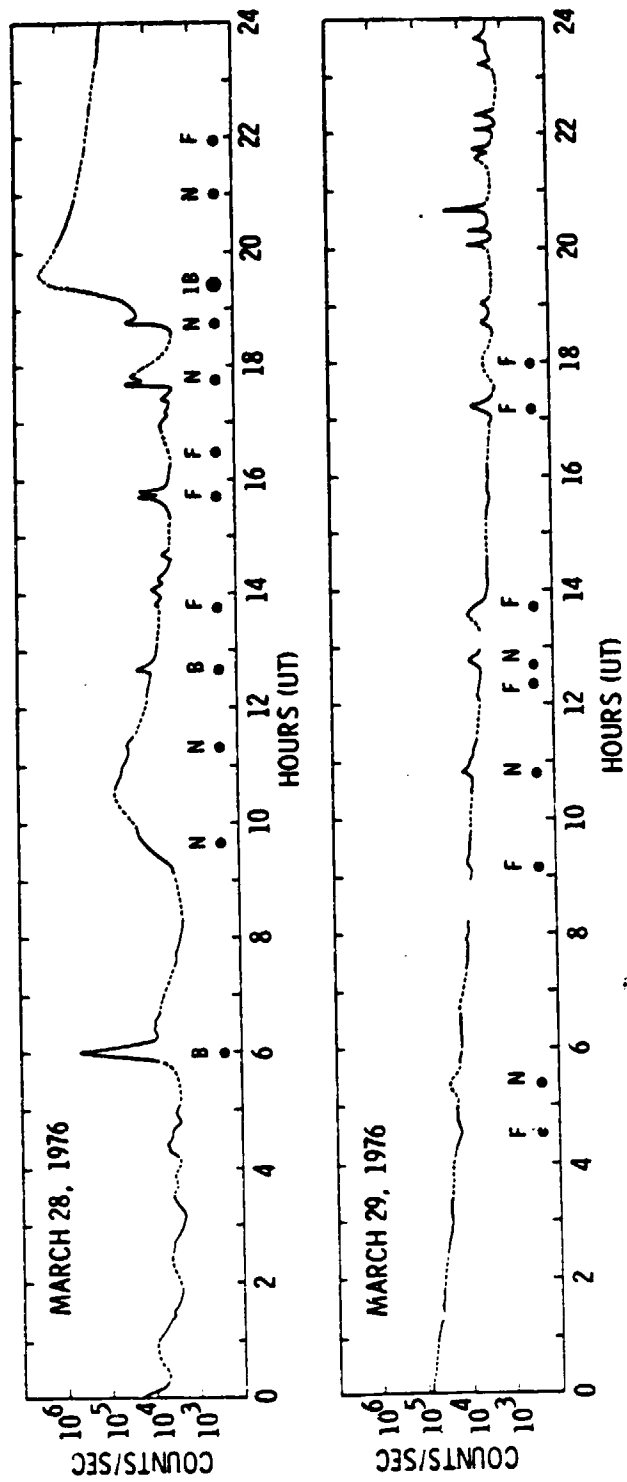


Figure 3. Light Curve of X-ray Emission from McMath 14143

2.1 Frequency of Flare Occurrence

An examination of Figure 2 demonstrates that for about a day prior to the proton producing flare of April 30 the X-ray emission is quite bursty with the emission seldom dwelling at the baseline intensity of $\sim 10^3$ cts/s. After the flare there is a long decay with very few significant bursts. The lack of post flare bursts may be partially attributed to the high baseline during the early decay. However, by 0400 UT on May 1 the baseline is down to 5×10^3 cts/s and bursts of 5×10^3 cts/s would be easily seen. There are none until 2120 UT. In comparison, there are about 16 bursts with intensity increases of more than 5×10^3 cts/s during the 24 hours prior to the major flare.

Similar variations in the frequency of the H α flares, as well as full disk X-ray bursts, prior to and after major solar flares have been reported previously (Krivský, 1973; Dodson and Hedeman, 1976). Flare occurrence is usually considered to be closely correlated to the complexity of the active region magnetic field. However, searches for flare-associated magnetic field restructuring with photospheric magnetographs have produced ambiguous results. The above MXRH burst frequency comparison may indicate that such a restructuring toward a configuration of lower potential energy does occur, at least at the higher levels where the X-ray bursts appear to originate.

About 24 hours after the flare of April 30 a moderately large event is observed. This time for building back up to a flare-prone configuration is consistent with that stated by Svestka (1976) and with the calculated times for building up a stressed magnet γ -configuration containing the appropriate quantities of energy (Tanaka and Nakagawa, 1973).

The comparison of the frequency of significant flares prior to and after the March 28 event (Figure 3) is not as striking as for the April 30 event. This is partially because it takes nearly twice as long to decay to 5×10^3 cts/s. However, we do observe six bursts of 5×10^3 cts/s in the 20 hours prior to the event, and none until about 24 hours after; though there are four bursts of $\sim 2 \times 10^3$ cts/s. The general pattern of more activity prior to the event than after is therefore still maintained.

2.2 Pre-Flare Brightening

Some flare theories (Priest, 1976; Spicer, 1976) contain a pre-flare brightening or pre-flare heating phase that may be observable in the soft X-ray emission. The duration and magnitude of this phase are not uniquely specified, but a time of approximately 10 minutes to an hour is typically expected. Some observers have reported data consistent with a pre-flare brightening phase (Pallavicini et al., 1975; Petrasco et al., 1975) while others have reported a systematic lack of pre-flare brightening (Kahler and Buratti, 1976). None have had access to continuous high time resolution data of a single region such as the MXRH provides.

We have studied the MXRH data for the two periods of interest to see if pre-flare brightening is observed. Twelve X-ray bursts with appropriate pre-flare data were examined and not one compelling case of pre-flare brightening was found. Six bursts were clear counter examples. This result indicates that pre-flare heating does not usually involve significant amounts of material at temperatures of 2 million degrees or above. In contrasting our results with those from the Skylab soft X-ray imaging experiments, it should be noted that the MXRH low energy limit is about the same as the high energy limit of the Skylab instruments, so energy and temperature dependent phenomena may be observed differently by the two types of instruments.

A related observation is that flares from the same region show a wide variation in rise times and fall times, and that two (or more) bursts are frequently superimposed. A statistical evaluation of causality is beyond the scope of this paper. It is possible that some reported pre-flare brightenings were actually double flares where the early flare had a very slow rise time.

3. ENERGY OUTPUT

To obtain the X-ray energy radiated from the two major flares we first determine the parameters of the isothermal hot plasma which most closely reproduce the observed pulse height distributions during the flares. An updated version of the code developed by Tucker and Koren (1971) for the emission from a low density, high temperature plasma is used for this determination. Two parameters, temperature and emission measure ($\int n_e^2 dV$), are derived. The radiation predicted by the model for any wavelength interval can then be calculated. The 1-8 Å wavelength band was chosen because it corresponds reasonably well to the MXRH sensitivity range and is the commonly used interval for the SOLRAD and NOAA full sun monitors. The resultant MXRH fluxes are typically consistent with the NOAA monitor fluxes when the region of interest dominates the disk and is non-flaring, while the MXRH values are somewhat lower near the peak of large flares.

The MXRH did not observe the peak of either major flare. For the April 30 flare our observations began at 2121 UT, about 7 minutes after peak emission. For the March 28 flare our observations ended at 1918 UT and began again at 2004 UT while flare maximum was about 1940 UT. The MXRH fluxes were extrapolated through these gaps. We obtain a total X-ray output (1-8 Å) of 6×10^{29} ergs for the April 30 flare and 1×10^{30} ergs for the flare of March 28.

4. RELATED OBSERVATION

The possibility of combining the X-ray data with information from other experiments should be greatly enhanced by interactions at this symposium. Our preliminary efforts in this direction have centered around examining particle observations for the April 29 to May 2 interval. This interval was selected because it contained a high energy proton event and because the source, McMath 14179, was on the western portion of the disk and thus had good access to the interplanetary magnetic field lines leading to the earth. The non X-ray data thus far examined are: 1) the IMP 7 and 8 relativistic electron fluxes as provided to us by J.M. Krimingis of John Hopkins Applied Physics Laboratory, 2) the IMP 7 and 8 high energy proton fluxes as presented in SGD, and 3) radio observations from SGD.

The high energy proton data show a five order of magnitude increase correlated with the major flare of April 30, but no detectable increases with any of the other flare activity. These data will not be discussed further.

The > 0.22 MeV electron data from IMP-7 and IMP-8 are shown in Figure 4 along with a compressed version of the X-ray fluxes previously presented in Figure 2. Periods when Type II and Type IV radio noise was detected, indicative of significant particle acceleration, are also shown. The electron curve is dominated by the major event at 2115 UT on April 30. Increases are also seen associated with the modest X-ray bursts (K_r subflares) at 0600 UT

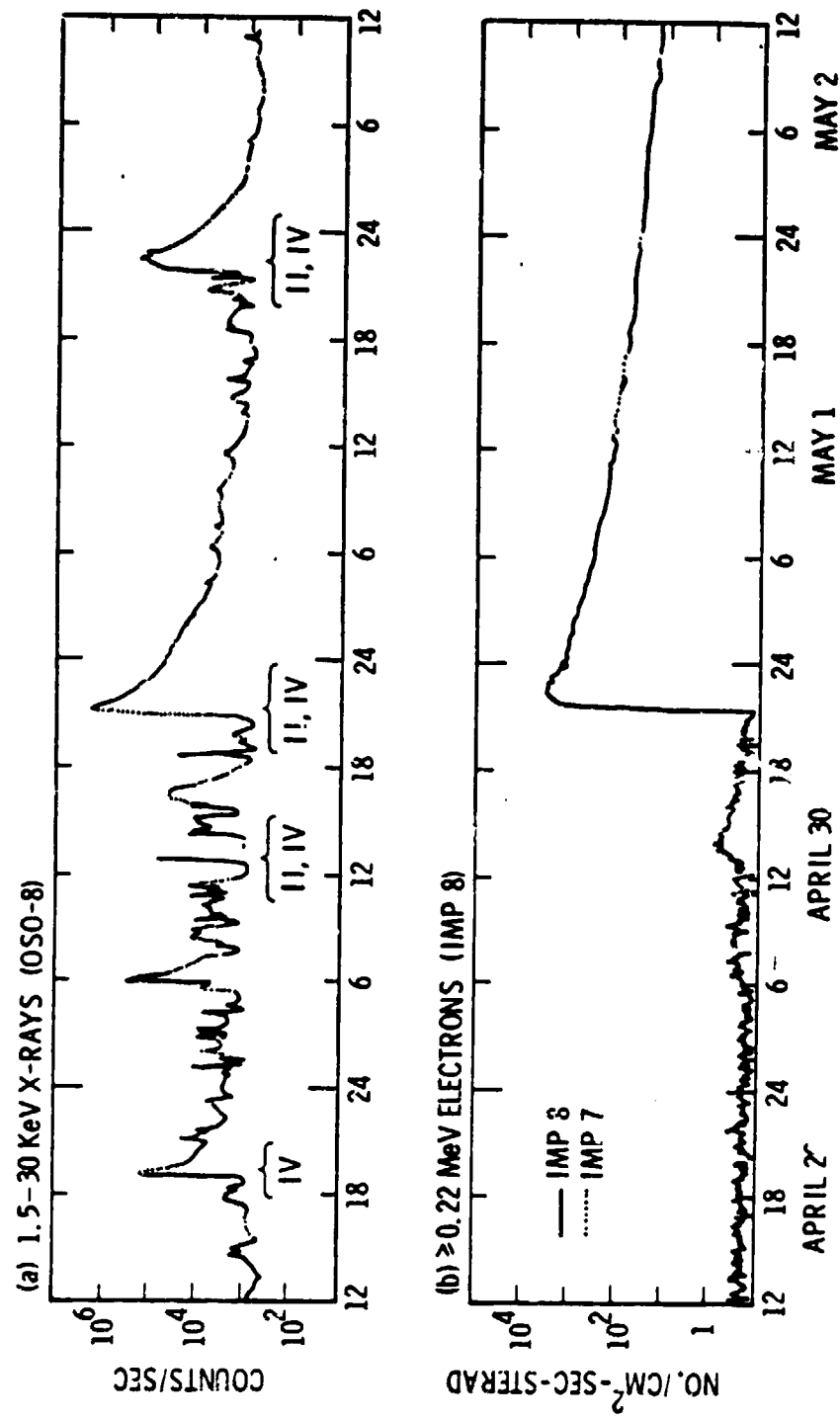


Figure 4. Light Curves of X-ray Emission and Electron Fluxes. Type II and Type IV radio events, as reported in Solar Geophysical Data, are also indicated.

and 1250 UT on April 30. However, no detectable electron enhancements occurred in conjunction with the burst at 1930 UT on April 29 or with the flare at 2200 UT on May 1.

It is interesting to note that the time dependence of the electron flux for the subflare at 1250 UT resembles the major flare both in rise time to maximum and decay rate, indicating that the interplanetary propagation conditions and injection rates were similar at both times. The similarity in shapes also adds confidence to associating the electron enhancement with the subflare. The short time intervals (1.1 to 1.5 hr) required for the electron flux to reach maximum is consistent with a direct magnetic connection and a relative long scattering mean free path in the interplanetary medium (Lanserotti et al., 1973). The electron flux increase following the subflare at 0600 UT is much less pronounced and is too uncertain to provide propagation information.

The lack of a significant electron enhancement from the subflare at 1930 UT on April 29 is surprising, as this event was comparable in X-ray yield with the two subflares which did produce electrons. The active region was somewhat less favorably situated at that time (W30), but it seems unlikely that this is the dominant difference.

No electron enhancement was observed accompanying the flare late on May 1 although the flare was very favorably located (W60) for propagating electrons to earth and it might have been expected that the major flare a day earlier would have smoothed out inhomogeneities in the interplanetary field and improved the propagation characteristics (Bukata and Palmeira, 1967). However, at the time of the May 1 flare the decaying electron flux from the April 30 event was still two orders of magnitude above the quiet time background values and a moderate electron flux increase would not have been noted.

5. SUMMARY

Using data which were obtained with the Lockheed MXRH experiment on OSO-8, we have studied the solar soft X-ray emission for periods including the major flares of March 28 and April 30, 1976. Our data are consistent with models which predict significantly more activity prior to a major flare than after, and with approximately one day as the time required to build up the configuration for a subsequent large flare. The data are, in general, not consistent with a pre-flare X-ray brightening phase on the time scale of 5-60 minutes.

Examination of >0.22 MeV electron data for a period including the April 30 event shows that small enhancements were detected from two subflares prior to the IB flare and that a large flux was promptly detected in correlation with the IB flare. Somewhat surprisingly no electron enhancements were detected from the flares about a day earlier (1930 UT on April 29) and a day later (2200 UT on May 1). The lack of an enhancement on May 1 may be simply because the intensity was still quite high due to the major event.

Acknowledgments

The authors wish to acknowledge the team that conceived, designed, fabricated and presently operate the MIRI instrument, especially Project Engineer, C.W. Gilbreth and ground station scientist, K.L. Smith. Useful scientific discussions with J.W. Leibacher and J.M. Mosher are gratefully acknowledged. Special thanks are extended to R.F. Donnelly of NOAA and S.M. Krimigis of Johns Hopkins Applied Physics Laboratory for providing us with their data. This program has been supported by the National Aeronautics and Space Administration under Contracts NAS5-22411, NAS5-11360, and by the Lockheed Independent Research Program.

References

- Bukata, R. P., and R. A. R. Palmeira, The effects of the filamentary interplanetary field structure on the solar flare of May 4, 1960, J. Geophys. Res., 22, 5563, 1967.
- Dodson, H. W., and E. R. Hedeman, Some comments on flares after many years of observations, Solar Phys., 47, 267, 1976.
- Kahler, S. W., and B. J. Buratti, Preflare X-ray morphology of active regions observed with the A S and E telescope on Skylab, Solar Phys., 47, 157, 1976.
- Křížský, L., Sudden changes of activity before proton flares (events of August 1972), Bull. Astron. Inst. Czech., 24, 375, 1973.
- Lanzerotti, L. J., D. Venkatesan, and G. Wibberenz, Rise time to maximum flux of relativistic solar electron events and its relation to the high frequency component of the interplanetary field power spectrum, J. Geophys. Res., 78, 7986, 1973.
- Pallavicini, R., G. S. Vaiana, S. W. Kahler, and A. S. Krieger, Spatial structure and temporal development of a solar X-ray flare observed from Skylab on June 15, 1973, Solar Phys., 45, 411, 1975.
- Petrasco, R. D., S. W. Kahler, A. S. Krieger, and J. K. Sijk, The location of the site of energy release in a solar X-ray subflare, Ap. J. (Letters), 199, L127, 1975.
- Priest, E. R., Current sheet models of solar flares, Solar Phys., 47, 41, 1976.
- Spicer, D. S., An unstable arch model of a solar flare, NRL Report 8036 (Naval Research Laboratory, Washington, D.C.) 1976.
- Švestka, Z., Solar Flares, D. Reidel, Dordrecht, The Netherlands, 1976.
- Tanaka, K., and Y. Nakagawa, Force-free magnetic fields and flares of August 1973, Solar Phys., 33, 187, 1973.
- Tucker, W. H., and M. Koren, Radiation from a high temperature, low-density, plasma: the X-ray spectrum of the solar corona, Astrophys. J., 168, 283, 1971.

Wolfson, C. J., L. W. Acton, and C. W. Gilbreath, Mapping X-ray Heliometer for OSO-8, Final Report, NASA-CR-144710, 1975.

Wolfson, C. J., L. W. Acton, D. T. Roethig, and K. L. Smith, 2-30 keV X-ray data from OSO-8, Collected Data Reports for STIP Interval II 20 March - 5 May 1976, Edited by H. E. Coffey and J. A. McKinnon, World Data Center A for Solar-Terrestrial Physics Report No. UAG-61, 187, 1977.

Discussion

Kaufmann: In high sensitivity tracking of an active solar center at 13 mm wavelength, in July 1974, we observed time features very much comparable to the soft X-ray results presented here.

Wolfson: Thank you for that interesting comment. Kundu of the University of Maryland has told me that he does see evidence of preflare heating for some radio events.

Appendix I

X-RAY EMISSION ASSOCIATED WITH FILAMENT ACTIVITY

L.W. Acton and J.M. Mosher

Reprinted from Jensen, Maltby and Orrall, eds.,
I.A.U. Colloquium #44 (1978), pp. 269-272

C - 2

X-RAY EMISSION ASSOCIATED WITH FILAMENT ACTIVITY

L.W. Acton and J.M. Noshier
Lockheed Palo Alto Research Laboratory
Palo Alto, California

The purpose of this research is to investigate the temporal and spatial relationships of activated filaments, soft X-ray production, and H_α flares. The X-ray data are from the Lockheed Mapping X-Ray Heliometer (MXRH) on OSO-8 (Wolfson et al., 1975, 1977). This instrument has been operating continuously since July 1975. It responds to radiation from solar plasma above about 2×10^6 K, provides a time resolution of 20 sec, a spatial resolution of 2-3 arc min and has a basic sensitivity roughly equivalent to the 1-8 Å full disc monitors of, e.g., the SOLRAD and SMS/GOES satellites (threshold $\approx 2 \times 10^{-9}$ W/m²). However, because of its spatial resolution the MXRH permits study of small X-ray events in individual active regions even when the integrated solar X-ray emission is high.

The events finally chosen for study were selected from a sample of 114 hours of the very best, high resolution, H_α records of active regions gleaned from about 150 days of observations of active regions by Big Bear Solar Observatory, all with simultaneous MXRH coverage. In the final data set, 20 flares were chosen for detailed study. Of these 10 were significant flares and 10 were smaller flare-like events. The largest flare was an Importance 1 proton event on April 30, 1976. Blue wing observations were available for about half of these events.

We have examined these data for pre-flare filament activation and pre-flare X-ray enhancements with the object of discovering a link between the two phenomena - if they exist at all. To the limits set by these data we find no convincing evidence for consistent pre-flare effects in H_α or X-rays.

As to whether there is, even in H-alpha, a distinct pre-flare filament activation phase we should mention that our viewing of these films did not convince us of the general usefulness of the conclusions of Martin and Ramsey (1972) or of Martres et al. (1977). The effects of which they speak seem very subtle to less experienced observers like ourselves. In each flare there was undoubtedly some sort of preflare filament activity that could be pointed out somewhere in the region, but, by the same token, there seemed to be innumerable examples of similar filament activity which did not result in flares. We did not get the impression that the kinds of flares which we were looking at could be predicted by watching what was happening to the filaments. Perhaps this is because we are looking at small events.

Likewise, study of the pre-flare X-ray light curves of these events reveals no consistent evidence for pre-flare heating. This is in agreement with the results of Wolfson, et al. (1978) for a randomly selected sample of 46 flares. On the other hand, we find a general, although by no means proportional, correlation between soft X-ray light curves and H_a emission in agreement with the comments of Dodson and Hedeman (1976).

In summary, for these rather small flares and flare-like events, we would have to say that we do not see any striking correlation of filament activity with pre-flare periods, nor, at the sensitivity of our instrument, do we find the gradual systematic pre-flare X-ray enhancements that have been reported by some experimenters (Teske and Thomas 1969; Thomas and Teske 1971). As to the general relationship between filament activity and X-ray enhancements we are less certain. Aside from the disperition brusque, it seems clear that filament activity itself is not directly responsible for any dramatic effects in X-rays, and even there, the enhancement comes after the filament has disappeared (e.g. Webb et al., 1976). As to more subtle correlations, we are limited by the spatial resolution of our experiment, which sometimes makes it rather difficult to know exactly which chromospheric phenomenon is associated with the effects we see.

This research was supported by the U.S. National Aeronautics and Space Administration under contract NAS5-22411. We are indebted to Big Bear Solar Observatory, Tel Aviv and Catania Observatories for Ha films used in this study.

References:

- Dodson, H.W. and Hedeman, E.R.: 1976, *Solar Phys.* 47, 267-275.
Martin, S.F. and Ramsay, H.E.: 1972, *Solar Activity Observations and Predictions* (Vol. 30 of *Progress in Astronautics and Aeronautics series*), P.S. McIntosh and M. Dyer (eds.) 371-387.
Martres, M-J., Soru-Escaut, I. and Nakagawa, Y.: 1977, *Astron.Astrophys.* 59, 255-259.
Teske, R.G. and Thomas, R.J.: 1969, *Solar Phys.* 8, 348-368.
Thomas, R.J. and Teske, R.G.: 1971, *Solar Phys.* 16, 431-453.
Webb, D.F., Krieger, A.S. and Rust, D.M.: 1976, *Solar Phys.* 48, 159-186.
Wolfson, C.J., Acton, L.W. and Gilbreth, C.W.: 1975, Mapping X-Ray Heliometer for OSO-8 Final Report, NASA-CR-144710.
Wolfson, C.J., Acton, L.W., Leibacher, J.W. and Roethig, D.T.: 1977, *Solar Phys.* 55, 181-193.
Wolfson, C.J., Acton, L.W. and Leibacher, J.W.: 1978, presented at the 152nd AAS Meeting, June 1978.
Abstract: *Bull Am.Astron.Soc.* 10, 456.

Appendix J

**A SUMMARY OF LOCKHEED X-RAY DATA FOR MCMATH 14943 AND FOR
THE FLARE OF NOVEMBER 22, 1977**

J.M. Mosher, G.H. Bruner and C.J. Wolfson

Special report prepared for World Data Center A (1978)

A SUMMARY OF LOCKHEED X-RAY DATA FOR McMATH 14943 AND FOR
THE FLARE OF NOVEMBER 22, 1977

by

J.M. Mosher, G.H. Bruner and C.J. Wolfson
Lockheed Palo Alto Research Laboratory
Palo Alto, California

1. INTRODUCTION

Since June, 1975, the Lockheed Mapping X-Ray Heliometer (MXRH) onboard OSO-8 has provided essentially continuous coverage of solar activity in the 2-15 keV X-ray band via one-dimensional collimators and proportional counter detectors. The present contribution summarizes the data obtained for McMath 14943, during September, 1977, and for the flare of November 22, 1977.

2. INSTRUMENTATION

The design and operation of the MXRH instrument were described in our submission to UAG Report 61 (Wolfson et al., 1977). More detailed information is provided in Wolfson et al. (1975). For the present purpose, it is sufficient to know that the data are collected in a manner such that count rates can be extracted in various combinations of arc-minute wide linear strips laid across the sun in three orientations at 120° to one another. Within any strip the counts can be further subdivided into 15 pulse-height (i.e., energy) channels, on the basis of which the effective temperature and emission measure of a source within the strip can be determined.

The 550 km altitude of the OSO-8 orbits limits data collection to 60 minute daylight segments separated by 30 minute periods of darkness. Additional intervals of up to 32 minutes are lost when the detector high voltages are switched off as the spacecraft passes through the South Atlantic Anomaly. The resultant average coverage is about 50%, with a measurement every 10 seconds in one of the three collimator systems during the active periods.

3. GENERAL NATURE OF X-RAY OBSERVATIONS FOR SEPTEMBER, 1977

An examination of MXRH maps from September 8 to September 22, 1977 shows that the intense magnetic complex formed by McMath 14943 and its smaller companion region McMath 14942 was the dominant X-ray source on the sun during the entire course of its disk passage. No attempt has been made to separate the signals from the two, since at the resolution of the MXRH the sources are essentially unresolved. McMath 14943 is presumably the main contributor based on H-alpha flare reports.

Next to this complex, the second most important producer of X-ray emission was McMath 14952, in the opposite hemisphere. While in its non-flaring state it was roughly an order of magnitude dimmer than McMath 14943, it could, during flares, briefly dominate the sun. On two occasions

(September 18 at 1922 UT and September 19 at 1937 UT) the MXRH shows it reaching four times the brightness of McMath 14943 in the 2 - 15 keV band. On a number of other occasions it achieved approximate equality (e.g.: September 18 at 2326 UT, September 19 at 1534 UT, and September 22 at 0820 UT). The only other region to achieve this distinction was McMath 14930. On September 13 at 1125 UT when it was on the NW limb and McMath 14943 was at a low ebb, it reached about two-thirds of the intensity of McMath 14943.

4. OBSERVATIONS OF McMATH 14943

A. Light Curve

Variations in the X-ray intensity of McMath 14943 (or, more properly, of the unresolved activity complex formed by McMath 14943 and its companion region McMath 14942) from September 5 through September 25, 1977 were investigated by constructing eighty four 6-hour light curves using the Vertical detector system. Data in this system are collected once every 20 seconds; using the Vertical Large detector for count rates below 15,000 cps, and the 15 times less sensitive Vertical Small Flare detector for count rates above that level. The approximate energy coverage is 2 - 15 keV for either detector, with most of the counts coming at the low-energy end. Two small data gaps, one of 5 hours on September 10 and the other of 5 hours on September 11 were introduced by operational errors.

For an example of a typical Vertical collimator light curve, see Figure 3. A summary presentation of all individual light curve results for McMath 14943 is given in Figure 1, where each vertical bar represents the span of count rates encountered in a 90-minute orbit, and the connected dots are orbital averages. In preparing this plot, the problem of detector switching discussed in Wolfson *et al.* (1977) has been avoided by manually sliding the Small Flare data by a factor of 15 so as to obtain an effective count rate in Vertical Large. Even so, the magnitudes of five of the major flare events are not accurately represented since they were sufficiently intense to produce overflow and saturation even in this least sensitive of the MXRH detectors. The maxima of smaller flares will also be underestimated whenever their peaks happen to fall in MXRH data gaps.

Data have been shown only for September 6 through September 24, since before and after these dates the weakening signal from the source behind the limb became blended with comparable signals from smaller sources on the visible disk (McMath 14941 in the East and McMath 14943 in the West) in such a way that the two signals could not be easily disentangled at the resolution of the MXRH. For the interval shown, observations of McMath 14943 in the Vertical system should be clean.

One of the main observational results illustrated by Figure 1 is the sporadic nature of the flare occurrences, with two periods of distinct activity separated by a relatively long dry spell. This variation does not appear to be related to any obvious change in the photospheric magnetic structure.

In general the timings of the X-ray flares (particularly the start and peak times) coincide very well with the H-alpha times reported in Solar-Geophysical Data, but there can be a considerable variation in the magnitudes of X-ray events corresponding to a given H-alpha class, particularly sub-flares. For example, a class -N subflare reported by three observatories at 1850 UT on September 11 produced more than a hundred-fold enhancement in the 2 - 15 keV X-ray intensity, whereas some other events in this class cause scarcely a ripple.

In relating MXRH observations to terrestrial effects, it should be noted that for an average solar active region producing a count rate R (cps) in the Vertical Large detector, the 1-8 Å X-ray energy flux (I) it creates at the top of the earth's atmosphere is given approximately by:

$$I_{\text{1-8 } \text{\AA}} = 10^{-9} \times R^{0.75} \text{ W/m}^2$$

Individual regions, with distinctive spectral characteristics, deviate from this empirical relationship by factors on the order of 2 or 3.

B. Identification of Behind the Limb Bursts

Since for the bulk of its disk passage McMath 14943 was the dominant solar X-ray source, the data provided in Figure 1 are largely redundant with those provided by full-disk X-ray monitors, such as the ones on NOAA's SMS and GOES satellites. The MXRH is particularly useful, however, in the identification of behind the limb bursts.

Figure 2 shows MXRH maps for the first and last bursts that could definitely be attributed to McMath 14943 (and which terminate the plot in Figure 1). In each case, the approximate position of this source on the back-side of the sun is indicated, along with the location of the most plausible alternative source on the visible disk. The fact that no associated H-alpha activity was reported in these alternate sources, together with the fact that the location of the observed X-ray emission on the limb coincides with that of a source suspended radially above McMath 14943 would seem to confirm our identification, although a considerable height is implied. At the time of the September 7th burst, the center of McMath 14943 is 21° behind the limb, requiring that the detected X-ray emission comes from heights on the order of 50,000 km or more above the photosphere. For the September 24th event, the region is 27° behind the limb, giving heights of at least 82,000 km.

5. MXRH DATA FOR THE FLARE OF NOVEMBER 22, 1977

The light curve of McMath 15031 on the day of November 22, 1977, the main feature of which is a beautiful 2B flare around mid-day, is shown in Figure 3. Again the Vertical Collimator system was chosen, with Small Flare data (which appear at intensities of greater than 15,000 cps) being shifted by a factor of 15.

The flare is a classic, both in X-rays and in hydrogen light, a sequence of which is shown in Figure 4. The timing of the first enhancement in H-alpha at 1946 UT coincides quite precisely with the onset of the X-ray burst. The flash phase appears to be simultaneous with the disruption of a small filament along the neutral line, the brightening occurring primarily in two discrete ribbons situated over the opposite polarity plages, and lighting up in different places so as to produce an apparent spreading at about 10 km/sec during the first hour. In X-rays, the initial cooling is exponential, with a time constant of 29 minutes.

6. SUMMARY

The present report is intended to summarize MXRH data for McMath 14943 and for the flare of November 22, 1977. More detailed information for selected times, including high resolution light curves, temperature and emission measure profiles and X-ray maps can be supplied on request.

ACKNOWLEDGMENTS

Operation of the Mapping X-Ray Heliosimeter is made possible by NASA Contract NAS5-22411. The analysis program is supported both by this contract and by the Lockheed Independent Research Program. Loren W. Acton is Principal Investigator on the MXRH experiment. The preparation of this report benefitted materially from the extensive analysis of quick-look data performed by Kermit L. Smith. Special thanks are due to H. Zirin for providing the H-alpha photographs.

REFERENCES

- | | | |
|---|------|--|
| WOLFSON, C.J.
L.W. ACTON, and
C.W. GILBRETH | 1975 | Mapping X-Ray Heliosimeter for Orbiting
Solar Observatory-8, Final Report, <u>NASA-</u>
<u>CR-144710</u> |
| WOLFSON, C.J.
L.W. ACTON
D.T. ROETHIG and
K.L. SMITH | 1977 | 2-30 keV X-Ray Data From OSO-8, <u>Report</u>
<u>UAG-61</u> (World Data Center A), p. 187. |

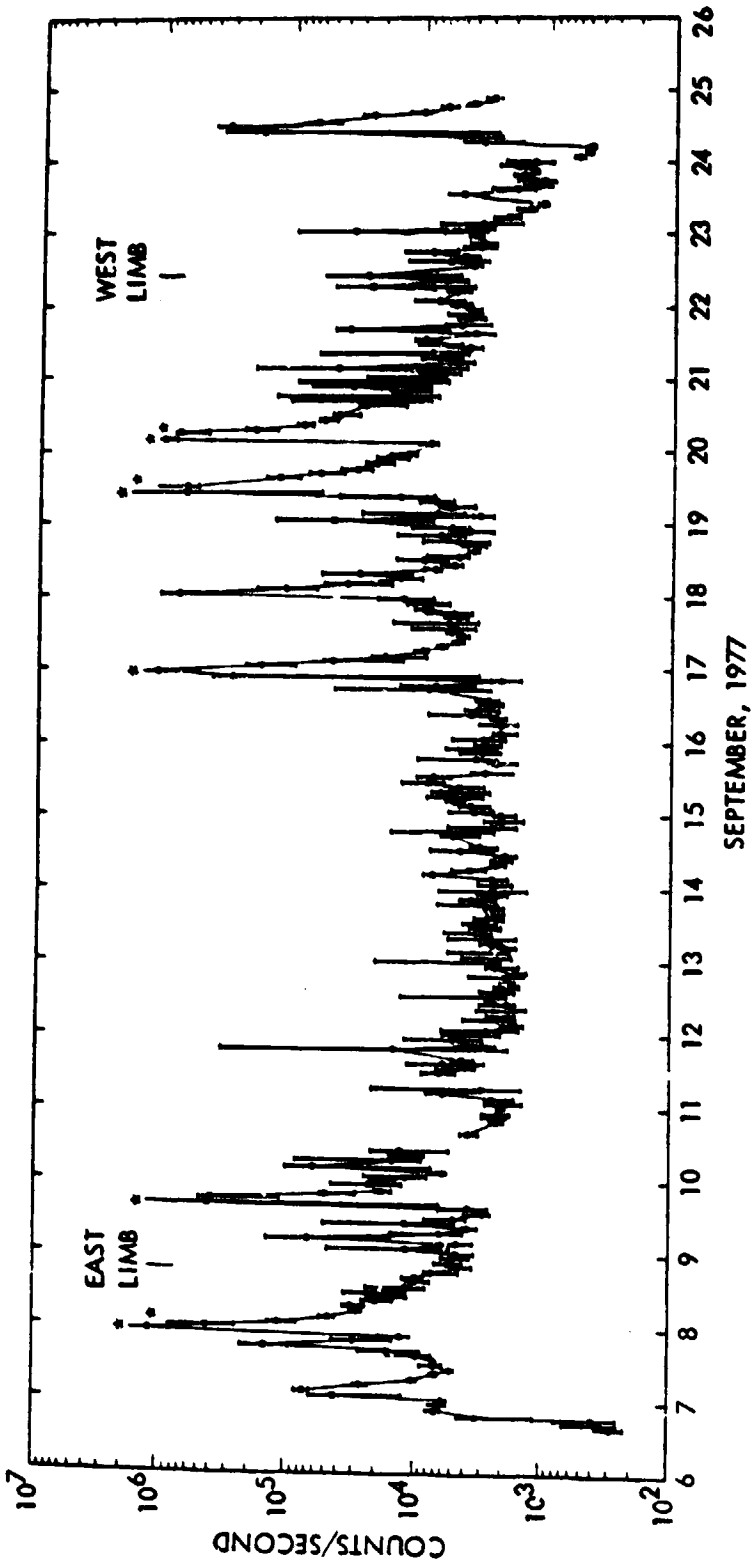


Figure 1:

Summary of 2 - 15 keV x-ray light curve data for McMath 14943. In orbits marked by asterisks the upper level is limited by saturation. Count rates are expressed in terms of an effective count rate in Vertical Large for the peak area segment. The Vertical Small Flare detector is used above 15,000 cps.

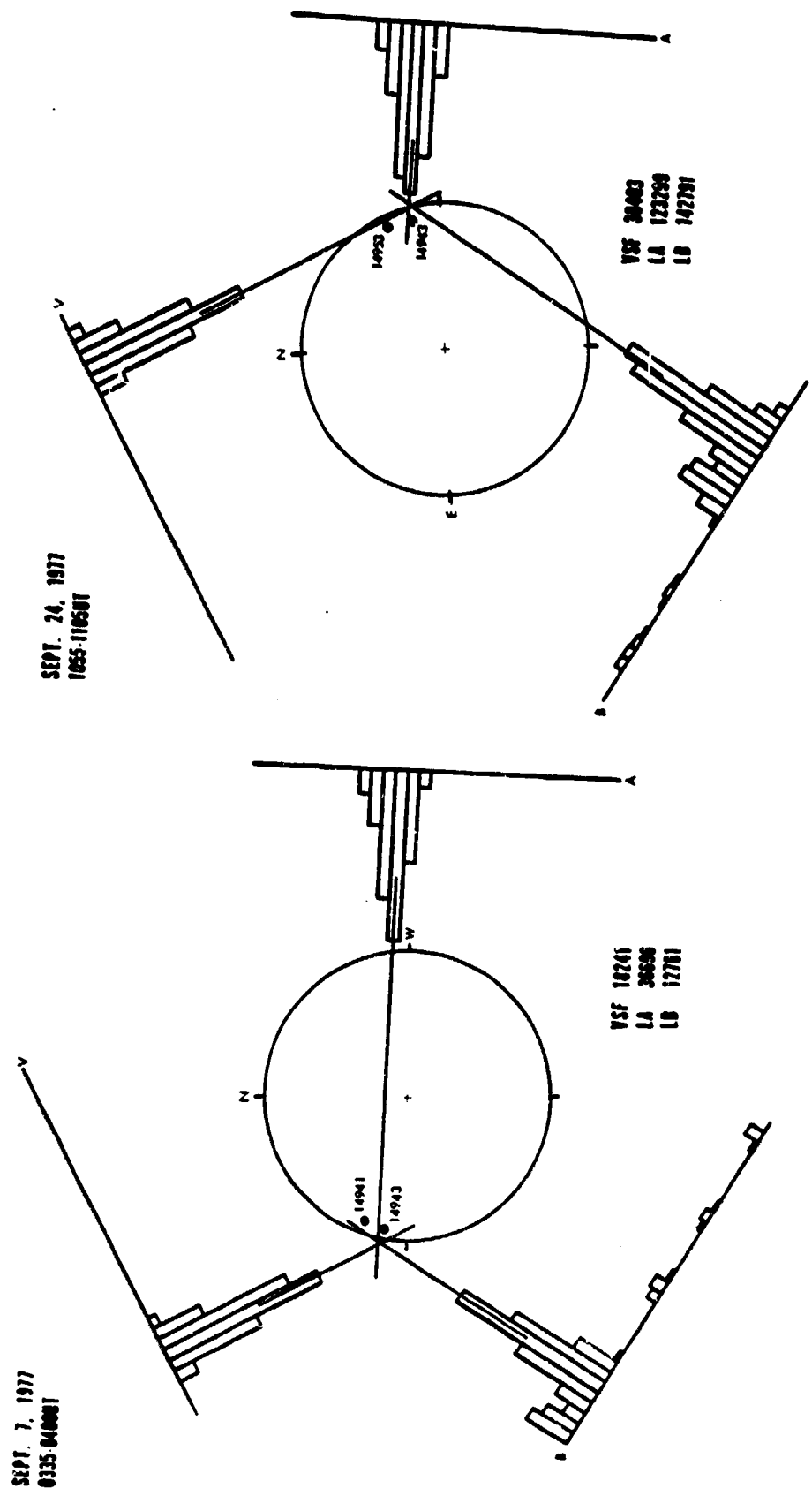


Figure 2: Typical X-ray maps for behind the limb bursts. For each detector the histogram is normalized to the peak count rate as indicated on the map. The dots for May 24th 14943 represent its approximate position behind the limb, while the second dot represents the position of a region on the visible disk. The secondary peak is due to a flaw in the collimator.

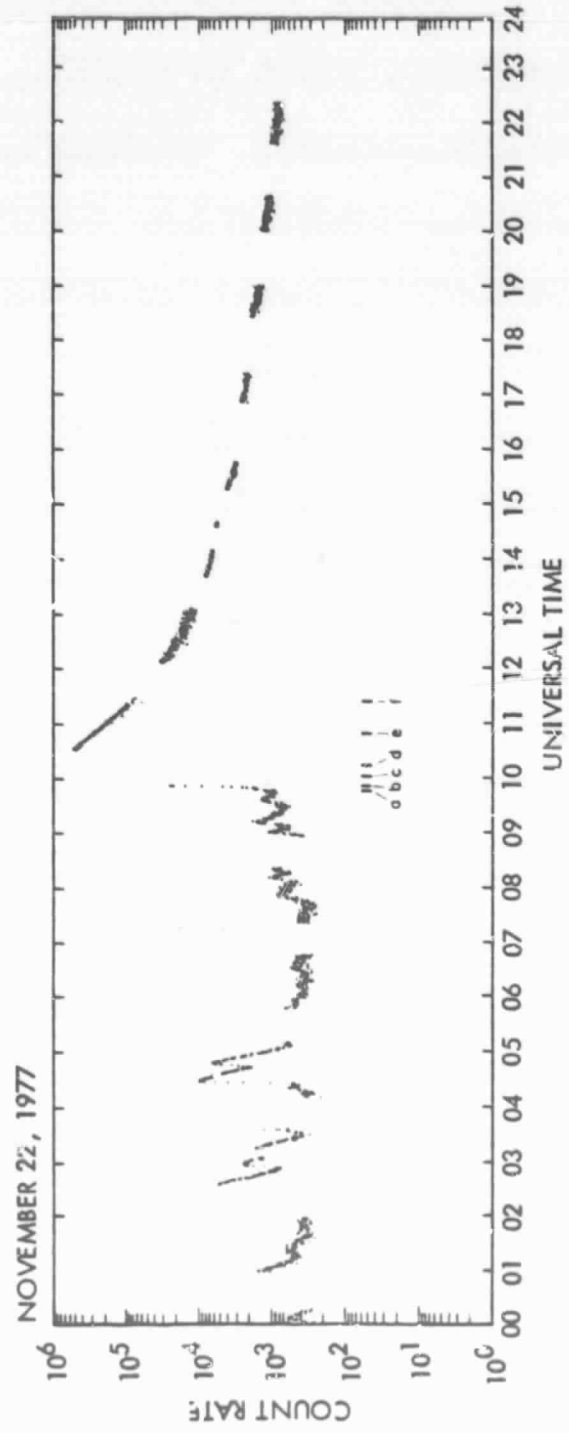


Figure 3: X-ray light curve for McMath 15031 on November 22, 1977. Times corresponding to the H-alpha photographs of Figure 4 are indicated. Frame 'b' corresponds to the second to last MXRI point shown on the rising slope. Detectors and energy coverage are as in Figure 1.

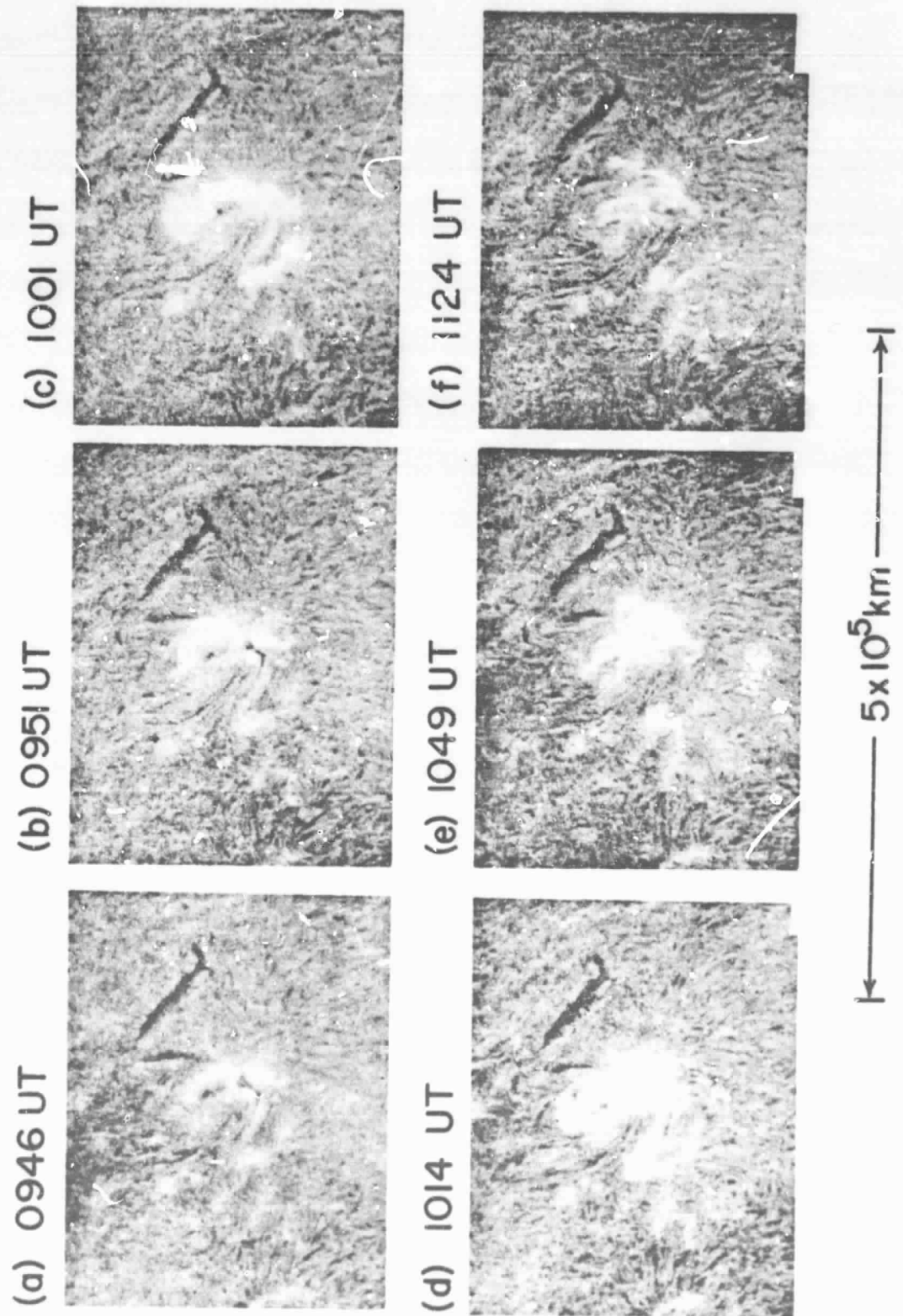


Figure 4: On-band H-alpha photographs of the flare of November 22, 1977 taken at Tel Aviv (courtesy H. Zirin, Big Bear Solar Observatory). North is at the top, and east is to the left.

ORIGINAL PAGE IS
OF POOR QUALITY

DOES THE EMISSION MEASURE DECREASE
DURING THE START OF A SOFT X-RAY FLARE?

C.J. Wolfson, L.W. Acton, and D.W. Datlowe

Reprinted from Solar Physics (1978)

Vol. 59, pp. 373-376

DOES THE EMISSION MEASURE DECREASE DURING THE START OF A SOFT X-RAY FLARE?

(Research Note)

C. J. WOLFSON, L. W. ACTON, and D. W. DATLOWE

Lockheed Palo Alto Research Laboratory, 3251 Hanover Street, Palo Alto, Calif. 94304, U.S.A.

(Received 24 May, 1978)

Abstract. Soft X-ray flare observations, interpreted as the emission from a single temperature plasma, frequently indicate a significant decrease in the inferred emission measure. It is shown that this effect results naturally from the isothermal assumption, and is eliminated when the preflare contribution to the total emission is removed.

The purpose of this note is to point out a straightforward explanation for a flare observation which might otherwise suggest complicated models. The observation is that, when the soft X-ray spectra of the emitting plasma is analyzed in terms of a single temperature and emission measure ($\int N_e^2 dV$), the emission measure shows a significant decrease during the initial flare rise. Such an effect was recently noted in the data of the Columbia OSO-8 Crystal Spectrometer which was presented at the OSO-8 Workshop (Figure 5 of Parkinson *et al.*, 1977); and possible mechanisms which might reduce the emission measure, either by collapsing the volume or decreasing the density, were discussed.

Another example of this effect is seen in Figure 1 where soft X-ray data, obtained with the Lockheed Mapping X-Ray Heliometer (MXRH) on NASA's OSO-8 spacecraft, are presented. Figure 1a shows the X-ray intensity from McMath region 14179 for a period which includes a modest (optical importance - F) flare. Figures 1b and 1c show the 'effective' (isothermal) temperature and emission measure for the emitting plasma. The inferred emission measure decreased an order of magnitude by 18:39 UT. The plasma parameters were determined, on a best fit basis, by folding theoretical X-ray spectra through the instrument response. The spectra were computed using an updated version of the code developed by Tucker and Koren (1971) for the emission from a low density, high temperature plasma.

The MXRH instrument which obtained these data is sensitive to X-rays with energies from 1.5-15 keV. Proportional counter detectors with 14 channel pulse height analyzers are used to obtain spectral information, superior to that available from ionization chambers and filter systems. The MXRH has an angular resolution of about 2 arc min and can therefore isolate single active regions, as opposed to viewing the entire disk, but cannot see spatial detail within an active region. A more complete description of MXRH observations may be found in Wolfson *et al.* (1977); instrumental details are given by Wolfson *et al.* (1975). Figure 1 demonstrates that the

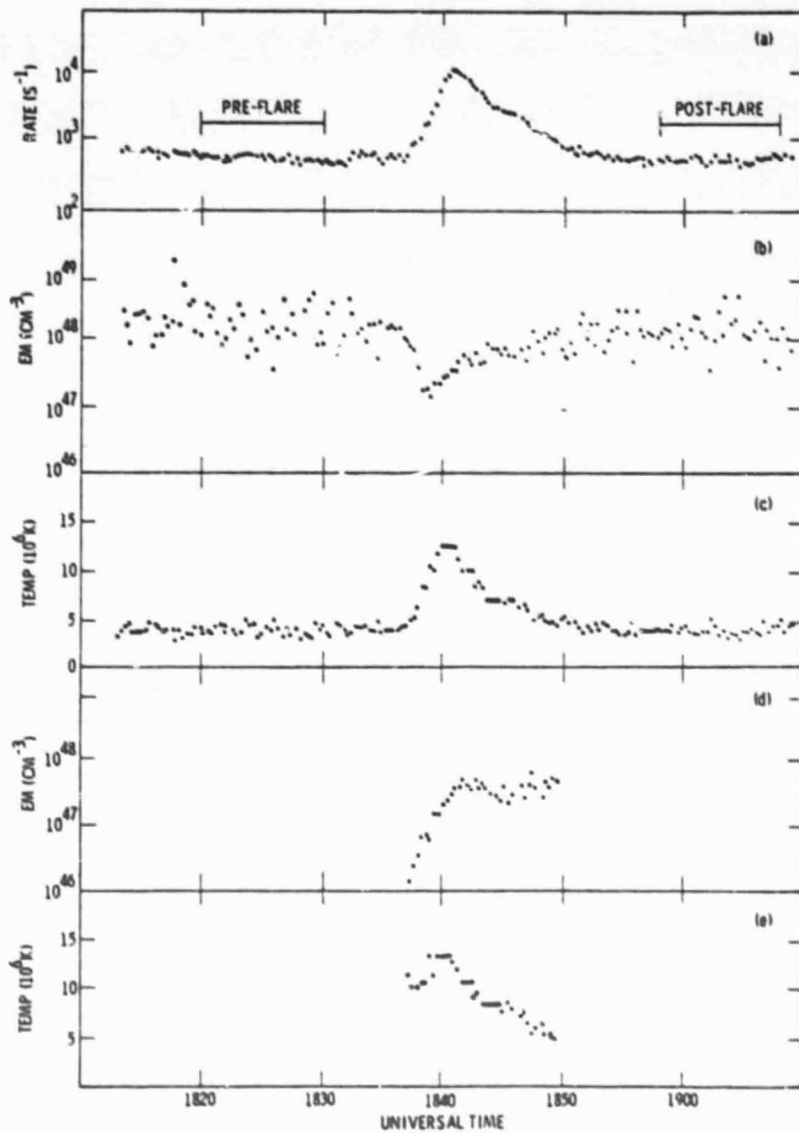


Fig. 1. Soft X-ray burst in McMath region 14179 on April 30, 1976. The X-ray intensity at each 20 s snapshot is shown in part (a). Parts (b) and (c) display the temperature and emission measure (EM) that are inferred when the data in part (a) are analyzed as the emission from an isothermal plasma. Parts (c) and (d) display the temperature and emission measure which result when the data indicated as 'pre-flare' are subtracted from the total data prior to the single temperature analysis. The parameters are only shown for the period when this net difference is statistically adequate for analysis.

MXRH has adequate sensitivity to parameterize the emission from a non-flaring active region. Instruments with sensitivity insufficient to detect emission from a non-flaring active region will not observe the effect we are discussing.

We suggest that the apparent emission measure dip is an artifact caused by not removing the emission from the stable active region prior to analyzing the flare. The flare initially adds a small amount of hot plasma to the existing larger amount of cool plasma, i.e. the high temperature plasma contains only a small fraction of the total emission measure. When one obtains an effective temperature and emission measure for the total plasma, the results are weighted averages of the two contributions. The weighting reflects both the temperature dependence of the solar emissivity and the energy sensitivity of the instrument. In the region of temperatures ($2-20 \times 10^6$ K) and energies (1-15 keV) with which we are concerned, a factor of two increase in temperature increases the measured signal by more than an order of magnitude. Thus, a small amount of hot flare plasma will dominate the total emission; the calculated, isothermal plasma parameters will trend towards those of the hot flare plasma, and a decrease in emission measure will be inferred. A similar effect will result from analysis which use the line ratio technique to determine an effective temperature since X-ray line emission, like the continuum, is much more sensitive to a variation in temperature than in emission measure.

The data of Figure 1 illustrates the situation just described. Assume that the average emission from 18:20 to 18:30 UT is representative of the stable active region throughout the flare. When this is subtracted from the total emission and the difference is analyzed, one obtains the effective temperature and emission measure shown in Figures 1d and 1e. The emission measure of the flare plasma is now seen to rise monotonically and then level off. The statistics become too poor to observe an eventual decrease.

We can make two additional arguments in favor of the picture of the flare phenomena as a flare plus a stable active region plasma rather than a contracting plasma or one of decreasing density:

(1) The observed data fits the model of a stable plasma plus a flare plasma better than it does the model of a single plasma. The Chi Square Statistic,

$$\chi^2 = \sum_{i=1}^N \frac{(D_i - F_i)^2}{\sigma_i^2},$$

where D_i and F_i are respectively the observed and expected counts in the i th pulse height analyzer channel and σ_i^2 is the statistical variance, typically decreases by more than a factor of 2.

(2) The plasma parameters in the post flare condition are indistinguishable from those during the preflare. This suggests, although it does not prove, that a portion of the emission came from an area of non-flaring plasma throughout the event. The observation that the flare appears to have made no significant change in the non-flare X-ray emission from the active region corona is not surprising in view of the general

lack of active region spatial restructuring reported for Skylab soft X-ray observations (Vaiana *et al.*, 1976), and the lack of photospheric magnetic field reconfiguration typically observed on ground based magnetograms (Rust, 1976).

Acknowledgements

The authors wish to acknowledge the team that conceived, designed, fabricated and presently operate the MXRH instrument; especially Project Engineer, C. W. Gilbreth and ground station scientist, K. L. Smith. Useful scientific discussions with J. W. Leibacher and J. M. Mosher are gratefully acknowledged. We thank H. S. Hudson for some comments which initiated our interest in clarifying this situation. This program has been supported by the National Aeronautics & Space Administration under Contract NAS5-22411, NAS5-11360, and by the Lockheed Independent Research Program.

References

- Parkinson, J. H., Kestenbaum, H. L., Long, K. S., and Novick, R.: 1977, Proceedings of the November 7-10, 1977 OSO-8 Workshop, p. 279.
Rust, D. M.: 1976, *Phil. Trans. Roy. Soc. London A* **281**, 427.
Tucker, W. H. and Koren, M.: 1971, *Astrophys. J.* **118**, 283.
Vaiana, G. S., Krieger, A. S., Timothy, A. F., and Zombeck, M.: 1976, *Astrophys. Space Sci.* **39**, 75.
Wolfson, C. J., Acton, L. W., and Gilbreth, C. W.: 1975, Mapping X-Ray Heliometer for OSO-8, Final Report, NAS-CR-144710.
Wolfson, C. J., Acton, L. W., Leibacher, J. W., and Roethig, D. T.: 1977, *Solar Phys.* **55**, 181.

AN INVESTIGATION OF THE 1.9\AA FEATURE IN
SOLAR-FLARE X-RAY SPECTRA

J.H. Parkinson, N.J. Veck, M.E.C. Ashfield,
J.L. Culhane, W.H.-M. Ku, J.R. Lemen,
R. Novick, L.W. Acton, and C.J. Wolfson

Reprinted from The Astrophysical Journal (1979)
Vol. 231, pp. 551-556

AN INVESTIGATION OF THE 1.9 Å FEATURE IN SOLAR-FLARE X-RAY SPECTRA

J. H. PARKINSON AND N. J. VECK

Columbia Astrophysics Laboratory, Columbia University; and
Mullard Space Science Laboratory, University College London

M. E. C. ASHFIELD AND J. L. CULHANE

Mullard Space Science Laboratory, University College London

W. H.-M. KU, J. R. LEMEN, AND R. NOVICK

Columbia Astrophysics Laboratory, Columbia University

AND

L. W. ACTON AND C. J. WOLFSON

Lockheed Palo Alto Research Laboratory

Received 1978 November 27; accepted 1979 February 5

ABSTRACT

The 1.9 Å feature, observed in the X-ray spectra of three solar flares with the Columbia University and Lockheed Palo Alto Research Laboratory spectrometers on the *OSO 8* satellite, is shown to be due to a blend of $1s-2p$ transitions in a range of Fe ions. In the temperature range $9-16 \times 10^6$ K, the feature has a mean wavelength of 1.900 ± 0.009 Å and is 0.04 Å wider than a single line, indicating that the main contributors are Fe xix-Fe xxii. Most of the emission originates from the dielectronic recombination process, and when inner-shell excitation is included together with normal collisional excitation, the observed intensity of the feature can be accounted for adequately. For these events, if the electron density is below approximately 10^{12} cm $^{-3}$, deviations from ionization equilibrium will be significant for ions more highly ionized than Fe xxii.

Subject headings: atomic processes — line identifications — Sun: flares — Sun: spectra — Sun: X-rays — X-rays: spectra

I. INTRODUCTION

Solar X-ray spectrometers have consistently reported a feature appearing at approximately 1.9 Å during active times. First reported by Fritz *et al.* (1967), the feature has been studied both with Bragg crystal spectrometers (e.g., Neupert and Swartz 1970; Doschek *et al.* 1971; Grineva *et al.* 1973) and with proportional counter spectrometers (e.g., Culhane and Phillips 1970; Acton, Catura, and Roethig 1977). The majority of these observations were made around the peaks of large events when electron temperatures exceeded $15-20 \times 10^6$ K, so most of the above authors attributed the bulk of the 1.9 Å feature to transitions in Fe xxiv and Fe xxv. For temperatures in the range $20-50 \times 10^6$ K, Bhalla, Gabriel, and Presnyakov (1975, hereafter BGP) have accounted for the intensities of the lines in the high-resolution observations of Grineva *et al.* (1973) by including both dielectronic recombination and inner-shell satellite lines in Fe xxiv in addition to the helium-like Fe xxv lines.

At temperatures around 10×10^6 K, less than 2% of Fe is stripped as high as Fe xxv, so it appears that the transitions invoked at higher temperatures are unlikely to contribute significantly in this lower temperature regime. This was confirmed by Acton, Catura, and Roethig (1977), who found the 1.9 Å feature to be one to two orders of magnitude stronger

than predicted for Fe xxv plus Fe xxiv satellite lines around 10×10^6 K. However, the wavelength of approximately 1.9 Å, is strongly suggestive of $1s-2p$ transitions in Fe ions, and Acton, Catura, and Roethig (1977) claimed that by including inner-shell ionization and excitation in ions below Fe xxiv, the remaining discrepancy could be removed. Merts, Cowan, and Magee (1976, hereafter MCM) have made detailed predictions of the spectrum around 1.9 Å as a function of temperature and have included dielectronic recombination and inner-shell excitation in ions below Fe xxiv in addition to the above-mentioned processes in Fe xxv and Fe xxiv.

In this paper we report observations of the intensity and wavelength of the 1.9 Å feature made with two solar spectrometers on board the *OSO 8* satellite. We show that, for temperatures around 10×10^6 K, the 1.9 Å feature arises from $1s-2p$ transitions, principally in Fe xix-Fe xxii, and we demonstrate the generally good agreement for the intensity of the feature with the calculations of MCM.

II. INSTRUMENTATION

The observations presented in this paper were obtained from two spectrometers on board the *OSO 8* satellite, namely, the graphite crystal spectrometer of the Columbia Astrophysics Laboratory and the

TABLE I
CHARACTERISTICS OF THE EVENTS USED IN THIS STUDY

ITEM	EVENT NUMBER		
	1	2	3
Date of observation.....	1976 April 29	1976 April 30	1977 Sept 10
Time of peak X-ray flux (UT).....	19 ^h 15 ^m	18 ^h 40 ^m	05 ^h 18 ^m
Position on Sun.....	S08°W31°	S08°W46°	N08°E75°
Classification of optical event.....	-N	-F	1N
Mean wavelength for feature (Å).....	1.902 ± 0.009	1.899 ± 0.006	1.900 ± 0.010

mapping X-ray heliometer of the Lockheed Palo Alto Research Laboratory. Both instruments are located in the rotating wheel section of the spacecraft and view the Sun once a revolution, nominally 10 s.

In the Columbia spectrometer, the uncollimated crystals are fixed relative to the wheel, and a scan in Bragg angle corresponding to 1.5–6.7 Å is achieved by the wheel rotation, the plane of dispersion being perpendicular to the spin axis. At 1.9 Å the spectral resolving power is given by $\lambda/\Delta\lambda \approx 24$. As this instrument views the whole Sun, at any time it will integrate the emission from all the visible active regions; however, flare observations are compromised only on the rare occasions when there are two simultaneous events on the Sun. The Lockheed spectrometer has 14 channel pulse-height analyzers, connected to proportional counters working between 1.5–15 keV, and has an angular resolution of 2'. Both instruments provide measurements of the continuum temperature (T_e) and emission measure ($N_e^2 V$) as well as the flux in the 1.9 Å feature. The Columbia spectrometer is able to measure the wavelength of the 1.9 Å feature in addition to observing more than 20 other lines.

Further details of the Columbia instrument are given by Kestenbaum *et al.* (1976); early results can be found in Parkinson *et al.* (1978). The Lockheed instrument is described in detail by Wolfson, Acton, and Gilbreth (1975), and typical observations are given by Wolfson *et al.* (1977).

III. OBSERVATIONS

We report X-ray observations of three solar flares and list relevant details in Table I. These events were chosen for study because they were observed without interruption by both instruments simultaneously, and observations of the active regions in which they occurred were available just prior to the commencement of each event. In addition, the continuum temperatures around the time of the peak 1.9 Å flux covered a wide range, from 9 to 16×10^6 K.

Parts of two graphite crystal spectra, showing the 1.9 Å feature in the 1976 April 30 event, are presented in Figure 1. In fitting a thermal continuum to each complete spectrum, we have followed the suggestion of Wolfson, Acton, and Datlowe (1978) and have first evaluated the temperature and emission measure of the active region in which each event occurred. We then fitted an isothermal continuum to the difference

between this active region contribution and each flare spectrum using the empirical continuum expression of Culhane and Acton (1970). The fitting was made to 104 bins, out of the total of 512 wavelength bins, spread throughout the spectrum and chosen so as to be free from line emission. Triangular line profiles were then fitted to the strong lines in order to determine their wavelengths and intensities (Parkinson *et al.* 1978). The wavelengths were then corrected for the position of the event on the solar disk. For the 81 independent observations of the wavelength of the 1.9 Å feature presented in this paper, we find a

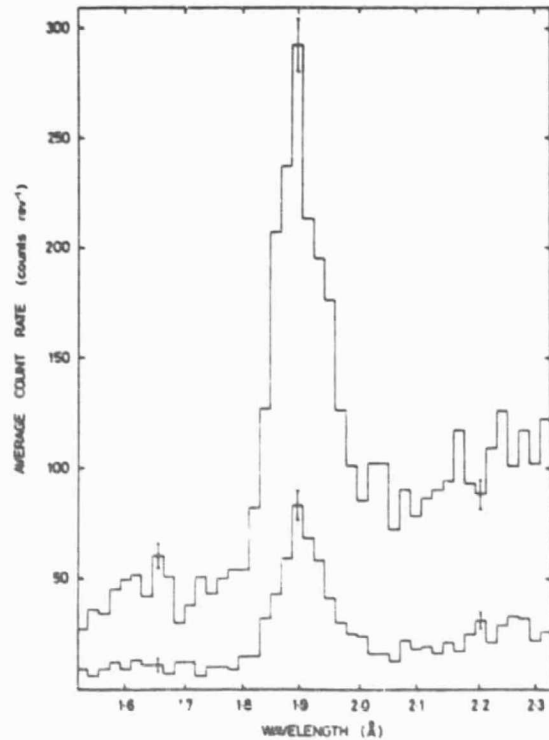


FIG. 1.—Sections of two graphite crystal spectra of the 1976 April 30 event. The lower trace was obtained between 19:08:23 and 19:08:44 UT; the best-fitting continuum to the whole spectrum has $T_e = 15.3 \times 10^6$ K and $N_e^2 V = 7.6 \times 10^{41} \text{ cm}^{-3}$. The upper trace was obtained between 19:11:49 and 19:12:10 UT. The continuum parameters are $T_e = 16.5 \times 10^6$ K and $N_e^2 V = 2.6 \times 10^{41} \text{ cm}^{-3}$.

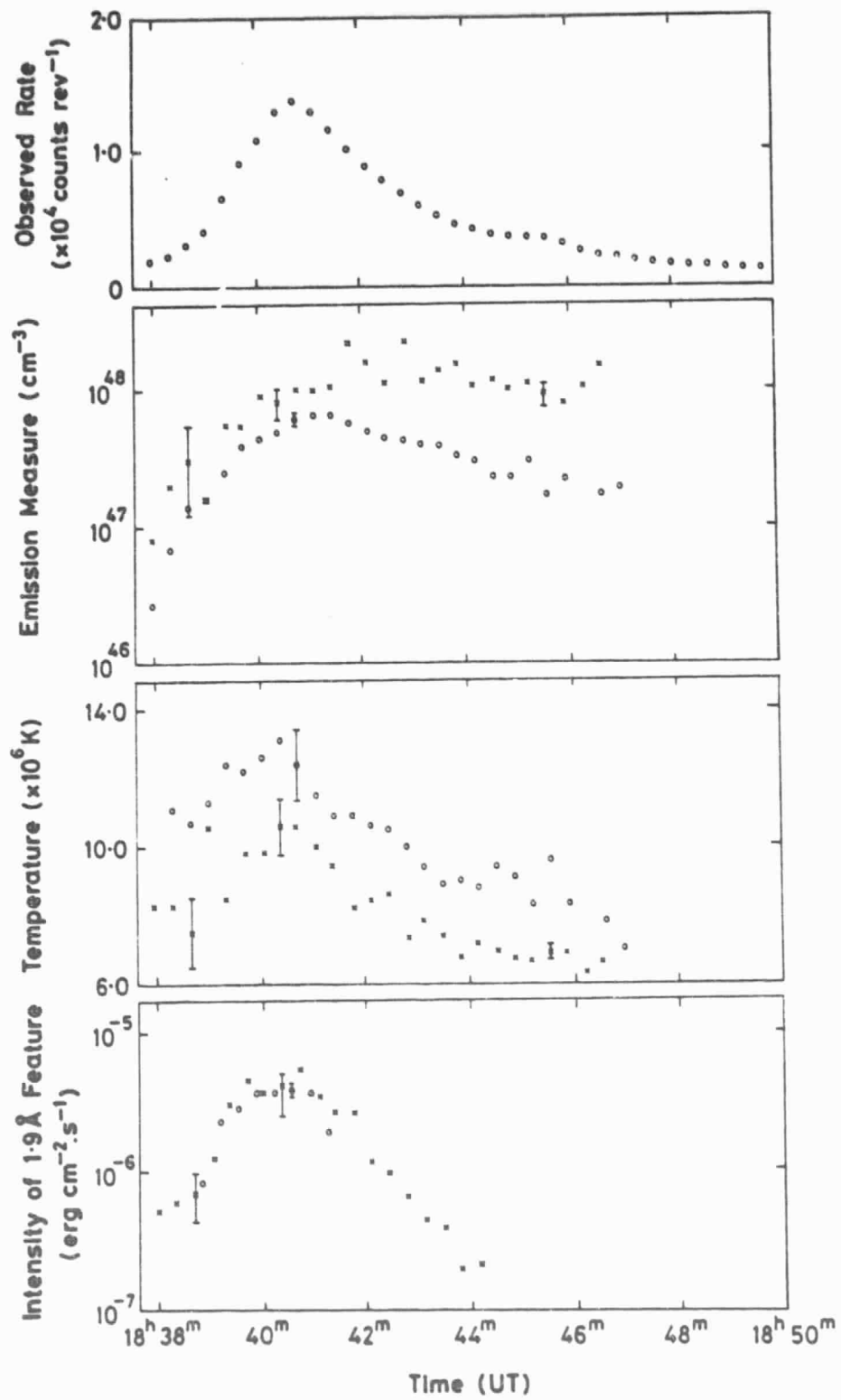


FIG. 2.—The 1.5–6.7 Å counting rate, the continuum emission measure and temperature, and the intensity of the 1.9 Å feature as a function of time for the 1976 April 30 event. Circles, Columbia graphite crystal spectrometer observations; crosses, Lockheed observations.

mean centroid wavelength of 1.900 Å with a standard deviation of 0.009 Å. No observations fell outside the wavelength range of 1.882–1.925 Å. No significant trend was found within the range of temperatures considered. Systematic errors such as those due to uncertainties in the measurement of the absolute spacecraft angles are estimated to be less than 0.05, or 0.006 Å. The best-fitting triangular profile was found to have a full width at half-maximum (FWHM) of 0.8, or 0.09 Å, whereas a single line would be expected to have a FWHM of 0.7, or 0.08 Å. At 1.9 Å this excess width corresponds to a line broadened by approximately 0.04 Å.

The Lockheed observations have been analyzed in a similar way: the preflare signal was subtracted from each spectrum, and then the best-fitting isothermal temperature, emission measure, and 1.9 Å flux were determined simultaneously. Again, the empirical expression of Culhane and Acton (1970) was used for the continuum together with an allowance for line emission at wavelengths greater than 3 Å.

The parameters derived for the 1976 April 30 event for the two spectrometers are compared in Figure 2. It is apparent that the Lockheed temperatures are always approximately 2×10^6 K lower than the Columbia temperatures and that the Lockheed emission measures compensate for this difference by being approximately a factor of 3 higher than the Columbia values. It is not clear why there should be such differences as both instruments obtain most of their data in the same energy range, 2–8 keV, and both sets of observations are fitted with the same continuum expression. However, we tend to prefer the parameters derived from the Columbia observations because the continuum data are not contaminated by line emission. It is pleasing, however, to note that the 1.9 Å line intensities agree so well, which indicates that the sensitivity calibrations of the two instruments around 6 keV are in good agreement.

The 1.9 Å fluxes per unit emission measure are plotted against temperature in Figure 3, with different symbols for each of the three events listed in Table 1. Although the temperature ranges for each of these events do not overlap, the observations delineate a well-defined temperature dependence.

IV. INTERPRETATION

At temperatures between 5 and 20×10^6 K, Fe exists in a range of ionization stages; for example, at 10×10^6 K all of the ionization stages between Fe XVII and Fe XXV have fractional abundances above $\approx 1\%$. Thus, if any particular electron transition is studied, then that transition in a wide range of ionization stages must be included. For the temperature regime considered here, 1s-2p transitions in all Fe ions between Fe XVII and Fe XXV must be taken into account. The resulting spectral feature will have components due to each ionization stage, which, unfortunately, are not resolved by the graphite crystal spectrometer.

The most extensive set of calculations for 1s-2p

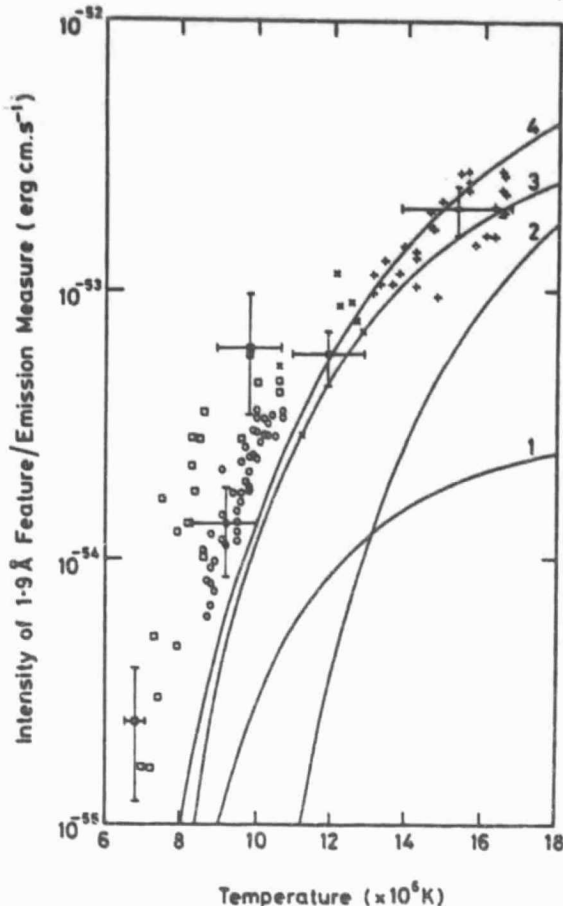


FIG. 3.—The observed intensity of the 1.9 Å feature compared with the intensity predicted assuming the plasma is in thermal equilibrium (MCM). Plus signs, Columbia observations of the 1976 April 29 event; crosses, of the 1976 April 30 event; circles, of the 1977 September 10 event; squares, Lockheed observations of the 1976 April 30 event. Curve 1 is collisional excitation in Fe XXIV and below; curve 2, collisional excitation in Fe XXV; curve 3, dielectronic recombination in Fe XXV and below; and curve 4, total intensity of all the contributions to the 1.9 Å feature.

transitions in Fe have been made by MCM. They found the two most important processes to be: (1) collisional excitation from the 1s to the 2p shell or higher, followed by the radiative decay of a 2p electron; and (2) dielectronic recombination, where a 1s electron is collisionally excited to the 2p shell, or higher, the colliding electron is captured in an unfilled orbital, and a 2p electron radiatively decays. For both of these processes, MCM calculated the wavelengths and intensities of the line that would be expected from 1s-2p transitions in Fe XVIII–Fe XXVI for a laboratory iron-seeded hydrogen plasma. Hill *et al.* (1978) subsequently found that the intensities of the features that they observed in the Princeton Large Torus agreed with the MCM calculations to within a factor of 2.

The calculations of MCM can be directly compared with the present work by changing the abundance of Fe to the coronal value of $N_{Fe} = 4.7 \times 10^{-8} N_H$ found by Withbroe (1971). We have also assumed that the reduction of the electron density by two to four orders of magnitude from the value $N_e = 10^{14} \text{ cm}^{-3}$ would not significantly affect the dielectronic recombination rate (Summers 1978).

For coronal conditions, we have evaluated three contributions to the intensity of the 1.9 Å feature:

1. A $1s-2p$ inner-shell contribution in Fe XVIII–Fe XXIV. This was obtained by subtracting the Fe XXV and Fe XXVI collisionally excited $1s-2p$ transition rates from the sum of the individual collision rates for all applicable Fe ions included by MCM.

2. An Fe XXV helium-like resonance (1^1S-2^1P), intersystem (1^1S-2^3P), and forbidden (1^1S-2^3S) contribution. The Fe XXV resonance line intensity was estimated in (1), and, according to Gabriel (1972), the total intensity of these three lines is 1.7 times the intensity of the resonance line.

3. A dielectronic recombination contribution. Here we have simply scaled the results of MCM.

The temperature dependence of these three components is shown in Figure 3. Over the temperature range $9-16 \times 10^6 \text{ K}$, the largest contribution always arises from dielectronic recombination, and above $13 \times 10^6 \text{ K}$ the Fe XXV helium-like triplet intensity exceeds that due to inner-shell collisional excitation. When the sum of these contributions is compared with the Columbia observations, there is excellent agreement above about $12 \times 10^6 \text{ K}$. At $9 \times 10^6 \text{ K}$ the flux measured by the Columbia spectrometer is twice the calculated flux; here the Lockheed values are 3 times the calculated flux.

V. DISCUSSION

In § III, the mean wavelength of the emission centroid was found to be $1.900 \pm 0.009 \text{ \AA}$ and appeared to be some 0.04 Å wider than would be expected for a single line. In the wavelength range 1.88–1.92 Å, the principal contributions will be from the ions Fe XIX–Fe XXII. In § III it was also shown that there were no significant variations with temperature in the range $9-16 \times 10^6 \text{ K}$. However, the MCM (1976) calculations predict a centroid wavelength close to 1.900 Å at a temperature of $9 \times 10^6 \text{ K}$ with an approximately linear decrease in wavelength to 1.865 Å at $15 \times 10^6 \text{ K}$, after which there is a slower decrease to 1.850 Å at $23 \times 10^6 \text{ K}$. Hence, for the temperature range over which we have made observations, we would have expected to see a change from 1.900 Å to 1.860 Å if the plasma were in ionization equilibrium.

Apart from MCM, the only other authors who have calculated dielectronic recombination and inner-shell rates for $1s-2p$ transitions were BGP, who examined Fe XXIV. For the dielectronic recombination process, the BGP rates are always higher than the MCM values; the difference increases from a factor of 1.4 at $12.5 \times 10^6 \text{ K}$ to a factor of 2 higher at both $11 \times 10^6 \text{ K}$ and $15 \times 10^6 \text{ K}$. In contrast, the inner-

shell rates are always close to 0.8 of the MCM values. When these two factors are combined appropriately, the two sets of calculations for the total Fe XXIV intensity agree to within a factor of 2 between 10 and $17 \times 10^6 \text{ K}$. Such differences are within the accuracy of the MCM calculations, as they state that the dielectronic recombination rates that they have used may be in error by a factor of 2 and the collisional excitation rates by as much as an order of magnitude.

Up to this point we have assumed that the plasma we are observing is always in thermal equilibrium with both the free electron velocities and the bound-electron occupation numbers described by a single temperature. However, for the events considered in this paper, if the electron density $N_e \lesssim 10^{12} \text{ electrons cm}^{-3}$, stages more highly ionized than Fe XXI will not reach equilibrium in a time less than the total duration of the event itself (Kafatos and Tucker 1972; Shapiro and Moore 1977). Because lower ions reach equilibrium

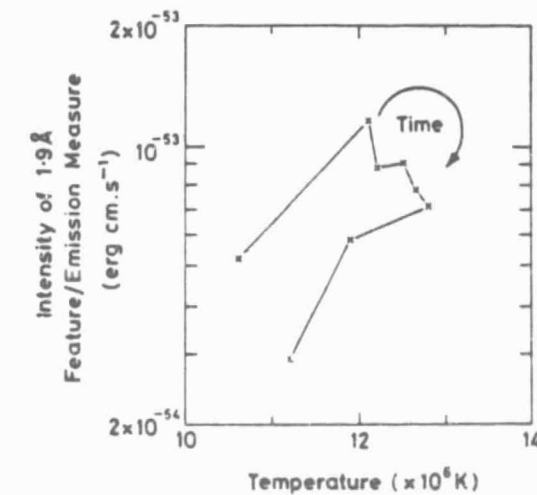
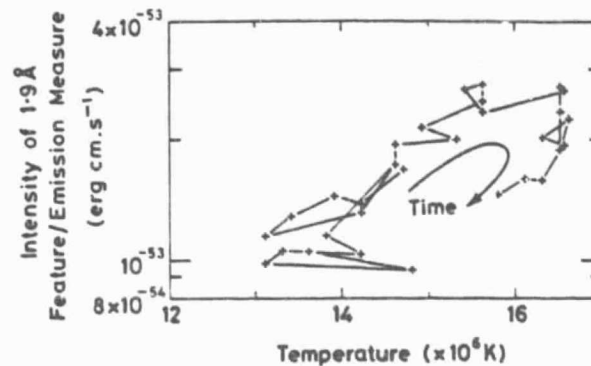


FIG. 4.—Time sequence of two of the events shown in Fig. 3. Upper panel, 1976 April 29; lower panel, 1977 September 10.

more rapidly than higher ions during the rising portions of an event, lower Fe ionization stages will be radiating more than would be expected from the value of the electron temperature if the plasma were in ionization equilibrium. This means that the centroid of the observed feature would be at a longer wavelength, corresponding to a plasma that is under-ionized. It appears therefore that deviations from ionization equilibrium may explain the apparent lack of dependence of the wavelength of the feature on temperature.

In the previous section we showed that most of the 1.9 Å emission originated from the dielectronic recombination process. As a consequence, the intensity of the feature will be only slightly affected by deviations from ionization equilibrium. In Figure 3 we chose not to indicate the time sequence of each set of observations for reasons of clarity. However, for all the events in which we have studied the 1.9 Å feature, a definite time structure emerges, and Figure 4 shows the Columbia observations of the 1976 April 29 and 1977 September 10 events in more detail. It appears that at any particular temperature, the intensity of the 1.9 Å feature is marginally stronger in the rising portion of the event than in the falling portion. We interpret this as supporting evidence for the flaring plasma not being in ionization equilibrium.

Finally, we draw attention to a weak feature observed at 1.64 ± 0.01 Å, which is barely visible in Figure 1. As this feature lies on the long wavelength side of the Ni xxvii helium-like transitions, we identify the feature with $1s-2p$ transitions in a range of Ni ions, exactly analogous to those in Fe that we have discussed above. The ratios of the two features will be principally dependent on the relative abundances of Fe and Ni. The observed flux ratio, Fe:Ni = 11 ± 2 ,

is in good agreement with measured relative abundances of Fe:Ni which are in the range 10–17 (Parkinson 1977, and references therein).

VI. CONCLUSIONS

We have investigated the feature at 1.9 Å which is observed in X-ray spectra of solar flares and have found that it is due to a blend of $1s-2p$ transitions in a range of Fe ions. The mean wavelength of 1.900 ± 0.009 Å and excess width of 0.04 Å indicate that the main contributions are from Fe xix–Fe xxii for temperatures between 9 and 16×10^6 K. The bulk of the emission arises from the dielectronic recombination process, and when inner-shell excitation is included together with normal collisional excitation, the observed intensity of the feature can be accounted for adequately. If the electron density $N_e \lesssim 10^{12}$ electrons cm $^{-3}$, then deviations from ionization equilibrium may account for the absence of any change in the feature wavelength with temperature.

We thank R. S. Wolff and H. L. Kestenbaum, formerly of the Columbia Astrophysics Laboratory, for helpful discussions in the early stages of this work. N. J. V. and M. E. C. A. acknowledge the receipt of SRC Research Studentships. The National Aeronautics and Space Administration supported this work under contract NASS-22408 at Columbia University and under contracts NASS-22411 and NASS-11360 at the Lockheed Palo Alto Research Laboratory, where the work was also supported by the Lockheed Independent Research Program. This article is Columbia Astrophysics Laboratory Contribution No. 165.

REFERENCES

- Acton, L. W., Catura, R. C., and Roethig, D. T. 1977, *Ap. J.*, **218**, 881.
- Bhalia, C. P., Gabriel, A. H., and Presnyakov, L. P. 1975, *M.N.R.A.S.*, **172**, 359 (BGP).
- Culhane, J. L., and Acton, L. W. 1970, *M.N.R.A.S.*, **151**, 141.
- Culhane, J. L., and Phillips, K. J. H. 1970, *Ap. J.*, **160**, 309.
- Doschek, G. A., Meekins, J. F., Kreplin, R. W., Chubb, T. A., and Friedman, H. 1971, *Ap. J.*, **170**, 573.
- Fritz, G., Kreplin, R. W., Meekins, J. F., Unzicker, A. E., and Friedman, H. 1967, *Ap. J. (Letters)*, **148**, L133.
- Gabriel, A. H. 1972, *M.N.R.A.S.*, **160**, 99.
- Grineva, Yu. I., Karev, V. I., Korneev, V. V., Krutov, V. V., Mandelstam, S. L., Vainstein, L. A., Vasilyev, B. N., and Zhitnik, I. A. 1973, *Solar Phys.*, **29**, 441.
- Hill, K. W., et al. 1978, *Phys. Rev.*, in press.
- Kafatos, M. C., and Tucker, W. H. 1972, *Ap. J.*, **175**, 837.
- Kestenbaum, H. L., Cohen, G. G., Long, K. S., Novick, R., Silver, E. H., Weisskopf, M. C., and Wolff, R. S. 1976, *Ap. J.*, **210**, 805.
- Merts, A. L., Cowan, R. D., and Magee, N. H. 1976, Los Alamos Scientific Laboratory Report No. LA-6220-MS (MCM).
- Neupert, W. M., and Swartz, M. 1970, *Ap. J. (Letters)*, **160**, L189.
- Parkinson, J. H. 1977, *Astr. Ap.*, **57**, 185.
- Parkinson, J. H., et al. 1978, *Solar Phys.*, **60**, 123.
- Shapiro, P. R., and Moore, R. T. 1977, *Ap. J.*, **217**, 621.
- Summers, H. 1978, private communication.
- Withbroe, G. L. 1971, in *The Menzel Symposium on Solar Physics, Atomic Spectra, and Gaseous Nebulae*, ed. K. B. Gebbie (Washington: NBS Special Pub. No. 353), pp. 127–148.
- Wolfson, C. J., Acton, L. W., and Datlowe, D. W. 1978, *Solar Phys.*, in press.
- Wolfson, C. J., Acton, L. W., and Gilbreth, C. W. 1975, NASA CR-144710.
- Wolfson, C. J., Acton, L. W., Leibacher, J. W., and Roethig, D. T. 1977, *Solar Phys.*, **55**, 181.

L. W. ACTON and C. J. WOLFSON: Space Sciences Laboratory, Code 52-12, Building 202, Lockheed Palo Alto Research Laboratory, 3251 Hanover Street, Palo Alto, CA 94304

M. E. C. ASHFIELD, J. L. CULHANE, J. H. PARKINSON, and N. J. VECK: Mullard Space Science Laboratory, Department of Physics, University College London, Holmbury St. Mary, Dorking, Surrey, England

W. H.-M. KU, J. R. LEMEN, and R. NOVICK: Columbia Astrophysics Laboratory, Departments of Astronomy and Physics, Columbia University, 538 West 120th Street, New York, NY 10027

PREDICTIONS OF SOLAR X-RAY FLUXES

BASED ON SUNSPOT STRUCTURE

J.M. Mosher

Reprinted from R.F. Donnelly, ed.,
Solar-Terrestrial Predictions Proceedings, Vol. III:
Solar Activity Predictions (1980), pp. C159-164

PREDICTION OF SOLAR X-RAY FLUXES BASED ON SUNSPOT STRUCTURE

J. M. Mosher
Lockheed Palo Alto Research Laboratory
Palo Alto, California 94304

A comparison is made between the sunspot structure and the slowly-varying x-ray output from individual solar active regions. Using data from the Lockheed Mapping X-Ray Heliometer experiment on OSO-8, it is found that the 1-8 Å x-ray intensity is approximately proportional to either sunspot area or count. If the product of these two parameters is used, the correlation improves and two-thirds of all regions lie within a factor of two of the average trend. An additional class of sources producing x-ray fluxes up to about 10^{-7} W/m² is associated with spot-free regions.

1. Introduction

Monitoring the flux of soft x-rays incident on the earth's atmosphere has been an important scientific objective of experiments on rockets and satellites for more than twenty-five years. As a result of the research which has been done, it is now well appreciated that nearly all of this radiation comes from solar active regions, but relatively little attention seems to have been directed towards the problem of defining or attempting to predict the typical level of emission from an individual region. Because of the limitations of most earlier instruments, what interest has been expressed has focussed primarily on the comparison of full disk fluxes with total spot areas (Michard and Ribes, 1968) or Zurich sunspot numbers (Teske, 1969; Parkinson and Pounds, 1971). In the present study, two and one half years of data from the Lockheed x-ray experiment on OSO-8 are examined in an attempt to determine within what limits the x-ray flux from an individual active region can be anticipated on the basis of the underlying sunspot structure.

2. X-ray Data

This study is based on results generated during the quick-look analysis of data from the Lockheed Mapping X-Ray Heliometer (MXRH) experiment onboard OSO-8. The MXRH, which is capable of assigning individual intensities to each of several solar active regions approximately once every 40 seconds, has been described in detail by Wolfson *et al.* (1975; 1977).

As a part of the quick-look analysis, a map is constructed showing the 'typical' appearance of the x-ray sun for each day. Since the x-ray fluxes are highly variable, the decision as to what constitutes 'typical', based on the examination of about four hours worth of solar data, is obviously rather arbitrary; yet, avoiding obvious flare peaks as much as possible, the objective has been to choose an interval of five to ten minutes which seems representative of the available sample-- that is, neither the quietest nor the most active time.

The intensities of the sources on the daily map are then evaluated in counts per second summed over the spectral range of the detectors, which is nominally 1.5-15 keV. Data from as many as three independent detector systems may be used in making the intensity evaluation. For the purposes of the

present paper, these intensities have been converted into estimated 1-8 Å energy fluxes (the standard wavelength range used by the SMS/GOES and SOLRAD monitor satellites) using an empirical power law relationship which incorporates the observed average dependence of temperature (spectral hardness) on intensity; which, in this spectral range, varies from $2-3 \times 10^6$ °K for the weakest sources to $6-7 \times 10^6$ °K for the strongest. Note that 1 W/m² at earth represents an output of 2.82×10^{30} ergs/sec from the region.

3. Analysis

The relationship between 1-8 Å x-ray intensity I (as determined from MXRH counts/second) and sunspot structure has been investigated by comparing the daily MXRH quick-look maps with the sunspot information published in Solar-Geophysical Data (Prompt Reports), the specific section used being the tabulation giving the daily sunspot area, A (the sum of umbral and penumbral areas in millionths of a hemisphere), and sunspot count, C, for each McMath Region.

Data examined cover the period July, 1975 through December, 1977. However, not every region was considered. In particular, since sunspot reports are not considered reliable for regions too near the limb, a comparison was made only if the source was within about $0.5 R_\odot$ of disk center, and in addition, only those x-ray values were used which could be independently evaluated by at least two of the three detector systems.

Although by its nature, the MXRH is limited, at any one moment, to evaluating the signal from the strongest sources present on the sun, special attention was given to trying to form an accurate impression regarding the association of x-rays with sunspots for weak sources. Numerous examples were found in which a decayed active region continued to emit detectable x-rays even after the visible sunspot structure had disappeared. On the other hand, no example could be found of a region with reported spot structure failing to produce at least some x-ray signal, although in a few cases the observed 1-8 Å flux was as low as a few times 10^{-9} W/m².

4. Predictions

The primary purpose of this paper is to present in a quantitative fashion the observed relation between soft x-ray flux and sunspot structure for individual solar active regions, and not to advocate a particular theory of x-ray production. It is easy to appreciate that nearly any theory will predict an increase in x-ray intensity with spot count and area, since the count is presumably a measure of the number of coronal flux tubes, and the area a measure of the coronal volume. In addition, it is easy to see that if the relation of x-ray flux to either of these parameters separately is imperfect (as it is), then its relation to some simple combination of them (such as their product) should be better. That is, of all the regions with a given value of area, the ones with the greatest complexity (i.e., count) would be expected intuitively to be the most x-ray productive; and, conversely, of all the regions with a given count, the ones with the greatest available magnetic energy (i.e., area) would seem likely to be the strongest in x-rays. In other words, one expects to find less scatter when the x-ray prediction is based on, for example, the product AxC than when it is based on either A or C separately.

In comparing the present results to theory, two notes of caution should be raised. First, as previously stated, the average x-ray temperature of regions

in the bandpass viewed by our detectors increases systematically with intensity. Hence, since the spectrum flattens, a proportionality which applies at 8 Å cannot be expected to apply precisely at any other wavelength, either higher or lower. Second, the plots shown are for the 'typical' daily x-ray levels. During flares, the intensity from a region can briefly rise to values orders of magnitude above this baseline, and hence the numbers reported may reflect only a tiny fraction of the integrated daily x-ray output from the region.

5. Results

The results of this first-order investigation of the relation between soft x-ray intensity, I , and sunspot structure are illustrated in Figures 1 and 2. When plotted against sunspot area, A , or count, C (Figure 1), or against the product of the two (Figure 2), a fairly clear correlation is seen, accompanied by a large amount of scatter.

On each of the graphs, a pair of lines has been drawn representing the range required to encompass two-thirds of the points with non-zero sunspot parameters. These lines have been drawn at a slope representing the average trend

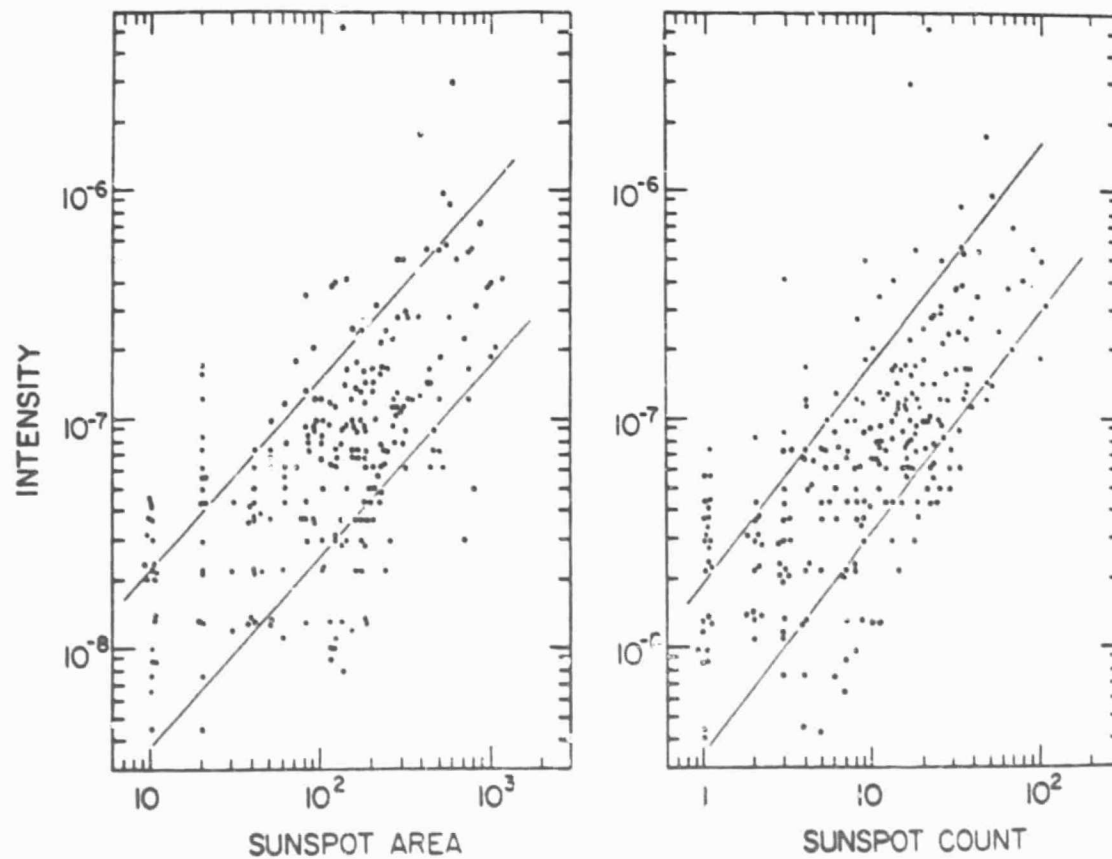


Fig. 1. Scatter plot of I vs A and C for all regions with non-zero spot parameters. Intensity is the 1-8 Å x-ray flux in units of W/m^2 at earth. Areas are measured in millionths of a solar hemisphere. Between the 10^{-8} and 5×10^{-8} W/m^2 levels there are an additional 40 x-ray sources for which the spot area and count are zero.

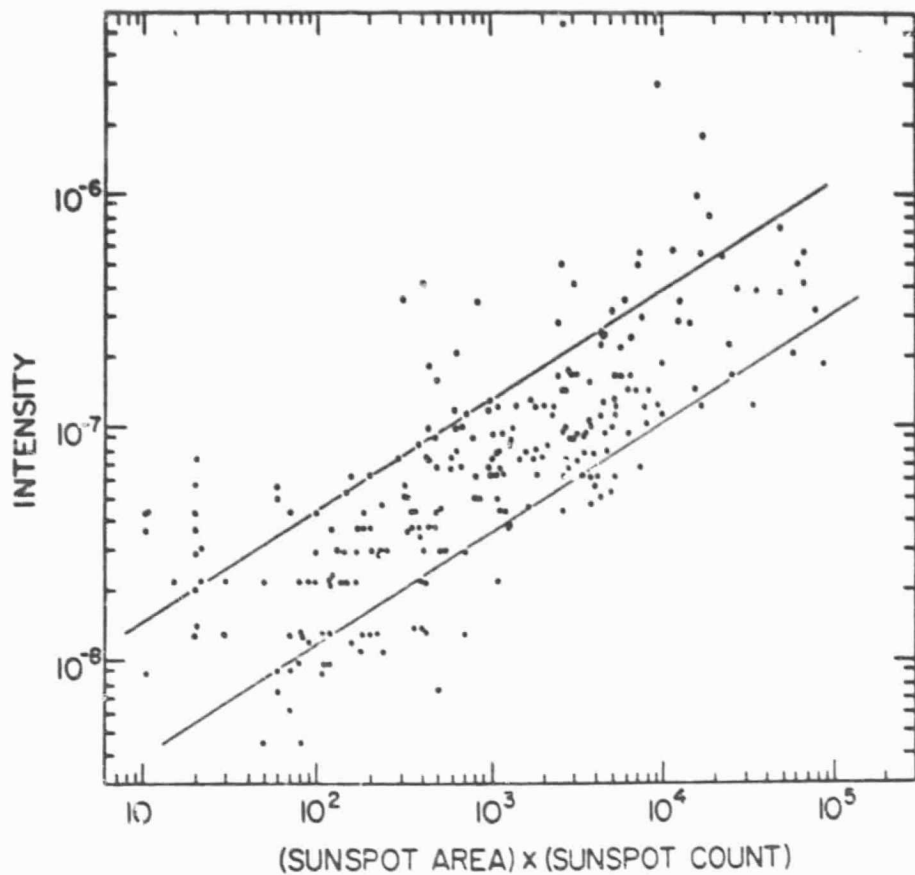


Fig. 2. Scatter plot of I vs. AxC with same format as Fig. 1. In a few instances a single McMath region contained more than one sunspot group. In these cases an average was made between the values of AxC obtained using separate and combined parameters.

of the data as determined by eye. The trends used were:

$$I = 1.34 \times 10^{-9} A^{0.84} \text{ W/m}^2 \quad (1)$$

$$I = 8.33 \times 10^{-9} C^{0.96} \text{ W/m}^2 \quad (2)$$

$$\text{and} \quad I = 2.57 \times 10^{-9} (AxC)^{0.47} \text{ W/m}^2 \quad (3)$$

The difference in the thickness of the 1σ scatter bands (which depends somewhat on the choice of slope) is not significantly different when the x-ray data are plotted against area, as opposed to count: a factor of ± 2.45 in the former case, and ± 2.34 in the latter. The 1σ scatter is reduced to a factor of ± 1.9 when the product AxC is used.

The scatter in the plots arises from several sources:

- (a) There are random errors in the choice of a 'typical' x-ray intensity whenever the region in question is variable (which is almost always).
- (b) There are genuine variations in the temperature of regions at any given level of intensity, so that the conversion from counts per second to W/m^2 cannot be uniformly accurate for all regions.
- (c) There are random errors of unknown magnitude in the reported values of A and C.
- (d) There is undoubtedly an intrinsic scatter in the true relationship between I and A or C or AxC.

The precise amount of the total scatter due to the last source is not entirely clear since we do not have accurate estimates of the contributions due to the other three, but the next section will indicate that at least some of the deviations from the average trend are real.

To within the accuracy of the present data, it would be fair to say that for regions with reported sunspot structure, the $1-8 \text{\AA}$ x-ray flux is observed to be proportional to either the sunspot area or count separately, or alternatively, and with somewhat less scatter, to the square root of the product of area times count.

6. Exceptional Regions

It seems useful to attempt to identify the origin of points lying unusually far either above or below the average trend. Regions with unusually high x-ray outputs are almost always found to have been in a flaring or semi-flaring state at the time of the daily map. As an example, the highest intensity shown is $I = 5.3 \times 10^{-6} \text{ W/m}^2$ for McMath 14607 at 1934 UT on January 12, 1977. This young, growing region with $A = 130$ and $C = 21$ happened to be near a flare peak at the time of the map. Earlier the flux had been as low as $5 \times 10^{-8} \text{ W/m}^2$, and a typical 'quiescent' value for the day, based on the full 24 hours of data, would be something like $1.5 \times 10^{-7} \text{ W/m}^2$.

Anomalously low x-ray intensities, on the other hand, are almost always associated with decayed regions, which tend to be relatively stable. McMath 14564, for example, which had $A = 130$ and $C = 4$ on December 21, 1976, had an x-ray output of only about $7.5 \times 10^{-9} \text{ W/m}^2$ -- a factor of 5 to 10 lower than would normally be expected for a group of its size. The pictures in Solar-Geophysical Data indicate an extremely simple region magnetically, consisting almost entirely of a single spot which is at least one, and perhaps nearly two rotations old.

7. X-rays from Spotless Regions

A logical extension of the last category is the x-ray sources associated with totally spot-free regions. Of the weak sources which could be studied with $1-8 \text{\AA}$ x-ray outputs in the range 1×10^{-8} to $5 \times 10^{-8} \text{ W/m}^2$, nearly one-third were of this variety, and invariably the spotless region represented the decayed remnant of a region which had or appeared previously to have had spots (possibly on the backside). The highest flux encountered in association with a spotless region during the course of this study was $I = 1.5 \times 10^{-7} \text{ W/m}^2$ for

McMath 14616 at 0800 UT on January 26, 1977. In retrospect, this unusually high flux was associated with a very gradual flare-like enhancement (possibly of the type described by Webb *et al.*, 1976). In the absence of this transient event, the region would probably have been at or near the threshold of detectability for the MXRH.

8. Conclusions

A quantitative comparison of MXRH daily x-ray intensities with sunspot areas and counts indicates that the 1-8 Å x-ray flux from individual solar active regions can be roughly anticipated on the basis of the underlying sunspot structure. To within the accuracy of the present data, the x-ray intensity appears to be proportional to either the area or spot count considered separately, or, alternatively, to the square root of their product. In the latter case, the scatter of individual regions around the average trend is by a factor of about 2. In addition to the sources which obey this proportionality, there is a class of x-ray sources (typically with intensities below 5×10^{-8} W/m²) associated with decayed and apparently spotless regions.

The implication of this study is that rough estimates of solar x-ray intensities incident at earth can be made even at times when direct measurements are not available simply by examining the sunspot structure. It should be noted, however, that the present results apply only to the slowly-varying component of the x-ray signal, and that the bulk of the integrated x-ray output from a region will usually be produced by flares. A separate study would be required to determine if the flare contribution can also be anticipated on the basis of sunspot structure.

Acknowledgements

Dr. L.W. Acton is principal investigator for the MXRH experiment. The great majority of the daily quick-look analysis has been performed by K.L. Smith. This work is supported by NASA Contract NAS5-22411 and by grants from the Lockheed Independent Research Program.

REFERENCES

- Michard, R. and E. Ribes (1968): La Composante Lentement Variable des Rayons X Solaires en Relation Avec la Structure des Centres d'Active. In Kiepenheuer (ed.) Structure and Development of Solar Active Regions, 420.
- Parkinson, J.H. and K.A. Pounds (1971): X-ray Observations of Solar Active Regions from OSO-5. Solar Physics, 17:146.
- Solar-Geophysical Data: National Geophysical and Solar Terrestrial Data Center, U.S. Department of Commerce, Boulder, Colorado.
- Teske, R.G. (1969): Observations of the Solar Soft X-ray Component: Study of Its Relation to Transient and Slowly Varying Phenomena Observed at Other Wavelengths. Solar Physics, 6:193.
- Webb, D.F., A.S. Krieger, and D.M. Rust (1976): Coronal Enhancements Associated with H-alpha Filament Disappearances. Solar Physics, 48:159.

Wolfson, C.J., L.W. Acton, and C.W. Gilbreth (1975): Mapping X-Ray Heliometer
for Orbiting Solar Observatory-8, Final Report. NASA CR-144710, 89 pp.

Wolfson, C.J., L.W. Acton, J.W. Leibacher, and D.T. Roethig (1977): Early
Evolution of an X-ray Emitting Solar Active Region. Solar Physics, 55:181.

THE HEIGHT STRUCTURE OF SOLAR ACTIVE REGIONS
AT X-RAY WAVELENGTHS AS DEDUCED FROM
OSO-8 LIMB CROSSING OBSERVATIONS

J.M. Mosher

Reprinted from Solar Physics (1979)
Vol. 64, pp. 109-119

THE HEIGHT STRUCTURE OF SOLAR ACTIVE REGIONS AT X-RAY WAVELENGTHS AS DEDUCED FROM OSO-8 LIMB CROSSING OBSERVATIONS

J. M. MOSHER

Lockheed Palo Alto Research Laboratory, 3251 Hanover Street, Palo Alto, Calif. 94304, U.S.A.

(Received 26 March; in revised form 31 May, 1979)

Abstract. Twenty limb crossing light curves of solar active region emission in the 1–4 keV energy band have been constructed from data gathered by the Lockheed Mapping X-Ray Heliometer experiment on OSO-8. These light curves indicate that 50% of the observed counts arise from heights below 20 000 km and 90% from heights below 57 000 km. The best fit is obtained for a model in which the emission density increases steadily down to the lowest observable levels, but the possibility of a small emission free gap at the base cannot be ruled out. On the average, the temperature of the plasma appears to be slightly higher at the base of a region than in its upper levels.

1. Introduction

Until very recently, the spatial resolution of solar X-ray telescopes has been insufficient to show directly the horizontal or vertical distribution of emission within a single solar active region. As a result, a number of indirect schemes have been used to estimate these functions. Of these schemes, one of the simplest is that of deducing the height structure from the variation of intensity with time as a region passes over the limb, the idea being that the change in brightness between times t and $t + \Delta t$ can be attributed to the portion of the region which disappeared from view during that interval.

This method was employed by Parkinson (1973) in the interpretation of the limb crossing of three typical solar soft X-ray sources using data from OSO-5. The appearance in that data of a 1 day delay between the predicted time of limb crossing and the actual start of X-ray occultation led to the conclusion that there was an emission-free gap of about 20 000 km thickness separating the base of the X-ray emitting plasma from the photosphere – a result which appears to be in direct conflict with the photographic measurements of Vaiana *et al.* (1973) showing both average temperature and electron density increasing steadily down to at least 5 arc sec from the surface. In addition, a variation of the limb crossing technique employed by Catalano and Van Allen (1973), in which direct flare intensities were compared with the intensities seen by a second satellite for which the flare occurred a known distance behind the limb, showed that the majority of the soft X-ray plasma at flare peak is within $(8 \pm 2) \times 10^3$ km of the photosphere, again casting doubt on the possibility of a 20 000 km gap in the non-flaring region.

In the present study, data from the Lockheed Mapping X-Ray Heliometer experiment on OSO-8 has been analyzed in an effort to better define the average properties of limb crossings at X-ray wavelengths, and to reinterpret that average behaviour in terms of a reasonable height structure.

2. Instrumentation

The Lockheed Mapping X-Ray Heliometer (MXRH) on OSO-8 (Wolfson *et al.*, 1975) was operated from June, 1975 through September, 1978, in a period of mainly moderate to low solar activity. The experiment is designed to study solar X-ray emissions in the energy range 1–15 keV by means of six proportional counter detectors viewing the Sun through three independent collimator systems. A more detailed description of the instrument and of the sensitivities of the various detectors can be found in Wolfson *et al.* (1977). The limb crossing data used here are drawn almost exclusively from Thin Window Detector A, the most sensitive of the six MXRH detectors at low energies, and hence the one with the highest intrinsic count rates. It contains an argon-CO₂ gas mixture behind a 3 cm² window of 76 micron thick Beryllium. Due to a systematic variation of average active region temperature with intensity, the count rates in this detector are very nearly proportional to the 1–8 Å output of the region, with 10 000 cps corresponding to about 1.6×10^{23} ergs s⁻¹.* The observed counts are produced almost entirely by photons in the range 1–4 keV. When the total Thin A count rate exceeds about 70 000 cps, as during most flares, the experiment automatically switches to a less sensitive detector, and in these cases an equivalent Thin A count rate has been used in preparing the limb crossing light curve.

Thin Window Detector A views the Sun through a one dimensional collimator having 13 useable fan beams of transmission. This provides the equivalent of a single 2.5 arc min half-width beam sweeping the Sun once every 40 s. Data from the other two collimator systems are used to confirm that no other significant X-ray source was present in the swath observed by Thin A.

Each point on the present limb crossing light curves (Figures 1 and 2) represents the average intensity of an orbit-long (90 min) segment of data. The effective integration time is about 2 s per point.

3. Selection of Data

In its 3½ years of operation, the MXRH observed the disk passage of several hundred significant X-ray emitting active regions. The present study is confined to 20 of the best examples, chosen from among sources which were cleanly resolved by Thin A, sufficiently strong to be potentially observable behind the limb, sufficiently steady for a reasonably definite unocculted intensity to be assigned, and free from the possibility of confusion by nearby but unrelated activity when behind the limb. An effort

* All count rates given in this paper are totals summed over the full width of the region.

was also made to obtain a roughly equal number of east and west limb crossings so that there would be no systematic bias towards growing or decaying regions. The final selections are listed in Table I, and a composite of the twenty limb crossing profiles, normalized to the intensities of the regions when on the disk, is shown in Figure 1. In preparing Figure 1, the east limb passages have been time-reversed so that they may be superimposed on the west limb ones. The two kinds of limb crossings are distinguished by an E or W following the McMath number in Table I.

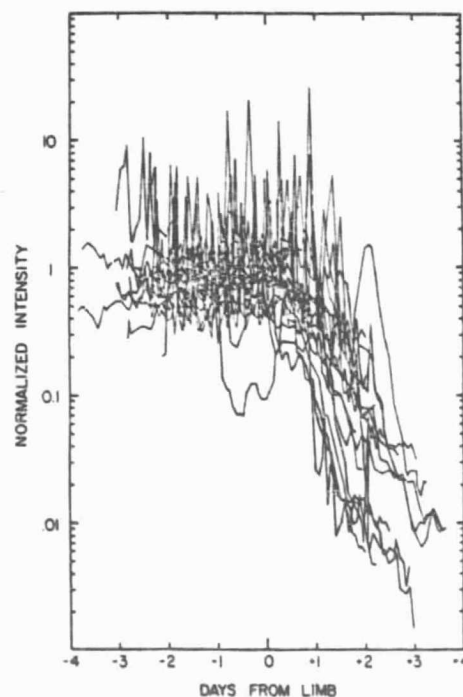


Fig. 1. Composite of the twenty limb crossing examples (east limb crossings time-reversed), each normalized to its average intensity when 1–2 days onto the disk.

Table I, as well as identifying the regions, gives the calculated limb passage date for the center of the McMath plage, the maximum longitudinal extent of the region as measured from the magnetograms and H-alpha photographs published in *Solar-Geophysical Data*, and the average unocculted X-ray intensity (evaluated 1–2 days onto the disk). The 'gap' and 'scale height' describe an exponential height distribution of emission whose predicted limb crossing characteristics would approximate the apparent non-flare 'baseline' of the actual region

$$I(z) dz = \frac{I_0}{H_0} \exp - \left(\frac{z - H_1}{H_0} \right) dz, \quad (1)$$

TABLE I
Twenty MXRH limb crossing selections

McMath No.	Limb date	Latitude	Maximum width	Intensity (10^3 cps)	Exponential approximation	
					Gap (10^3 km)	Scale height (10^3 km)
13736W	6-30.0-75	8° S	7.4	42.1	10	20
13738W	7-7.8-75	7° N	17.6°	8.8	5	20
13750W	7-16.6-75	6° N	14.5°	54.1	10	10
13766W	7-26.8-75	7° S	22.2°	12.7	5	10
13777E	7-20.9-75	8° N	18.2°	5.9	10	20
13786E	7-29.6-75	6° N	21.2°	34.9	0	10
13790W	8-16.3-75	9° N	19.2°	120.4	10	10
13826W	9-11.8-75	8° N	30.4°	34.9	5	40
13832W	9-19.0-75	8° S	32.0°	3.7	20	10
13892W	10-11.1-75	13° S	15.8°	9.4	10	20
14029W	1-25.3-76	12° S	15.0°	4.4	0	20
14127W	3-26.0-76	6° N	15.0°	1,2.0	0	10
14143E	3-24.1-76	8° S	13.6°	321.4	5	10
14143W	4-7.1-76	8° S	13.6°	17.6	0	10
14161E	4-8.1-76	5° N	19.4°	11.1	10	20
14375E	8-18.6-76	12° S	18.7°	8.4	5	5
14579E	12-24.1-76	20° S	17.6°	44.2	10	20
14607W	1-19.5-77	28° S	9.6°	47.7	5	20
14726E	4-11.6-77	22° S	19.0°	157.8	10	40
14726W	4-25.8-77	22° S	19.0°	17.8	5	20

where H_0 is the scale height and H_1 is the gap (see Section 4.3). These two parameters, together with the disk intensity, I_0 , give a fairly accurate impression of the appearance of the individual light curves, as is shown in Figure 2. A small scale height indicates that the intensity fell rapidly, whereas a large one indicates that it fell slowly. A gap of 'zero' indicates that the intensity began falling at or before the predicted limb crossing time, whereas a large gap indicates that the start of the occultation appeared to be delayed.

4. Interpretation of Limb Crossing Data

The interpretation of the limb crossing data was accomplished by searching for 'best fits' between the observed intensities and those predicted for model regions. In the models, a family of possible height and width distributions of emission (assumed to be constant with time) is considered. The converse process, of attempting to go directly from a single limb crossing light curve to an inferred height distribution (assuming only a horizontal width for the region) is much more difficult and generally leads to uncertain results.

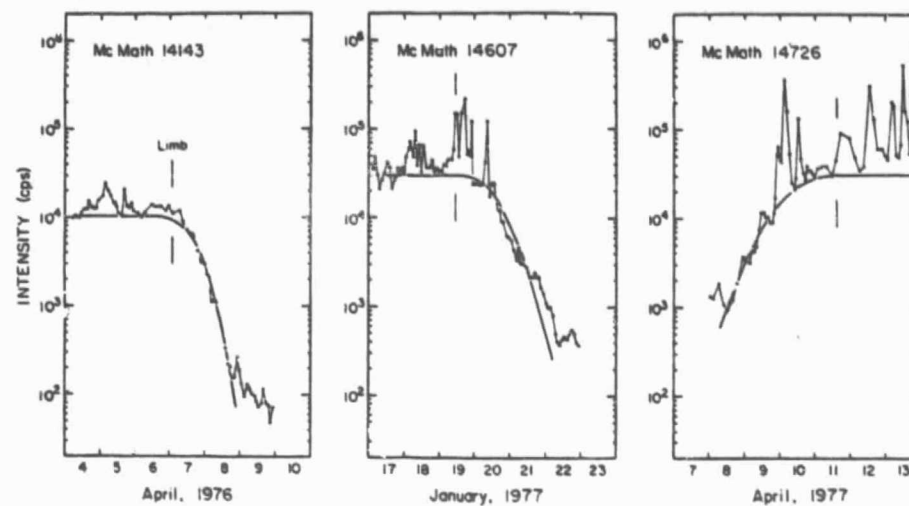


Fig. 2. Light curves of three individual regions illustrating a 'fast', 'normal', and 'slow' limb crossing. The smooth curves are those predicted for exponential emission distributions with the gap, scale height, latitude and longitudinal extent specified in Table I.

4.1. MINIMUM VISIBLE HEIGHT

In making the model calculations, it is necessary to be able to evaluate the minimum visible height for a vertical column whose latitude and longitude correspond to a position behind the limb. This minimum height is given by

$$H_{\min} = R_{\odot} \left(\frac{1}{\sin \theta} - 1 \right), \quad (2)$$

where R_{\odot} is the radius of the Sun (696 000 km plus the thickness of the occulting layer) and θ is the angular distance of the base of the column from disk center, which is given by

$$\theta = \cos^{-1} (\sin B_0 \sin \lambda + \cos B_0 \cos \lambda \cos \phi), \quad (3)$$

where B_0 is the tilt of the Sun's polar axis ($-7\frac{1}{4}^\circ \leq B_0 \leq +7\frac{1}{4}^\circ$), λ is the latitude, and ϕ is the longitude measured from central meridian (see Figure 3).

The longitude is assumed to advance at the rate given by Newton and Nunn (1951) for recurrent sunspots:

$$\phi = (13.39 - 2.77 \sin^2 \lambda) T, \quad (4)$$

where T is the fractional number of days since central meridian passage. The limb crossing occurs when $\theta = 90^\circ$. For the present purpose, the McMath calcium plage latitudes and central meridian passage dates listed in *Solar-Geophysical Data (Prompt Reports)* were found to be adequate and convenient, and were used in evaluating the limb crossing times given in Table I.

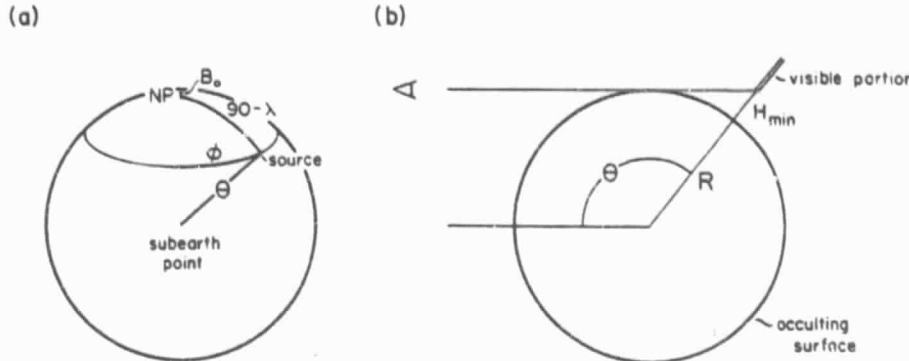


Fig. 3. (a) Relation of the angular distance θ to the latitude, λ , longitude, ϕ , and polar tilt, B_0 . (b) Method of calculating H_{\min} , the minimum visible height along a radial column with $90^\circ \leq \theta < 180^\circ$. The diagram is constructed in the plane containing the source, observer, and Sun center, so that θ assumes its full value. R includes the thickness of the occulting layer, and H_{\min} is measured from its top.

Since the effect of the Sun's polar tilt is very small, it was found that the model curves could be calculated assuming $B_0 = 0$, provided only that they were registered to a properly calculated limb crossing point in the observed data.

The graphs shown in Figure 4, although intended for a different purpose, are essentially a plot of H_{\min} as a function of time behind the limb.

4.2. HEIGHT OF THE OCCULTING LAYER

By means of the limb crossing interpretation, the height structure is automatically evaluated with respect to some occulting level above which, at grazing incidence, the radiation is transmitted and below which it is absorbed. To estimate the height of this level for the occultation of 2 keV X-rays in the solar atmosphere, we may use the recent results of Fireman (1974) and Cruddace *et al.* (1974) which indicate a total absorption cross section of about $3 \times 10^{-23} \text{ cm}^2 \text{ atom}^{-1}$, and evaluate the column densities along grazing paths using the chromospheric model of Allen (1973) from 0–2000 km (above the photosphere), and the spicular model of Beckers (1972) from 2000–10 000 km. One finds that the column density falls from $3 \times 10^{23} \text{ atoms cm}^{-2}$ to $3 \times 10^{21} \text{ atoms cm}^{-2}$ between 500 and 1000 km, which would mean that the atmosphere goes from transparent to opaque between these levels. Hence the zero of our height scale for the occultation of soft X-rays will be a position about 750 km or 1 second of arc above the photosphere.

4.3. MODEL REGIONS

In the calculations, the solar active region was visualized as consisting of a series of horizontal slabs of 5000 km thickness and of 0 to 18° width in longitude (18° is the average of the maximum dimensions listed in Table I). Regions with a more complicated horizontal structure can be approximated by a series of zero-width

regions separated in longitude. Once un-occulted intensities have been assigned to the various slabs, the predicted intensity of the region at any time can be evaluated simply by calculating the fraction of each slab exposed to view.

The horizontal slab picture is obviously not an accurate physical representation of the true distribution of plasma within a region – the true distribution is presumably one in which the plasma is confined to closed magnetic loops – but it seems mathematically sufficient if the object is simply to determine the fraction of the observed X-ray brightness originating in the various height intervals. That fraction can be thought of as resulting from some combination of the brightness and number of loops at each height. Our conclusions will show that the average height of the plasma observed by the MXRH Thin Window A detector (which is roughly comparable to AS&E's Skylab filter No. 5) is quite small relative to the probable width of the region (i.e., 20 000 km vs 100–200 000 km), implying that the majority of 1–4 keV X-rays come either from very low-lying loops, or from the foot-points of larger ones.

The simplest family of model regions is that in which the intensity falls off exponentially with height, possibly with an emission-free gap at the base, but more arbitrary height distributions were also considered. Each variation in the model produces a different sort of effect in the predicted occultation curve, but in nearly all cases, the calculations predict that the 50% attenuation point will be a reasonably accurate indicator of the median X-ray height. This relationship is shown in Figure 4. Unfortunately, the X-ray sources are often too variable for the 50% point to be easily determined. The interpretation of other percentage points, such as 10% and 90% occultation, is less obvious and depends on the detailed assumptions about the horizontal and vertical structure of the region.

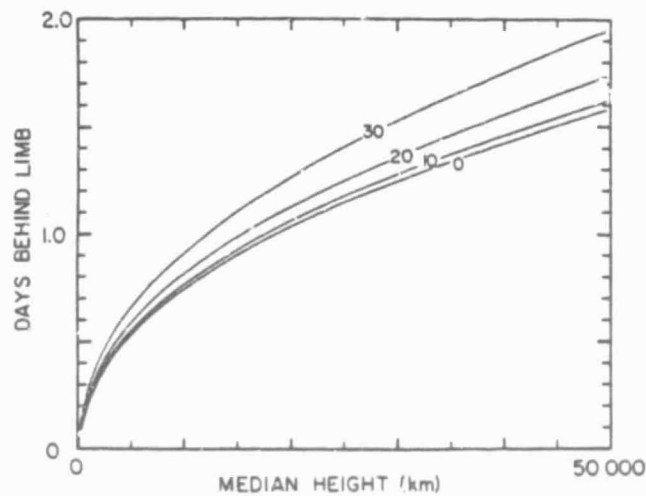


Fig. 4. Interpretation of the 50% occultation point of model regions in terms of the median X-ray height at four latitudes from 0 to 30°.

5. Interpretation of the Observed Average X-Ray Limb Crossing Profile

In order to successfully apply the limb-crossing technique, it is necessary that the intrinsic brightness of the solar region be constant during the period of observation. It is evident from Figures 1 and 2 that this is not true for X-ray regions, and that the effort to establish a 'non-flare baseline' (such as was used in determining the 'gap' and 'scale height' in Table I) can lead to quite arbitrary results. Only if a sufficiently great number of cases is averaged together can we hope that the assumption of constant brightness will be approximated. Such a numerical average of the normalized intensities of the 20 regions, at intervals of 0.1 days from 2 days preceding to 2 days following the date of limb passage is shown in Figure 5, together with two interpretations in terms of height structure based on the two extreme assumptions regarding the horizontal width of the region: 0 and 18° (215 000 km). The true average width of the regions involved is almost certainly between these extremes. The MXRH itself generally shows the brightness in Thin A spread over a half-width which, after correction for instrumental response, is less than 100 000 km or 8° in longitude, but the X-ray source may be offset somewhat from the assumed center of the region.

The model height distributions in Figure 5 were obtained by starting with the closest-fitting exponential (having a scale height of about 30 000 km), and then manipulating the brightnesses of the various 5000 km thick layers until the closest fit

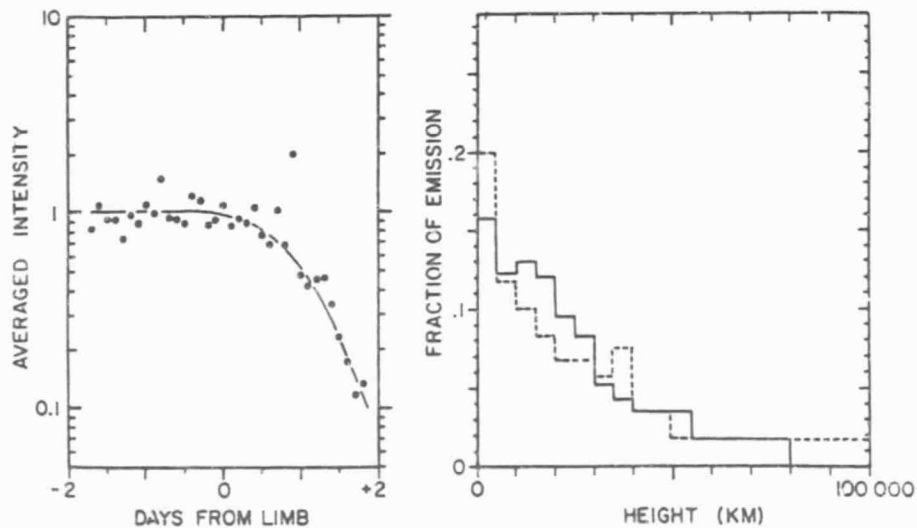


Fig. 5. Numerical average of the twenty normalized limb crossing light curves and its interpretation in terms of the fraction of the total emission arising in various 5000 km thick height intervals. The solid histogram is based on the assumption of an 18° spread in longitude, whereas the dashed one assumes zero width.

to the observed data was obtained (the smooth curve in the left half of Figure 5). These distributions indicate that 50% of the observed counts come from below 19–20 000 km and 90% from below 53 000–60 000 km. An additional 750 km should be added to account for the thickness of the occulting layer.

While no other height distribution would produce a significantly better fit to the averaged data, there are many other possible distributions whose fit would not be significantly worse. In particular, even though there would seem to be no compelling reason for doing so, one can consider the possibility of emission-free gaps between the photosphere and the base of the X-ray emitting plasma in the manner of Parkinson (1973). When this is done, it is found that gaps of up to about 15–20 000 km can be accommodated within the scatter of the averaged data; however, the gapped models seem less pleasing since the emission is forced into a thinner and thinner zone so as to maintain a roughly constant median height.

6. Dependence of X-Ray Height on Age and Brightness of the Region

Table I, as well as Figures 1 and 2, indicate that there is a considerable variety in the limb crossing characteristics of individual active regions. Part of the scatter undoubtedly arises from errors introduced into the calculation of the limb passage date by using the central coordinates of the McMath plage. Such errors are probably mostly less than $\pm 4^\circ$, however, which would shift the curves horizontally by only about $\pm \frac{1}{2}$ day. One might think that the additional scatter would be largely a reflection of systematic effects arising from differences in the size, age or brightness of the regions being considered, but this does not appear to be the case. The 'gaps' and 'scale heights' listed in Table I do not correlate systematically with either the size (and therefore age) nor with the unocculted brightness of the regions. We conclude that the apparent differences are predominantly artifacts arising from changes in the intrinsic brightness of the regions during the period of observation.

7. Temperature Structure

While the primary objective of the present study was to define the variation of soft X-ray intensity with time during the limb passage of a typical region, the data examined also contain information as to the spectral hardness of that radiation over the relatively narrow range of wavelengths available, and this hardness parameter is in turn an indication of the temperature of the plasma producing the observed counts.

In each of the 20 cases, a comparison was made between the temperature observed in several quiet periods when the region was on the disk near the limb with that observed when the integrated intensity of the region had been reduced to about one third of its original non-flare level. The average unocculted temperature was $(2.45 \pm 0.05) \times 10^6$ K, compared to $(2.26 \pm 0.05) \times 10^6$ K for the two-thirds occulted

regions. While consistent with a model in which the plasma is hottest at its base, this difference is not very dramatic. A comparison between the relative count rates in the Thin Window A detector versus those in the Large Vertical detector (which is up to about 50 times more sensitive to photons above 4 keV) similarly failed to reveal any large temperature effect.

The present result, if verified, should not be thought of as implying that individual magnetic loops are necessarily hotter at their footpoints than at their tops, but rather, only that the lower lying structures are, on the average, slightly hotter than the more extended ones.

8. A Possible Explanation of Parkinson's Result

This study of twenty MXRH limb crossings has not confirmed Parkinson's (1973) conclusion from OSO-5 that the onset of soft X-ray attenuation is systematically delayed by 1 day from the nominal limb crossing of the corresponding photospheric region. While a few of the individual regions might be viewed as exhibiting this behavior (see Table I), the objective numerical average of Figure 5 shows a maximum possible delay of less than 0.5 days.

It is suggested that this discrepancy results from Parkinson's accidental use of a sidereal (instead of synodic) solar rotation rate in the calculation of his limb passage dates from central meridian crossing (see Parkinson, 1971). Such an error would lead to east limb passages occurring 0.5 days before predicted, and west limb passages happening 0.5 days after the predicted date.

9. Comparison With Flare Heights

The result of Catalano and Van Allen (1973) of $(8 \pm 2) \times 10^3$ km for the median height of the soft X-ray flare peak plasma is significantly below the median height of 20 000 km derived here for the X-ray active region in general. If correct, this result would imply that flares affect primarily the lower X-ray loops, and that the importance of flares relative to non-flare background should fall off systematically with time behind the limb.

The sample available here is really too small to objectively test this hypothesis. For example, in a typical 1 day interval of unocculted observation on the disk, the 20 regions together produced 6 flares raising the orbital average X-ray level by 10 or more times above its 'background' level. If one were to look during a comparable interval from 1 to 2 days beyond limb passage, the results of Catalano and Van Allen would suggest that the flare intensities should be attenuated by about 10 times, whereas Figure 5 indicates that the general X-ray level is down by about 5 times. Thus a 10 times flare should be converted into a 5 times one, and in fact 7 times 5 flares were found in the sample during this interval. This is consistent with the suggested difference in scale heights, but the statistics are obviously poor.

10. Summary and Conclusions

The average profile of X-ray intensity versus time for twenty regions passing behind the limb has been interpreted in terms of the quantity of 1–4 keV X-ray emitting plasma present at various heights above the photosphere. It is found that on the average, 50% of these counts observed by the Lockheed MXRH come from below 20 000 km, and 90% from below 57 000 km. This result is greater than the typical height of origin of soft X-ray flares reported by Catalano and Van Allen (1973), but lower than the previously reported general X-ray heights derived by Parkinson (1973) from OSO-5 data. The present data, in themselves, provide no compelling reason for supposing that the plasma within a region is separated from the photosphere by an emission-free gap in the manner described by Parkinson, and specifically contradict the existence of gaps greater than 15–20 000 km. The limb crossing characteristics of individual regions appear to be dominated by intrinsic changes in brightness rather than by systematic variations in age, size, or brightness. X-ray temperature variations during occultation are slight, with the lowest parts of the region appearing hottest.

Acknowledgements

Loren W. Acton is Principal Investigator on the MXRH experiment. The present study has benefitted from useful discussions with C. J. Wolfson and K. L. Smith. The MXRH project has been supported by NASA under Contract NAS5-22411, NAS5-11360 and by the Lockheed Independent Research Program.

References

- Allen, C. W.: 1973, *Astrophysical Quantities*, 2nd Edition, Athlone Press, p. 174.
Beckers, J. M.: 1972, *Ann. Rev. Astron. Astrophys.* **10**, 73.
Catalano, C. P. and Van Allen, J. A.: 1973, *Astrophys. J.* **185**, 335.
Crudace, R., Paresce, F., Bowyer, S., and Lampton, M.: 1974 *Astrophys. J.* **187**, 497.
Fireman, E. L.: 1974, *Astrophys. J.* **187**, 57.
Newton, H. W. and Nunn, M. L.: 1951, *Monthly Notices Roy. Astron. Soc.* **111**, 413.
Parkinson, J. H.: 1971, University of Leicester Thesis, p. 153.
Parkinson, J. H.: 1973, *Solar Phys.* **28**, 137.
U.S. Department of Commerce: *Solar-Geophysical Data*, (Part I: Prompt Reports), Boulder, Colo., U.S.A.
Vaiana, G. S., Krieger, A. S., and Timothy, A. F.: 1973, *Solar Phys.* **32**, 81.
Wolfson, C. J., Acton, L. W., and Gilbreth, C. W.: 1975, Mapping X-Ray Heliometer for OSO-8, Final Report, NASA-CR-144710.
Wolfson, C. J., Acton, L. W., Leibacher, J. W., and Roethig, D. T.: 1977, *Solar Phys.* **55**, 181.

Appendix 0

X-RAYS, FILAMENT ACTIVITY AND FLARE PREDICTION

J.M. Mosher and L.W. Acton

Reprinted from Solar Physics (1980)

Vol. 66, pp. 105-111

X-RAYS, FILAMENT ACTIVITY AND FLARE PREDICTION

J. M. MOSHER and L. W. ACTON

Lockheed Research Laboratory, Palo Alto, Calif., U.S.A.

(Received 21 May; in revised form 30 October, 1979)

Abstract. 127 hr of high-resolution H α movies of young active regions have been compared with simultaneous 1.5–15 keV X-ray measurements from the Mapping X-Ray Heliometer experiment on OSO-8, with particular attention to preflare periods and to the possibility of X-ray emission associated with filament activity during that time. The period studied included 8 confirmed flares or subflares, 16 unreported events of comparable magnitude, and numerous examples of filament activity. We found no evidence for X-ray emission from areas of enhanced filament activity unless simultaneous brightenings were present in H α . In addition, we detected no peculiar behavior of either filaments or X-rays during the period of approximately 20 min preceding these small flares which, even in retrospect, would have allowed them to be 'predicted'.

A quantitative definition of H α filament activity is not easy to arrive at, but in general it must be agreed that it is manifested by rapid fluctuations in the size and darkness of the filament at line center, and by fluctuating visibility and streaming motions in the line wings. Some forms of surge activity would be included in this definition. An extreme example of filament activity is the sudden disappearing filament or *disparition brusque*, which when observed at the limb is seen as an eruptive event.

Activity in dark chromospheric features is by no means universally associated with simultaneous activity in bright features (flares), but numerous examples can be found suggesting connections between the two, both in the sense of flares appearing to trigger activity in filaments and of filament activity appearing to trigger flares (Tandberg-Hanssen, 1967, and references therein). In addition, a rather intimate relationship has long been suggested between filament activity and X-ray emission (Kreplin *et al.*, 1962; Zirin *et al.*, 1969). So frequent has been the reference to these observations that it has led by many authors (e.g., Bruzek, 1964, 1969; Kiepenheuer, 1964; Rust, 1976; Švestka, 1976; Dodson-Prince and Bruzek, 1977) to the formulation of a more or less standard sequence of flare events in which the 'flash' or 'explosive' phase (during which both optical and X-ray emission rise rapidly) is said to be preceded by a 'preflare' or 'preflash' phase, lasting up to tens of minutes, during which gradually rising X-ray emission appears to be correlated with an erupting filament (Roy and Tang, 1975; Rust *et al.*, 1975), possibly, but not necessarily, accompanied by simultaneous faint brightenings in the chromosphere. Indeed, it has been suggested that for major flares, the peculiarity of the filament activity during this preflare period could be used as a predictive tool (Smith and Ramsey, 1964; Martin and Ramsey, 1972).

While we would not dispute that such a picture, at least as regards preflare filament activation, may be valid for major flares (particularly those in old regions with

decayed spots: Dodson and Hedeman, 1970), it has never been very clearly stated how many examples of major filament activity are 'resolved' without flaring, nor to what extent the principles of prediction may be applied to the more common small flares which occur in young regions. The role of X-rays in the preflare activity is especially unclear. Wolfson *et al.* (1978) have found that for a randomly selected sample of small flares with good preflare coverage it is just as common to find a declining X-ray flux for 20 min prior to the flash phase as to find a rising one. Further, in those flare events in which the temporal separation between filament activation and chromospheric brightening is most distinct - namely in the *disparitions brusque*, where the complete disappearance of the filament at line center may precede the first recognizable chromospheric brightening - the onset of X-ray emission is said to be delayed, and to coincide most nearly in time with the optical brightening if the latter is bright enough to be detected (Sheeley *et al.*, 1975; Dodson and Hedeman, 1976; Webb *et al.*, 1976).

In the present study we have compared a considerable volume of high-resolution H α observations with simultaneous spatially-resolved X-ray observations in an effort to form an independent opinion as to whether for ordinary flares in young active regions:

- (a) The observation of unusual filament and/or X-ray activity is a useful indication of impending flares; and
- (b) presence of filament activity alone is sufficient 'cause' for an X-ray enhancement, or if the latter is observed only when there is a simultaneous brightening in the chromosphere.

The X-ray observations used here come from the Lockheed Mapping X-Ray Heliometer (MXRH) experiment on OSO-8. This instrument, which has been described by Wolfson *et al.* (1975, 1977), observes the Sun in the energy range 1–15 keV with a spatial resolution of about 2.5 arc min in three one-dimensional systems. Under favorable circumstances, it can separate the X-ray signals from the several strongest active regions present on the disk, monitoring each with 10-s time resolution for about half of each 90-min orbit (interrupted by spacecraft night and by areas of unusably highly background).

These data were compared with simultaneous high-resolution H α filtergram movies provided by the Big Bear Solar Observatory. The filtergrams, which were taken with a 10" refractor and $\frac{1}{2}$ to $\frac{1}{4}$ Å bandpass birefringent filters, cover a field of about 4×6 arc min, and are usually centered on a young flare-productive region. Since there is little variation in the quality of the X-ray observations over the $3\frac{1}{2}$ year span of that experiment's operation (July, 1975–September, 1978), the procedure adopted was to first survey a large quantity of movies in search of interesting events occurring during times of good seeing. In all, guided by the observing notebooks and discussions, about 200 days of coverage were examined; from which the reels containing the highest quality images were selected for comparison with the X-ray data. These selections are listed in Table I.

TABLE I
Summary of regions studied and activity observed during the period of simultaneous coverage

McMath region number	Dates used	No. of orbits studied	Area of spots (millionths)	Minimum 1-8 Å output (10^{23} ergs s^{-1})	Maximum 1-8 Å output (10^{23} ergs s^{-1})	No. confirmed flares and subflares	No. unconfirmed subflares	Total No. X-ray fluctuations
13766	7-24, 25-75	7	170	2	3	0	1	3
13783	7-25, 26, 27-75	10	60	1.5	9	0	0	5
13786	7-31-75	15	300	3	200	0	2	14
	8-2, 10-11-75							
13790	8-11, 12, 13, 14-75	22	500	6	40	1	4	28
13937	11-15-75	1	200	5	80	1	0	2
14127	3-21-76	5	380	10	400	0	3	8
14143	3-30, 31-76	15	500	2	30	1	1	17
	4-1, 2-76							
14179	4-29, 30-76	11	200	~4	≥ 700	3	1	12
14203	5-15-76	6	90	1.5	4	0	0	3
14785	5-30, 31-77	29	250	2.5	10	0	2	30
	6-1, 2-77							
14832	7-4, 5, 6-77	17	200	2	9	0	0	3
14967	10-3, 4-77	7	140	≤ 3	4	0	0	1
14979	10-7, 9-77	10	280	5	70	0	1	5
15124	2-2-78	4	250	10	70	2	1	6

In all, a total of 169 orbits, or about 127 hr, of simultaneous coverage are involved. Roughly half of the H α data is at line center, and half at 0.6 Å in the blue wing, where the rising preflare filament motions are supposed to be particularly evident (Smith and Ramsey, 1964). In addition to listing the names of the regions studied, Table I gives the approximate size of the associated spot group, its maximum and minimum 1–8 Å X-ray output, and the number of flare events occurring during the period of simultaneous coverage. 'Confirmed' flares refers to events listed in *Solar-Geophysical Data*. 'Unconfirmed' events are of comparable magnitude, but did not appear in the official flare lists. The two largest flares studied were of Importance 1 (April 30, 1976 and February 2, 1978). All of the others are subflares. Finally, the total number of all X-ray fluctuations representing more than about a 50% variation in intensity over one orbit or less is given.

Now the exact level of X-ray enhancement which was looked for is difficult to specify in quantitative terms, as is the level of filament activity with which we sought to correlate it. For a point source, the intrinsic sensitivity of the MXRH corresponds to about 3×10^{21} ergs s $^{-1}$ in the 1–8 Å band, but for stronger sources (because the X-ray output of a region is never perfectly steady) some subjective combination of fluctuation amplitude and time scale – such as a 20% change in intensity over 20 min – is obviously required before a distinct X-ray 'event' will be recognized. Similarly, when the H α chromosphere is viewed at high spatial resolution, particularly in off-band pictures, some degree of filament activity is almost always present. A second potential problem is that within the general area monitored by the X-ray detectors several different chromospheric events may be simultaneously in progress, and the assignment of a particular X-ray enhancement to any one of them is difficult. In any event, the problem was to see to what extent periods of enhanced filament activity could be convincingly related to periods of enhanced X-ray emission, and whether either of these kinds of activity appeared to happen unusually often in the period immediately preceding flares.

The main impression with which we were left by the total quantity of film viewed tends to confirm the observations of Dodson and Hedeman (1976); that is, fluctuations in the X-ray output of a region appear to be closely associated with simultaneous fluctuations in the intensity of bright H α features, and very little related to fluctuations in dark features (such as filaments). Most potential counterexamples to this rule could easily be explained. When a fluctuating bright chromospheric feature could not be found at the time of an X-ray enhancement, the plages in the region involved were usually already quite bright, so that a small additional variation in brightness could have passed unnoticed. Similarly, when an obvious change in H α brightness produced no noticeable change in the X-rays, the X-ray level was usually already quite high. In spite of this good general correlation, it should be noted that the magnitude of the X-ray fluctuation corresponding to a particular change in plage brightness is not perfectly predictable, as is demonstrated by the ability of repetitive and seemingly homologous H α flares to produce a variety of X-ray signatures. As an example, one small flare in McMath 13783 on July 27, 1975 at 14:30 UT produced a

factor of 2 increase in the X-ray output, whereas a larger and brighter repeat of this event in H α at 16:40 UT produced no noticeable effect (i.e., less than about 20% enhancement) in spite of a similar background level.

The impression that fluctuating dark features within the field of view are not the key to the X-ray enhancements is reinforced by numerous examples in which filament activity was the dominant process and X-ray enhancements were not observed. A typical instance of this lack of association, at least at the sensitivity of the MXRH, would be the observations of McMath 14785 on June 1, 1977. In this case, a large filament located 2 arc min northwest of the main activity center exhibited strong off-band streaming motions from 20:50 to 23:55 UT. During this interval, the 1-8 Å flux actually declined from 1×10^{24} to 3×10^{23} ergs s $^{-1}$ (evidently recovering from a small flare in the main region), and there was no significant change in the position of the center of mass of the X-ray emission compared to its position before or after the period of enhanced filament activity. We conclude that the amount of X-ray emission arising at the site of the filament activity could not have been more than about 10^{23} ergs s $^{-1}$. Another example would be the observations of McMath 15124 on February 2, 1978. This region exhibited unusually violent and dramatic dark surge-like motions in the superpenumbra of the main spot throughout the period of observation from 17:30-24:00 UT. During this period, the rise of each of the three main X-ray enhancements observed by the MXRH was clearly coincident with a bright chromospheric flare, and no connection could be found between the rest of the X-ray light curve and the timing of the activity in the superpenumbra. Rust *et al.* (1977) have also noted a lack of X-ray emission from non-flaring surges.

As to the tendency of peculiarities in either filament activity or X-ray output to anticipate the onset of flares, we could see nothing that would make these of significant predictive value for the sort of small flare studied here. As suggested by Table I, minor filament activity and minor X-ray fluctuations are a more or less constant occurrence, and in contradiction to the results of Martres *et al.* (1977) we could find no systematic change in their character during the interval of 10-20 min prior to onset of a small flare; and in the few instances where the X-ray level did rise slowly before the flash phase, as for about 10 min before the start of the Importance 1 proton flare at 20:47 UT on April 30, 1977, it appeared that the chromospheric plages were also brightening slightly at the same time. The only systematic correlation between flare and filament activity which we could see was that in virtually every flare studied a substantial disturbance occurred in the filamentary material lying between the flare ribbons at the time of the flash phase. The onset of this disturbance did not appear to significantly precede the onset of flare brightening, and while it is difficult to disentangle cause and effect, the X-ray light curves certainly seemed to follow most nearly the pattern of H α brightening, independent of how much filamentary activity was involved.

Because the high-resolution H α films concentrated on young active regions, our sample did not include a useable example of a classic *disparition brusque* event, that is a sudden disappearing filament in a region of small or no spots. To complete our

study, one such example was taken from the patrol films obtained at Big Bear's Tel Aviv station. This event occurred on November 14, 1977 between 11:45 and 16:00 UT in the decayed region preceding McMath 15025. As reported by Webb *et al.* (1976) and by others, we found that the start of the X-ray event occurred well after the start of the filament disruption. In this particular instance, a delay of 45 min was observed from the first observation of rising motions in the filament to the beginning of the X-ray enhancement (which was simultaneous with the appearance of faint brightness in the chromospheric flare ribbons). The total 1–8 Å output of this event was about 4×10^{27} ergs in 3 hr.

In summary, we were unable to find any evidence of a direct association between filament or surge activity and X-ray emission in the absence of simultaneous chromospheric emission (presumably indicating a close link between the mechanisms producing the latter two kinds of output). In addition, we were unable to detect any systematic peculiarity in either the filament or X-ray activity which would have allowed us to predict the onset of the flares studied here, except for the one *disparition brusque* event described above.

Acknowledgements

This research was supported by the U.S. National Aeronautics and Space Administration under contract NAS5-22411. We are indebted to Dr H. Zirin for use of the H α films from Big Bear Solar Observatory and Tel Aviv.

References

- Bruzek, A.: 1964, in W. N. Hess (ed), *AAS/NASA Symposium on the Physics of Solar Flares*, p. 301.
- Bruzek, A.: 1969, in C. de Jager and Z. Švestka (eds.), *COSPAR Symposium on Solar Flares and Space Research*, p. 61.
- Dodson, H. W. and Hedeman, E. R.: 1970, *Solar Phys.* **13**, 401.
- Dodson, H. W. and Hedeman, E. R.: 1976, *Solar Phys.* **47**, 267.
- Dodson-Prince, H. W. and Bruzek, A.: 1977, in A. Bruzek and C. J. Durrant (eds.), *Illustrated Glossary for Solar and Solar-Terrestrial Physics*, D. Reidel Publ. Co., Dordrecht, Holland, p. 81.
- Kiepenheuer, K. O.: 1964, in W. N. Hess (ed.), *AAS/NASA Symposium on the Physics of Solar Flares*, p. 323.
- Kreplin, R. W., Chubb, T. A., and Friedman, H.: 1962, *J. Geophys. Res.* **67**, 2231.
- Martin, S. F. and Ramsey, H. E.: 1972, in P. S. McIntosh and M. Dryer (eds.), *Solar Activity Observations and Predictions*, MIT Press, p. 371.
- Martres, M.-J., Soru-Escaut, I., and Nakagawa, Y.: 1977, *Astron. Astrophys.* **59**, 255.
- Roy, J.-R. and Tang, F.: 1975, *Solar Phys.* **42**, 425.
- Rust, D. M.: 1976, *Solar Phys.* **47**, 21.
- Rust, D. M., Nakagawa, Y., and Neupert, W. M.: 1975, *Solar Phys.* **41**, 397.
- Rust, D. M., Webb, D. F., and MacCombie, W.: 1977, *Solar Phys.* **54**, 53.
- Sheeley, N. R., Jr., Bohlin, J. D., Brueckner, G. E., Purcell, D., Scherrer, V. E., Toussey, R., Smith, J. B., Jr., Speich, D. M., Tandberg-Hanssen, E., Wilson, R. M., DeLoach, A. C., Hoover, R. B., and McGuire, J. P.: 1975, *Solar Phys.* **45**, 377.
- Smith, S. F. and Ramsey, H. E.: 1964, *Z. Astrophys.* **60**, 1.
- Švestka, Z.: 1976, *Solar Flares*, D. Reidel Publ. Co., Dordrecht, Holland, pp. 42, 216, and 307.
- Tandberg-Hanssen, E.: 1967, *Solar Activity*, Blaisdell Publ. Co., Waltham, Mass., p. 376.

- Webb, D. F., Krieger, A. S., and Rust, D. M.: 1976, *Solar Phys.* **48**, 159.
Wolfson, C. J., Acton, L. W., and Gilbreth, C. W.: 1975, 'Mapping X-Ray Heliometer for OSO-8', Final Report, NASA-CR-144710.
Wolfson, C. J., Acton, L. W., Leibacher, J. W., and Roethig, D. T.: 1977, *Solar Phys.* **55**, 181.
Wolfson, C. J., Acton, L. W., and Leibacher, J. W.: 1978, *Bull. Am. Astron. Soc.* **10**, 456.
Zirin, H., Ingham, W., Hudson, H., and McKenzie, D.: 1969, *Solar Phys.* **9**, 269.

BIBLIOGRAPHY

Note: for publications produced under the current contract, please see Appendix A.

Bruner, E.C., Jr. (1980): "The Lockheed OSO-8 Program: Analysis of Data from the High Resolution Ultraviolet Spectrometer Experiment," NASA GSFC Final Report (NAS5-22411, Task II).

Donnelly, R.F., Grubb, R.N., and Cowley, F.C. (1977): "Solar X-Ray Measurements from SMS-1, SMS-2 and GOES-1: Information for Data Users", NOAA Technical Memorandum ERL SEL-48.

Lockheed Palo Alto Research Laboratory (1975): "Technical Manual for the Mapping X-Ray Heliometer Instrument on OSO-1," Technical Report, NAS5-11360, Item 18.

Orrall, F.Q., ed. (1980): Energy Balance and Physical Conditions in Active Regions (Skylab Solar Workshop III), University of Colorado, in press.

Pallavicini, R., Serio, S., and Vaiana, G.S. (1977): "A Survey of Soft X-Ray Limb Flare Images," Astrophys. J. 216, 108.

Peterson, L.E., Hudson, H.S., and Tsikoudi, V. (1976): "New Upper Limits on Jovian X-Rays," Icarus 22, 419.

Shapley, A.H. (Dec, 1976): private communication.

Tucker, W.H. and Koren, M. (1971): "Radiation from a High-Temperature, Low-Density Plasma: The X-Ray Spectrum of the Solar Corona," Astrophys. J. 168, 283.

Webb, D.F., Krieger, A.S., and Rust, D.M. (1976): "Coronal X-Ray Enhancements Associated with H-Alpha Filament Disappearances," Solar Phys. 48, 159.

Wolfson, C.J., Acton, L.W., and Gilbreth, C.W. (1975): "Mapping X-Ray Heliometer for OSO-8," Final Report, NASA CR-144710.

Wolfson, C.J., Acton, L.W., and Smith, K.L. (1978): "Final Report for the Orbital Operations Portion of the Mapping X-Ray Heliometer Program (OSO-8)", NASA GSFC Final Report (NAS5-22411, Task Ia).

INDEX

(Text only -- contents of articles not indexed)

	Page
Computer program development	5
Data available	3
Data processing, extent of	14
Data requests	21
Extra-solar program	33
Filaments	
Active	23
Eruptive	27
Follow-on Contract	14
Mapping X-Ray Heliometer (MXRH), description of	1
National Space Science Data Center, contribution to	18
New Technology	33
NOAA flare forecast center	16
Preflare enhancement	23
Presentations	39
Publications	37
Radio observations, correlation with X-rays	23, 32
References	39, 142
Reprints	49ff
Spectral features	26
Sympathetic flares	25
Transient UV brightenings	32
World Data Center (<u>Solar-Geophysical Data</u>)	16
X-ray plasma, height of	27
Young active regions, X-rays from	21, 26